Magnetization Reversal Study in CoFe Magnetic Nanostructures

THESIS

Submitted in partial fulfilment
of the requirements for the degree of

DOCTOR OF PHILOSOPHY

By

N.V.S.S.Seshagiri Rao
ID. No. 2013PHXF0014H

Under the Supervision of

Dr. V.Satyanarayana Murthy

BITS Pilani

Pilani | Dubai | Goa | Hyderabad

BIRLA INSTITUTE OF TECHNOLOGY AND SCIENCE, PILANI
2018

BIRLA INSTITUTE OF TECHNOLOGY AND SCIENCE, PILANI

CERTIFICATE

This is to certify that the thesis entitled **" Magnetization reversal study in CoFe Magnetic nanostrucutres "** and submitted by **N.V.S.S.SESHAGIRI RAO** ID No **2013PHXF0014H** for the award of Ph. D. of the institute embodies original work done by him under my supervision.

Signature of the Supervisor: _____

Name : **Dr. V.SATYA NARAYANA MURTHY**

Designation : **Assistant Professor**

Department of Physics

BITS Pilani-Hyderabad Campus.

Date:

Acknowledgements

It is a moment of gratification and pride to look back with a sense of contentment at the long travelled path, to be able to recapture some of the fine moments and to be able to thank the infinite number of people, some of whom were with me from the beginning, some who joined me at some stage during the journey, whose rally round kindness, love and blessings have brought me to this day. I wish to thank each and every one of them with all my heart.

Foremost, I would like to express my sincere gratitude to my advisor **Dr.V.Satyanarayana Murthy** for the continuous support of my Ph.D. study and research, for his patience, motivation, enthusiasm, and immense knowledge. His guidance helped me in all the time of research and writing of this thesis. Our interactions were always quite informal and friendly. I consider myself quite fortunate to have had such an understanding and caring adviser, throughout the course of my research at the Institute. I would also like to thank him for taking the time to help me develop my scientific writing skills. I know the preparation of this thesis has tried his patience, and I would like to let him know that his efforts have not gone unappreciated. I could not have imagined having a better advisor and mentor for my Ph.D. study.

I am thankful to acknowledge my Department Advisory Committee (DAC) members Prof. **P.K.Thriuvikraman** and Prof. **Meenakshi Viswanatham** for their support and encouragement during this period.

I would like to express my gratitude to Prof **P.K.Thiruvikaraman**, Head of the department-Physics, for providing me with all the necessary laboratory facilities and for having helped

me at various stages of my research work. I deeply acknowledge and my heartfull thanks to **Dr. Kannan Ramaswamy, Dr. K.V.S. Shiva Chaitanya, Dr Arvinda N.Raghavan,** Department of Physics, **Prof. Sanket Goel** Head Department of EEE, Prof. B.V.S.S.Prabhakar Department of Elelctrical and Electronics Engineering, Mr. Ramesh Prasanna C, Department of Computerscience BITS, Pilani-Hyderabad campus, for his valuable suggestions.

I am grateful to **Prof. Souvik Bhattacharya**, **Vice-Chancellor (BITS)** and **Prof. V. S. Rao, Ex- Director (Hyderabad campus)** and Present Director **Prof. G. Sundar BITS, Pilani (Hyderabad campus)** , for allowing me to carry out my doctoral research work in the institute.

I would like to express my sincere thanks to **Dr.Vidya Rajesh, Associate Dean, Academic Research (Ph.D. Programme), Prof. Yogeswari, Dean, SRCD, Venkata Vamshi Krishna Venuganti, Associate Dean AGSR of BITS-Pilani, Hyderabad campus** for their continuous support and encouragement during my research work.

I sincerely acknowledge the help rendered by faculty members of Department of Physics at the BITS-Pilani, Hyderabad campus. I would like to acknowledge non-teaching staff Mr. Upender reddy , RamaDevi and Sheik Shakoor of physics department, Praveen (ARD), Bhagya Lakshmi (SRCD Division), and Suresh (IPC- Division).

I take this opportunity to sincerely acknowledge the Department of Science & Technology (DST), Government of India, New Delhi, and Bits-Pilani, Hyderabad Campus for providing financial assistance.

I am very much grateful to all my friends and it's my fortune to gratefully acknowledge the support of all the individuals **Mr.Y.V.Subba Rao**, **Hemanth Kumar Narsetti** , Smriti Smita Lenka, **Shanmukha sundar**, Konka Raviteja, Rahul Thakur, **Waseeem Ahmed Wani** and Satheesh Kandukoori. I take this opportunity to thank one and all for their help directly or indirectly.

Finally I thank my parents, wife, children and other family members who kept with their continuous care, support and encouragement for their support throughout my Ph. D work .

Lastly, and above all, I would like to thank the God Almighty; for all that he has given to me.

To those I may have Wronged,

I ask Forgiveness.

To those I may have Helped,

I wish I did More.

To those I Neglected to help,

I ask for Understanding.

To those who helped me,

I sincerely Thank you

Date: *So much*

… N.V.S.S.Seshagiri Rao

Magnetization reversal study in CoFe magnetic nanostructures

Abstract

Keywords: Soft magnetic materials, micromagnetism, nanomagnets, nanostructures, exchange energy, magnetostatic energy, Zeeman energy, etc

This thesis presents the results of a study on magnetization reversal in soft magnetic CoFe nanostructures having varying geometries (elliptical, circular, rectangular and square) of thickness (10 nm – 60 nm). The reversal was studied by running the micromagnetic simulations using the open source code OOMMF developed by NIST. The magnetization reversal depends on the shape and size of the nanostructure. 10 nm and (or) 20 nm nanomagnets exhibited the reversal process by sudden change in the direction of magnetization in all the shapes. For thickness ≥ 20 nm the reversal is through the formation of S– type, double vortex and single vortex states in the case of elliptical and circular nanomagnets and by the formation of C – type, multivortex , double vortex and single vortex states in rectangular and square nanostructures. The magnetic states captured during the time of simulations shows the formation of the above said intermediate states. The competition between the magnetostatic energy which depends on shape and the exchange energy decides the formation of the above said magnetic states.

To verify the simulation results, experimental studies were done on 10 nm and 60 nm thick elliptical nanomagnets. The simulation results of the above said two nanomagnets are matching with the experimental observations. MFM images in the demagnetized state show the formation of single domain and vortex states in 10 nm and 60 nm thick nanomagnets respectively. The small deviations from the simulation results are explained.

TABLE OF CONTENTS

List of Figures

List of Tables

Notations

OOMMF	-	Object Oriented Micromagnetic Frame work.
NIST	-	National Institute of Standard and Technology.
UV	-	Ultraviolet
XRD	-	X-ray Diffraction
VSM	-	Vibrating Sample Magnetometer
AFM	-	Atomic Force Microscopy
MFM	-	Magnetic Force Microscopy
FDM	-	Finite Differnce Method
FEM	-	Finite Element Method.
TCl/TK	-	Tool Command Language/Tool Kit
MIF	-	Micromagnetic Input Format
LLG	-	Landau Lifshitz Gilbert Equation.
SWM	-	Stoner Wohlfarth Model
AR	-	Abrupt Reversal
DV	-	Double vortex
SV	-	Single Vortex
MV	-	Multi Vortex
H_{ndv}	-	Nucleation of double vortex
H_{nsv}	-	Nucleation of single vortex
H_c	-	Coercive field
H_a	-	Annihilation field
H_s	-	Saturating field

Chapter I

Introduction

1.1. Magnetism at Nanoscale

Nanomagnetism is the study of magnetic structures or particles at nanoscale. It is one of the most vital and fastest growing areas of research. Nanostructures can be produced in different geometries and in different magnetic materials. Nanostructures consist of number of atoms or molecules combined together in a cluster with at least one dimension less than 100 nm. A nanometer is 10^{-9} m or 10 Å. Spherical particles having a radius of about 1000 Å or less can be considered as nanoparticles.

The behavior of nanoparticles or nanostructures is different from that of the bulk because of the reduced dimensionality. Elementary models of the solid state explain why the changes of properties occur in nanoscale [1]. The different behavior in nanoscale can be broadly explained based on three factors –

(i) The dimensions are comparable to the characteristic length scales such as exchange length, domain and domain wall size, spin diffusion length, etc.

(ii) Reducing from bulk to nanometer range breaks the crystal translational symmetry. Because of this, the coordination number and the band structure of the material changes.

(iii) The surface to volume ratio increases,

Fig.1.1 shows the reduced number of neighbors and the energy band diagrams with the dimensionality. In the bulk, all the three dimensions are in the micron or above micron range. By reducing the one or more dimensions to nanoscale we can get the films, wires or rods and clusters or dots. If one of the dimension is reduced to the nanoscale by keeping the other two dimensions large then the structure is called thin film. In other case if two dimensions are reduced, while one remaining large, then it is called as a nanowire or nanorod. If all the three dimensions reaches to the nanometer range, it is called nanodot [2]. These different types of geometries is of great interest in soft and hard magnetic nanostructures. Among these, soft ferromagnetic nanostructures are of much importance because of their use in magnetic data storage, spintronics, sensors, etc.

1.2 Ferromagnetic domains

Ferromagnetic materials frequently break up into many regions each with different orientation of magnetization. Such a region of single orientation of magnetization is called a domain. Each domain is spontaneously magnetized to the saturation value M_s. Which happen only at low temperature. At high temperatures thermal energy will reduce the magnetization. Domains are separated by a transition region called domain wall. These domain walls are the interfaces between the regions in which the spontaneous magnetization is different. The size of the domain wall depends on the competition between magnetocrystalline anisotropy energy and exchange energy [2, 3].

The domains are basically responsible for the phenomena of hysteresis of magnetization which occurs on increasing and then decreasing the applied field. When the size of each magnetic

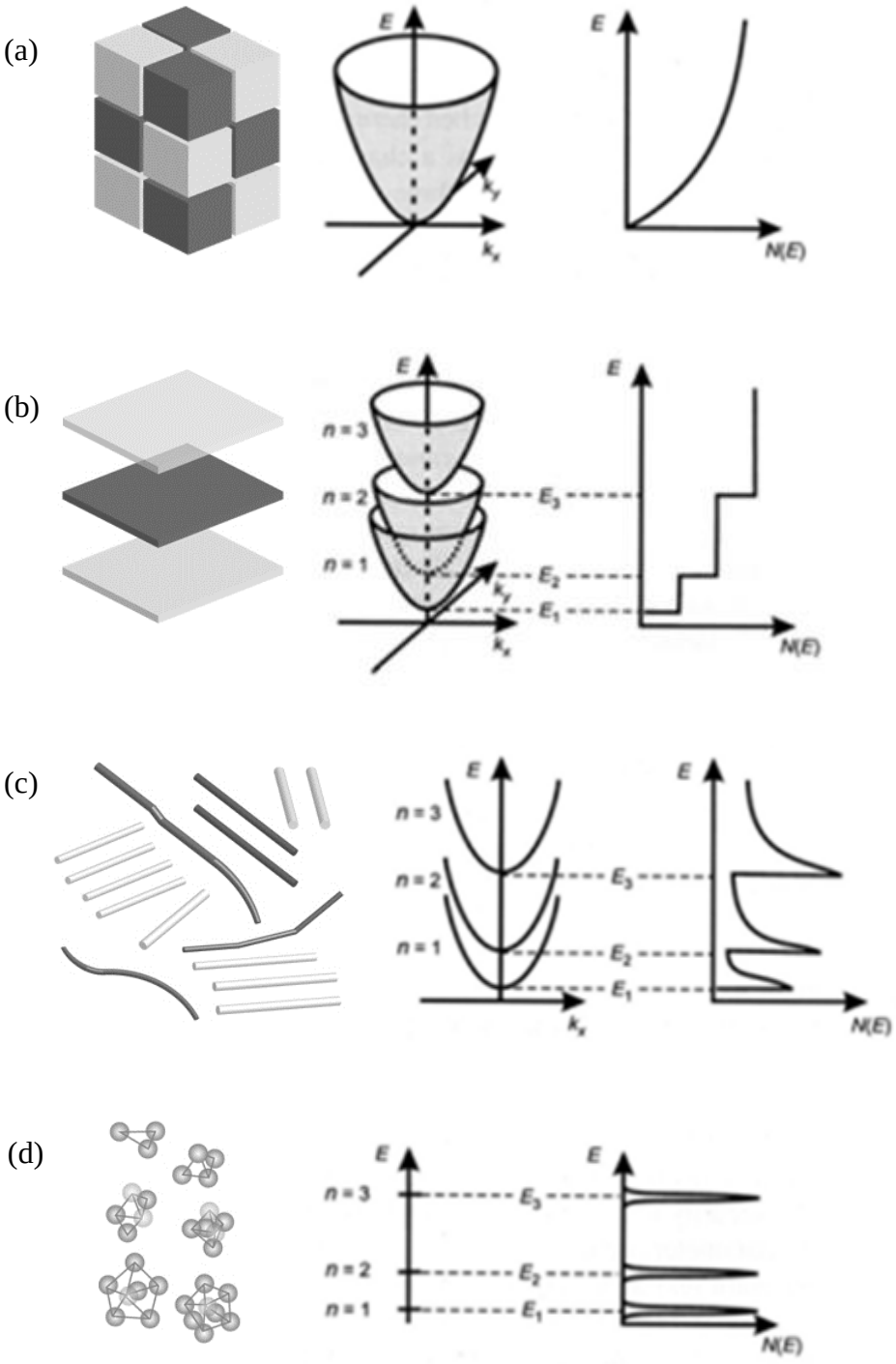

Fig.1.1: Variation of energy band diagrams with the dimensionality (a) bulk - 3D, (b) thin film – 2D, (c) nanowire or rod - 1D and (d) nanodots - 0D.

particle is reduced to some critical value it will not favor the formation of domains and the particle will have single domain [4]. The size of the single domain particle depends on the balance between the magnetostatic energy and the domain wall energy.

1.3 Magnetodynamics

The important equation of micromagnetism that is used to model the behavior of the hard disk drives is the Landau-Lifshitz-Gilbert equation. In Ferromagnet, the magnetization M can vary internally but at each point its magnitude is equal to the saturation magnetization Ms.

In its original form it was first proposed by L. D. Landau and E. M. Lifshitz in 1935. The Landau – Lifshitz- Gilbert equation predicts the rotation of the magnetization in response to torques and consists of a physically derived precession term and a phenomenological damping term. The LL equation is given by

$$\frac{d\mathbf{M}}{dt} = -\gamma \boldsymbol{M}\, x\, \boldsymbol{H}_{eff} + \lambda \mathbf{M} \text{ x } (\mathbf{M} \text{ x} \boldsymbol{H}_{eff}) \quad \text{---------- (1)}$$

Where γ is the electron gyromagnetic ratio and λ is a phenomenological damping parameter which is often replaced by $\lambda = - \alpha \frac{\gamma}{M_s}$ where α is dimensionless constant, M_s is the saturation magnetization, H_{eff} is the effective magnetic field. $\frac{dm}{dt}$ is the magnetic response to torque .

In 1955 Gilbert replaced the damping term in LL equation by time dependent of the magnetic field

$$\frac{d\mathbf{M}}{dt} = -\gamma \left(\boldsymbol{M}\, x\, \boldsymbol{H}_{eff} - \eta\, \boldsymbol{M}\, x \frac{d\mathbf{M}}{dt} \right) \quad \text{---------- (2)}$$

Here M is the magnetization at any instant of time, This is LLG equation ,where η is the damping parameter which is the characterstic of the material. It can transform in to LL equation

$$\frac{\mathrm{d}\mathbf{M}}{\mathrm{dt}} = -\gamma'\mathbf{M}\ x\ \boldsymbol{H}_{eff} + \lambda\mathbf{M}\ \mathrm{x}\ (\ \mathbf{M}\ \mathrm{x}\ \boldsymbol{H}_{eff}) \quad \text{----------} \quad (3)$$

where $\gamma' = \frac{\gamma}{1+\gamma^2\eta^2 M_s^2}$ and $\lambda = \frac{\gamma^2\eta}{1+\gamma^2\eta^2 M_s^2}$ in this form of the LL equation, the precessional term γ' depends on the damping term. This represents the better behavior or real ferromagnetrs when the damping is large. Fig.1.2 shows the schematic representation of these two terms.

1.4 Effective field (H_{eff})

The effective field is a combination of applied field, exchange field, anisotropy field and demagnetizing field [11, 12].

$$\mathbf{H}_{\mathrm{eff}} = \mathbf{H}_{\mathrm{ext}} + \mathbf{H}_{\mathrm{exch}} + \mathbf{H}_{\mathrm{ani}} + \mathbf{H}_{\mathrm{d}} \text{ ----------} \quad (5)$$

This field exerts torque on the magnetization causing the magnetization dynamics.

The Effective field related can also be written as

$$\mathbf{H}_{\mathrm{eff}} = -\ \frac{d\boldsymbol{E}}{d\mathbf{M}} \text{----------} \quad (6)$$

Where E is the total energy of the system. It is a combination of different energies involved which are explained in the following section.

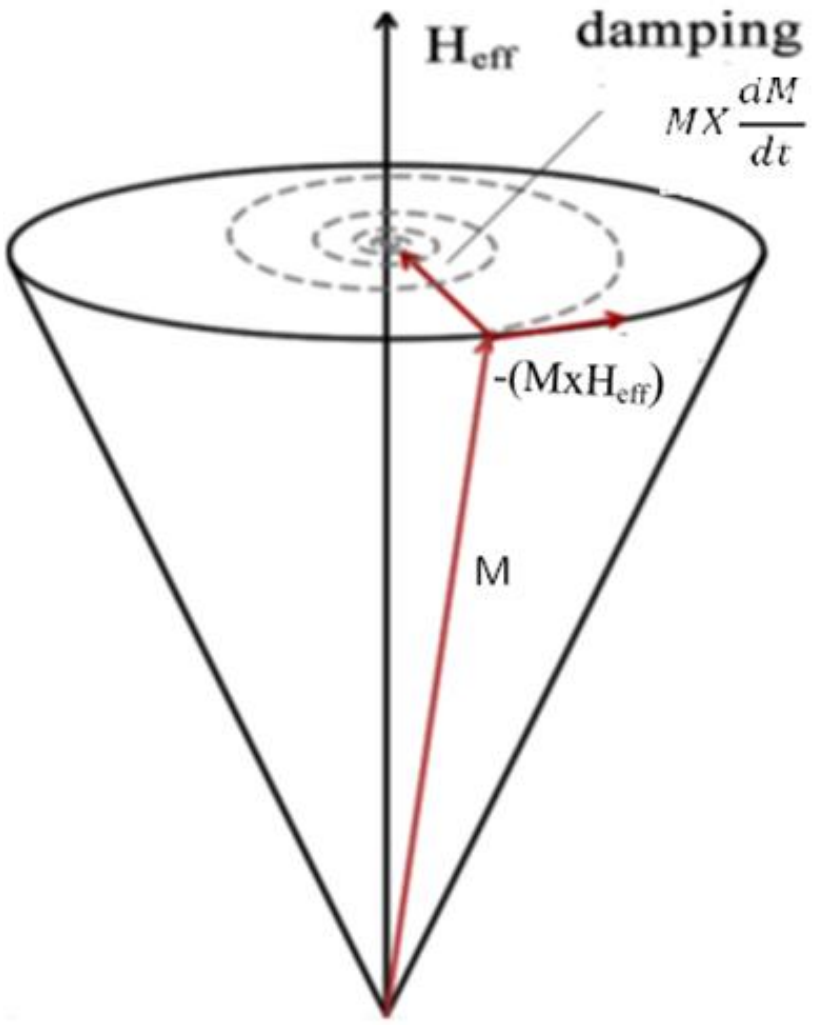

Fig. 1.2: The precession and damping terms of an atomic magnet in an effective field.

1.5 Energy Terms

According to the phenomenological theory used in micromagnetics the total energy of a ferromagnetic system can be written as a combination of several energies.

$$\mathbf{E}_{total} = \mathbf{E}_{ext} + \mathbf{E}_{exch} + \mathbf{E}_{ani} + \mathbf{E}_{d} \text{ ----------(7)}$$

Here E_{ext} is the energy contribution due to external field, E_{exch} is the exchange stiffness energy, E_{ani} is the anisotropy energy and E_d is the demagnetization energy [4, 13, 14].

1.5.1 Exchange Energy

It is the energy which acts on the relative orientation of spins of two electrons. This energy is quantum mechanical in origin. The exchange forces are fundamentally electrostatic [4, 8, 15]. If the spins align parallel then the material is ferromagnetic and if they are antiparallel then the material is antiferromagnetic. It forms an important part of total energy of the system. The exchange energy is given by

$$\mathbf{E}_{ex} = -2 J_{ex} \mathbf{S}_i . \mathbf{S}_j = -2 J_{ex} \mathbf{S}_i \mathbf{S}_j \cos\theta \text{ ----------} \quad (8)$$

Where J_{ex} is exchange integral, S_i and S_j are the atomic spins and θ is the angle between the spins. If $\theta = 0°$ i.e. the spins are parallel and J_{ex} is positive then minimum energy state of the system gives ferromagnetism. If $\theta = 180°$ i.e. the spins are antiparallel and J_{ex} is negative then minimum energy state gives antiferromagnetism.

1.5.2 Anisotropy energy

A magnetic material will have anisotropy energy if its internal energy depends on the direction of the crystallographic axes. It is called magnetocrystalline anisotropy energy. In a crystal, not all directions of the magnetization have the same energy [7, 16, 17]. Energetically the magnetization directions are called as easy and hard axes. The origin of magnetic anisotropy is due to the coupling of electron orbitals with lattice and electron orbitals with spins. The direction of easy or hard axes and the energy depends on the crystal structure of the material.

The crystal anisotropy energy in cubic crystals such as Fe and Ni is

$$E_{ani} = K_1(\alpha_1^2\alpha_2^2 + \alpha_2^2\alpha_3^2 + \alpha_3^3\alpha_1^2) + K_2(\alpha_1^2\alpha_2^2\alpha_3^2) + ... --- (9)$$

Here K_1 and K_2 are anisotropy constants α_1, α_2, and α_3 are the direction cosines.

In hexagonal crystals like cobalt

$$E_{ani} = K_2 \sin^2\phi + K_4 \sin^4\phi \text{----------} \quad (10)$$

Where ϕ is the azimuthal angle, The other types of anisotropies other than magnetocrystalline anisotropy are stress anisotropy and shape anisotropy. Stress anisotropy is related to the magnetostriction which is the expansion or contraction of ferromagnet along the direction of magnetization. It is also crystal structure dependent. Shape anisotropy becomes more important when the sample size becomes small. The origin of shape anisotropy can be understood by studying the demagnetizing fields or demagnetization energy.

1.5.3 Demagnetization energy

It depends on the level or strength of magnetization of the material. It is also called dipolar energy or stray field energy or magnetostatic energy. Demagnetizing fields are produced by the magnetization of the sample by applying the external field. The magnetostatic or demagnetizing field energy H_d is given by

$$\mathbf{H}_d = - N_d \mathbf{M} \quad \text{----------} \quad (11)$$

Here N_d is the demagnetizing factor, and it depends on the shape of the material. It can be calculated for different shapes [6 - 8, 11, 17].

When there is no external field the demagnetizing energy can be obtained from Maxwell's equation and written as

$$E_d = -\frac{1}{2}\int \mu_o \boldsymbol{H}_d \,.\, \boldsymbol{M}\, dv \quad (12)$$

Clearly the demagnetization energy can be reduced if the magnetization is reduced. As a result of this the material breaks into domains. The overall magnetization of the material which is the vector addition of all the domains magnetization is zero. But in the presence of field, because of the magnetization of the material, it will have some demagnetization energy. Hence in the total energy E_d is included.

1.5.4 Zeeman Energy

The energies E_{exc}, E_{ani} and E_d are the internal energies of a ferromagnetic material [4, 11, 18]. Zeeman energy comes because of the applied magnetic field and if the magnetization does not lie in the direction of applied field. Zeeman energy can be written as

$$E_{ext} = E_{ze} = - \mathbf{M}.\, \mathbf{H}_{ext} \text{----------} \quad (13)$$

1.5.5 Total Energy or Effective Field Energy

In nanomagnetism, micromagnetic modelling is a common technique to calculate magnetization. There are some more energies (magnetoelastic energy) other than the above four but they do not contribute significantly. The equilibrium spin configuration is determined by minimization of total energies [18].

$$E_{total} = E_{eff} = E_{ext} + E_{exch} + E_{ani} + E_d \text{ ----------(14)}$$

1.6 Applications of Nanomagnetic Structures

Magnetic nanostructures have tremendous applications such as hard disk media, magnetic random access memory (MRAM), spin transfer torque random access memory (STTRAM), sensors, etc. [2, 7]. The study of magnetization reversal is very much essential to understand the mechanism and behavior of nonmagnetic devices. Magnetization reversal in nanomagnets happens by the application of magnetic field or by passing current.

1.6.1 Magnetic Data Storage

The recording density of magnetic hard disk is increasing day by day. According to international magnetic storage industry consortium, by the year 2020 the storage capacity of single hard disk will reach 100 Tb. Fig.1.3 shows the roadmap of international magnetic storage industry consortium. Achieving this with the present granular film in magnetic hard disk is very difficult. In granular film few grains are used to store the data (0 or 1) [15, 16, 19]. The target can be reached with the use of nano magnetic structures. In this each single domain nanostructure will store 0 or 1.

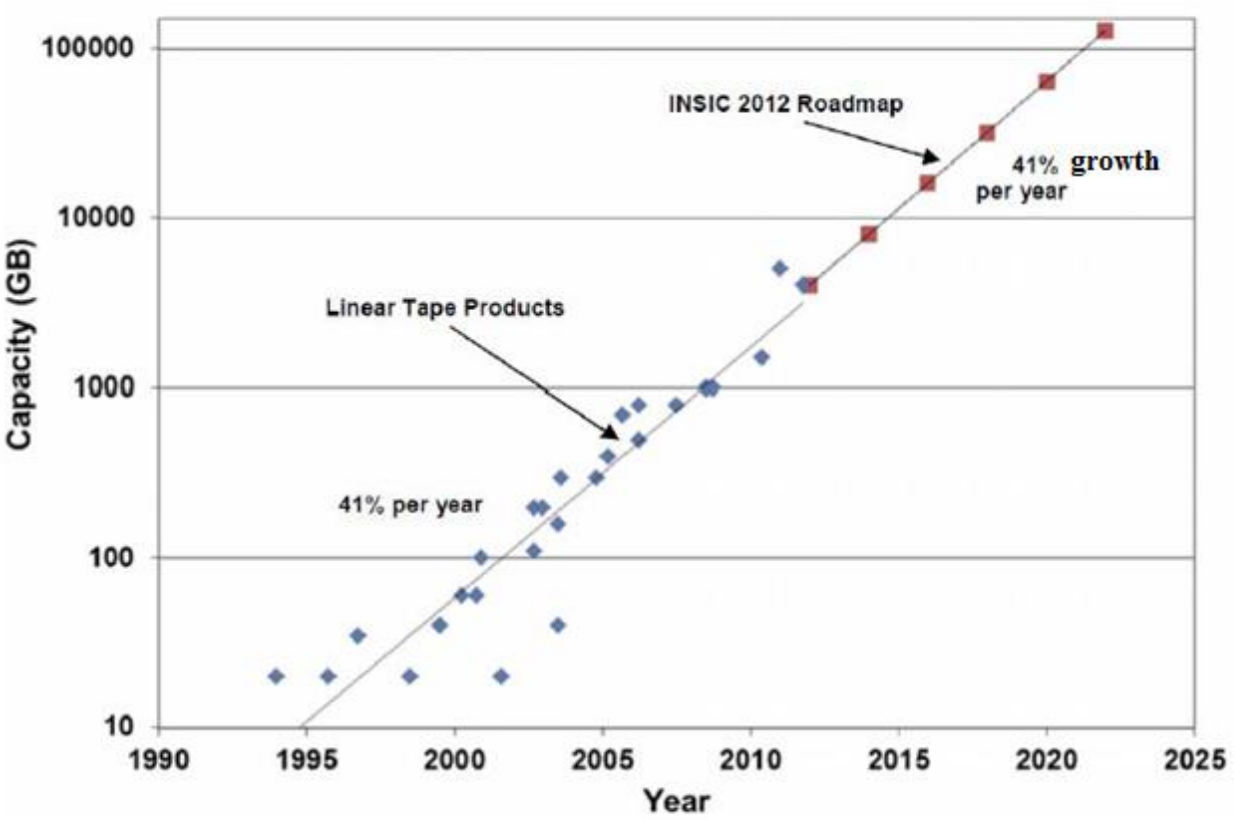

Fig.1.3: International magnetic storage industry consortium roadmap.

(http://www.insic.org)

The single domain nanomagnets shows square hysteresis loop, which is the most important parameter for magnetic data storage.

1.6.2 Magnetoresistive Random Access memory (MRAM)

Magnetoresistive random access memory (MRAM) is a nonvolatile random access memory technology developed by IBM research foundation. It is under development since 1990s. Unlike conventional RAM chip, the data is stored by magnetic storage elements, which are formed by ferromagnetic multilayer thin films each of which can hold magnetization separated by an insulating layer [20, 21]. The development of MRAM started with anisotropic magnetoresistance materials. The most important attribute of MRAM is nonvolatility. In the absence of electric power, magnetic moments maintain their alignment, thus data is kept undamaged. Micromagnetic simulations help us to understand which shapes of the nanomagnets are useful as part of an MRAM configuration [22 - 26].

1.6.3 Sensor Elements

Magnetic multilayer films that exhibit electron - spin dependent transport are used in sensing and storage devices. Spin tunnel junctions are favorable systems for applications in magnetic random access memory or field sensors [27]. The tunneling behavior becomes important by decreasing the lateral size of the elements and the uniformity of the magnetization. Recently, investigations have been reported on the magnetization reversal of the free layer using microscopy techniques in the transmission electron microscope [28]. The magnetization reversal of square elements showed the formation of complex domain structures that differ significantly according to the direction in which the field is applied.

1.6.4 Magnetic Nanostructures

Experimentally and theoretically the magnetic nanostructures are of great interest. The main function of nanostructures is that domain walls can be moved in any direction by spin polarized currents. Future magnetoelectronic devices and magnetic sensors will be based on this technology [29]. Here logical operations are executed by domain wall propagation through ferromagnetic nanostructures [30, 31]. Even though there is active research in recent years there is still a lot to fully understand the properties of magnetic nanostructures and their fabrication. More systematic study is needed for the magnetization reversal process and its associated dynamic effects in nanoscale systems.

1.7 Literature review

Scientific research and economic interests have recently turned to smaller and smaller magnetic structures, which can be used in hard disk drives, MRAM and other novel devices. Magnetic nanostructures have been studied on different materials like permalloys ($Ni_{80}Fe_{20}$), $Ni_{19}Fe_{81,}$ Super Permalloys ($Ni_{80}Fe_{15}Mo_5$), and Co nano-elements in different types of geometries like thin films, nanowires, nanodots and circular disks. Many applications require submicron size dot particles as they are the major issues for data storage devices. For submicrometer sized networks, both magnetostatic energy and exchange energy are important in determining the magnetization response [32]. In the last 20 years, there have been tremendous study for the development of magnetic nanostructures using special magnetooptical and other fabrication methods.

Magnetization reversal in nanostructures is very much dependent on the material constituents, size, shape and edge roughness, etc. Another important property is that in the case of the magnetically soft materials, the crystalline anisotropy (K_1) can be neglected as the magnetization reversal process and field evolution of the spin structure depends more on the shape and geometry of the nanostructure [33].

Magnetization reversal in submicron elliptical permalloy ($Ni_{80}Fe_{20}$) nanostructures have been investigated by P.Vavassori et. al [34] and they reported that the reversal mechanism is found to be dependent on the direction of the magnetic field.

F.Carace et.al studied magnetization reversal in [35] elliptical permalloy ($Ni_{80}Fe_{20}$) (magnetically isotropic) nanodots, that were fabricated using electron beam lithographic and lift –off process. They reported different kinds of magnetization reversal for different values of eccentricity. Experiments showed that the magnetization reversal is incoherent for elements that have less value of eccentricity and two relatively abrupt transitions of sharp switching of magnetization was observed resulting for vortex nucleation. Whereas for high values of eccentricity the reversal mechanism showed sharp switching of magnetization from one direction to other without vortex nucleation and almost showed perfect coherent magnetization rotation. This large variation of magnetization reversal on eccentricity is determined only by magnetostatic shape anisotropy.

For the as deposited thin film nanostructures in permalloy ($Ni_{80}Fe_{20}$) networks, the magnetization patterns for different networks was observed by Mei-Feng Lai et al. [36]. In films of the honeycomb network having three arm junctions, lowest energy of reduced ±1 magnetic pole density is observed at the junction center; while in the square network having four arm junctions

two lower energy configurations with the zero net magnetic pole density is observed in the junction center. Here in the square network the pattern of independently existent antivortex which has higher energy density is observed for the first time.

Another interesting magnetic nanostructure is the rectangular geometry. The magnetic configurations were studied in an array of rectangular permalloy ($Ni_{81}Fe_{19}$) elements in different aspect ratios [37]. It is observed that at low values of aspect ratio, single domain states or various stable states were obtained for each array and found that only one vortex state exist. For high value of aspect ratio multivortex and cross tie states exists [38].

In another case, there was a comparative study between rectangular and circular permalloy ($Ni_{80}Fe_{20}$) nanorings, investigated by G.Shimon et.al [39]. Ring shape strongly affects the reversal path and various transition field values. The thickness of the ring affects the domain wall structure and the reversal path and alters the field values for the two major transitions between magnetic states as compared to circular rings that vary with thickness [40]. The other one is at the corners of rectangular rings which provide the location of domain wall, in which the domain walls either annihilate to form a vortex state, or follow each other around the ring to reverse the ring without forming the vortex state. Simulation results provided good agreement with the experimental observations. These interactions between domain walls and corners in rings are important in the design of domain wall logic, memory and other devices [41].

In another study, the current induced magnetic switching behavior of memory cells was investigated by Jyh- shinn et.al [42]. Simulations showed that the switching current depends on

the end domain configuration and the remanent state of memory cells. The magnetic fields generated by small conducting line can alter the switching mode and makes the behavior somewhat complicated. The reversal process of field induced magnetic switching for the selected cell is divided into O, U, and S modes. The dynamic effects in magnetic nanostructures are becoming increasingly important at extremely small length and time scales [43]. A dependence on shape has been observed the oval cell requires small switching current than the elliptical one.

J.Fidler et.al investigated the magnetization reversal in rotational magnetic fields [44] on Co based nanostructures for different geometries like square, rectangular and circular shapes of different thickness. The switching behavior for instantaneously applied fields differs from the one in rotating magnetic field at high frequencies. Simulations were performed by using 3D Micromagnetic model. It is reported that the shape and Gilbert damping parameter strongly depends on the switching time and field. Magnetization reversal process in the unidirectional field proceeds by the nucleation and propagation of end domains towards the center of the nano particles of Cobalt whereas, the rotational fields reversal implicates the comparable rotation of the end domains towards the rotational field direction, Magnetization reversal process and simulations showed that during the reversal process at critical diameter (40 nm for Ni and 20 nm for Fe) the vortex structure is energetically unfavorable and the transition from vortex wall to transverse wall occurs.

Magnetization reversal in Co based nanowires of different diameters have been observed by Luu Van Thiem et.al [45]. The wire diameter and the magnetic anisotropy influences the

magnetization reversal. The reversal occurs via coherent rotation mode for wire diameter smaller than 276 nm while for diameter greater than 276 nm curling of magnetization takes place. The easy axis of the magnetization changes direction from parallel to perpendicular with respect to wire axis when the wire diameter exceeded a critical value of ~ 276 nm.

L.Torres et. al [46] have studied micromagnetic simulations in supermalloy ($Ni_{80}Fe_{15}Mo_5$) nanostrucutres and observed two different switching modes in planar square magnetic nanoelements of size ''*a*'' in the different exchange lengths of thickness $0.5l_{ex}$ and $1.5l_{ex.}$ The first one is found for very small nanoelements, while the second one takes place in the large nanosquares and presents an intermediate state. R.P.Cowburn et.al [47] have experimentally measured the magnetization reversal in supermalloy square nanomagnets and had verified using micromagnetic simulations.

1.8 Objective

The main objectives of this thesis is to study the shape viz., elliptical, circular, rectangular and square and size of the nanostructure on magnetization reversal using micromagnetic simulations. To achieve the above said objective the following steps were followed

- Understanding the Object Oriented Micromagnetic Frame Work (OOMMF) developed by National Institute of Standards and Technologies (NIST)
- Executed the micromagnetic simulations for nanostructures of different shapes and sizes

Verified the simulation results experimentally for one of the nanostructure (elliptical)

Chapter II

Experimental and Simulation Details

This chapter describes the preparation of the soft magnetic nanostructures and their magnetic characterization. This chapter also describes the micromagnetic simulation details of soft magnetic nanostructures using Object Oriented Micromagnetic Frame work (OOMMF).

2.1 Elliptical nanostructures

Commercially available elliptical nanostructures fabricated on Si wafer were used for the experimental studies [48]. The nanostructures were fabricated using deep ultra violet lithography technique at 248 nm wavelength. A silicon substrate of diameter 200 mm was used for the fabrication of large area nanomagnets (4 mm x 4 mm). First the Si substrate was coated with a antireflection coating of thickness 60 nm using a spin coater. A positive resist UV210 of thickness 280 nm to 480 nm (depends on the shape and size) was coated on the antireflection coating. A combination of alternating phase shift masks and chromeless phase lithography masks were used on top of the photoresist. Patterning is done using Nikon S203 scanner which contains deep ultraviolet laser of wavelength 248 nm. Elliptical patterns created using this technique have the length of the major and minor axes as 335 nm and 225 nm respectively. The separation between the nanostructures along the major and minor axes are 290 nm and 150 nm respectively.

2.2 Electron beam evaporation

$Co_{50}Fe_{50}$ alloy was deposited on the commercially available elliptical nanostructures using electron beam evaporation technique. In e - beam evaporation technique, the beam of electrons are ejected out in such a way that they will heat and vaporize the target material to be deposited [49]. Once the target material changes its state from liquid to a vapor, it will be able to condense itself on the substrate wafer. In other words, there is a change of phase from liquid state to vapor state by a beam of electrons. AJA electron beam evaporation unit was used to deposit $Co_{50}Fe_{50}$. Before deposition, a base pressure of $1x10^{-7}$ torr was created in the chamber. The material was deposited on the substrate with a rate of 0.4 A°/s. A bare Si substrate was also kept in the chamber during deposition. This is used as a reference film.

2.2.1 Working principle

Fig. 2.1 shows the block diagram of e - beam evaporator technique. The material that is to be deposited is taken in a water cooled copper crucible. The mechanism behind the working principle is divided in to two stages. In the first stage the electrons are emitted in thermionic process from a hot filament. The electron beam is accelerated by applying a voltage of 5 KV to 20 KV. In the second stage the evaporation of the target material will take place. The excited beam of electrons move in a certain path towards the material to be evaporated. Magnets are used to focus the electron beam on to the target material. The high energetic electron beam hits the target material and makes it to melt and evaporate. The evaporated material condenses on the substrate. The entire process happens in a high vacuum chamber [50-52]. The high vacuum allows the evaporated molecules to move freely in the chamber and condense on the target

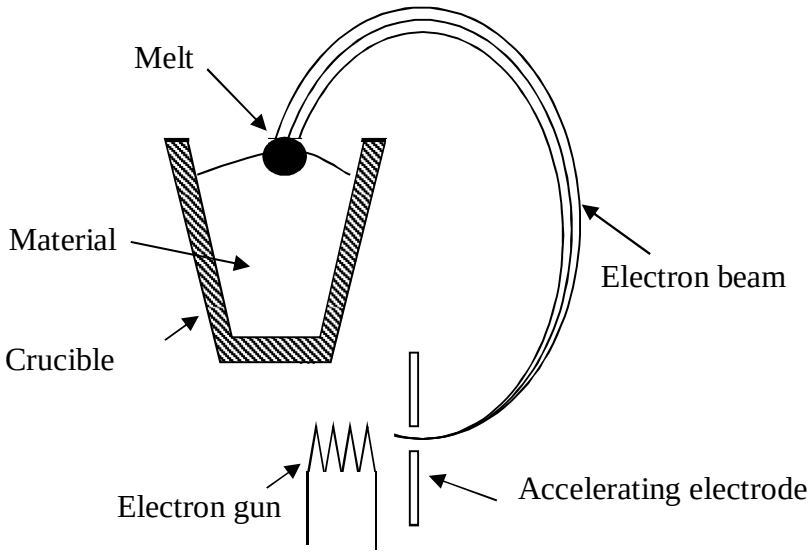

Fig. 2.1: Block diagram of electron beam evaporation technique

surface. In this process any material can be evaporated and the rate of deposition varies from angstroms to micrometers per second.

2.3 Characterization of magnetic nanostructures

The e – beam prepared elliptical nanomagnets were characterized using vibrating sample magnetometer (VSM) and magnetic force microscope (MFM).

2.3.1 Vibrating Sample Magnetometer (VSM)

Magnetization measurements were done at room temperature using a commercially available Lakeshore 7400 S vibrating sample magnetometer. The nanomagnets were attached to the sample holder using a double side tape. Since Si is diamagnetic, the magnetization of Si was measured and subtracted from the magnetization data of nanomagnets on Si. This gives the magnetization of only nanomagnets.

VSM was first invented by Simon Foner, in 1959 at the Lincoln laboratories. It is a measurement technique which allows us to determine the magnetic moment of a sample with very high precision. Fig. 2.2 shows the block diagram of VSM. It consists of an electromagnet, vibrator, lock in amplifier, pickup coils, a sample holder and power supply [53].

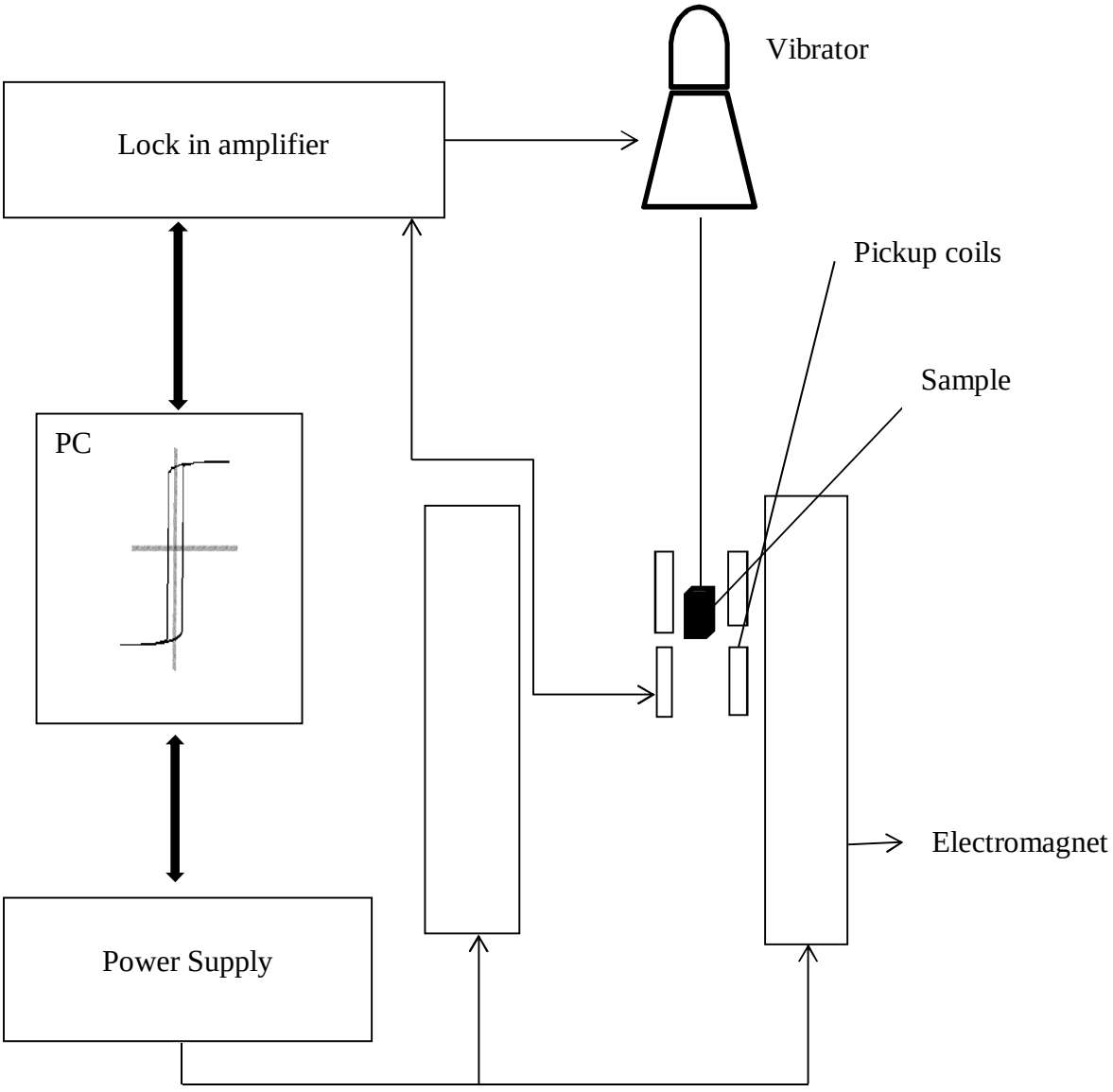

Fig. 2.2: Block Diagram of Vibrating sample Magnetometer (VSM)

2.3.1.1 Working principle

It works based on Faraday's law i.e ,changing magnetic fields induces voltage across the pickup coils. The sample to be studied is placed in a sample rod. One end of the sample holder is attached to a mechanical vibrator or to some loud speaker which in turn is connected to a lock in amplifier. The other end of the rod is in a uniform magnetic field produced by electromagnets. Electromagnets are connected to power supply that in turn are connected to PC where we can see the magnetization (M) vs field (H) variation. The sample rod is vibrated sinusoidally using a vibrator made up of linear actuators or modified audio speakers. The induced voltage in the pickup coil is proportional to the sample's magnetic moment, but does not depend on the strength of the applied magnetic field. In a typical setup, the induced voltage is measured through the lock-in amplifier using the piezoelectric signal as its reference signal. Lock-in principle of measurement allows the measurement of signal weaker than the noise. By measuring in the field of an external electromagnet, it is possible to obtain the hysteresis curve of a material [54].

2.3.2 Magnetic force microscope (MFM)

In the characterization of magnetic nanostructures, visualization with greatest resolution is interesting. Among the visualization techniques, MFM has become a powerful tool to see the submicron sized domains and to study surface roughness of thin films and also to understand the magnetic behavior of thin films and nanostructures. This is mainly due to its ease of use without any specific sample preparation and high lateral resolution of few 10 nm. It is also useful for observation of soft ferromagnets [55]. Digital instruments nanoscope III was used for the MFM measurements. CoCr coated Si cantilever tips magnetized along the tip axis are used as the scanning probe. The scan height was maintained at a distance of 70 nm.

2.3.2.1 Working principle

Magnetic force microscopy is a special mode of operation of the scanning probe microscopy. This method employs a magnetic tip that interacts with the magnetic field near the surface in noncontact mode. This was discovered after the invention of Atomic force Microscope (AFM). The tip which is coated with a magnetic material is attached to a cantilever and interacts with the stray field emanating from the sample thus measuring the force gradient as a function of position. MFM is a non-contact technique which operates in both static and dynamic modes. The static mode detects the magnetic force acting on the tip, dynamic mode measures the force derivative or force gradient that is acting on the tip. The cantilever or tip is the main element of a MFM [56, 57]. The magnetic forces act at greater distances than the Vanderwaals forces, the information provided by the magnetic force can be separated from surface topography by increasing the tip to sample distance. As the tip moves over the magnetic field gradient, it is either pulled toward or repulsed away from the sample depending on the magnetic moment direction of the sample. Fig. 2.3 shows the MFM imaging of magnetic sample.

2.4 Simulation details

Micromagnetic simulation has become an important tool in the study of both static and dynamic phenomena in ferromagnetic materials and for optimization of magnets in magnetic storage devices and sensors. For making better devices we require sound knowledge of reversal mechanism at submicron dimensions and dependence with shape, size and thickness, etc. of the material. To study these in simulations, each magnetic element is divided into cells and the

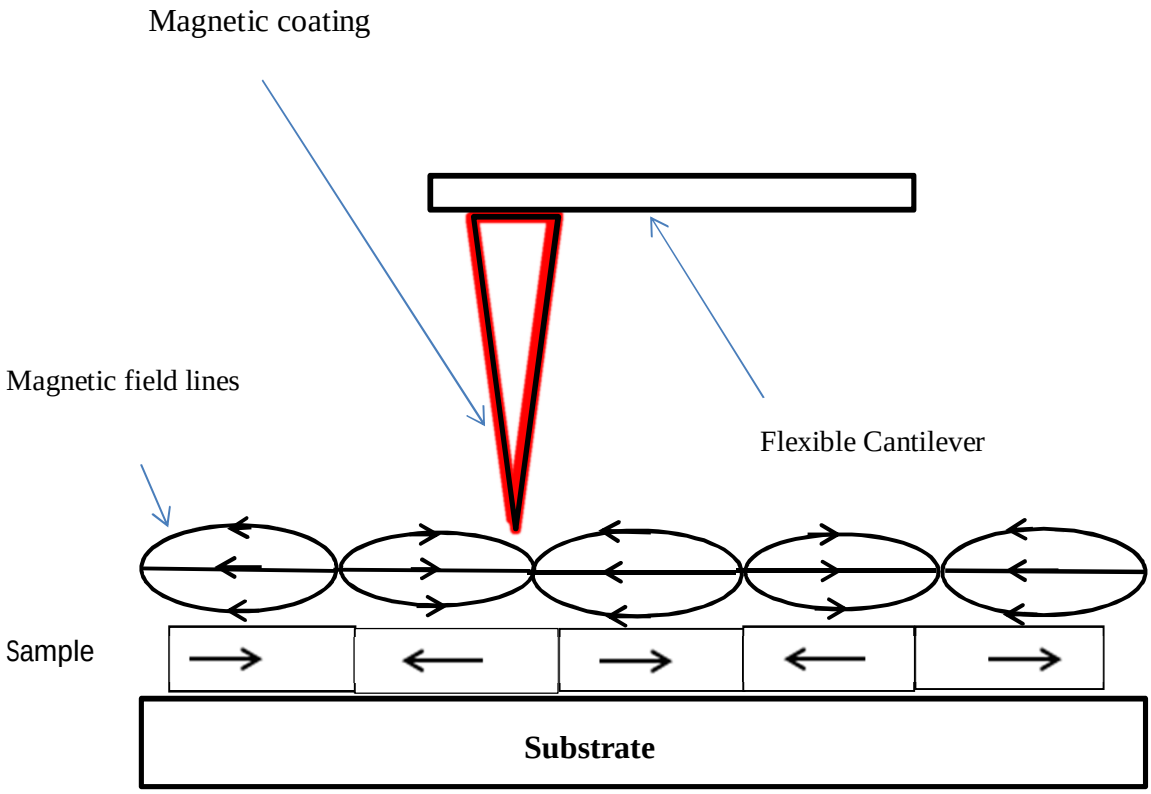

Fig. 2.3: MFM imaging of magnetic sample

magnetization of each cell is M_i i.e., $|Mi|$ = M_S. The magnetization distribution for the given value of the applied field is given by integrating the Landau – Lifshitz - Gilbert equation [58].

The magnetic properties of small structures, artificially prepared or occurring due to microstructure, can be understood using the principles of micromagnetism enunciated by W.F.Brown [59]. Here we consider the M_s vector of constant magnitude to have a direction which is a continuous function of positon (x, y, z) in the crystals, we then express the various energies namely exchange, anisotropy, magnetostatic, etc. in terms of directions throughout the crystals. The resulting equations are then to be solved for spin directions at all points [60 - 62]. Micromagnetism was developed for the purpose of energy minimization that tend to determine domain structures and classical nucleation theory to explain magnetization reversal mechanisms for many years.

There are different types of commercial and free domain packages available for running the micromagnetic simulations [63]. These packages work on either finite difference method (FDM) or finite element method (FEM) [64]. One of the free domain package is the Object Oriented Micromagnetic Frame work (OOMMF) developed by National Institute of Standards and Technology (NIST). The goal of the OOMMF project is to develop a portable, extensible public domain micromagnetic program and associated tools. This code forms a completely functional micromagnetic package, with the additional capability to be extended by other programmers so that people developing new code can build on the OOMMF foundation. OOMMF is written in C++, a widely-available, object-oriented language that can produce programs with good

performance. For portable user interfaces, we make use of Tcl/Tk so that OOMMF operates across a wide range of UNIX, Windows, and Mac OS X platforms. The step in using OOMMF the first method is to create the simulation environment by making MIF maker [65]. The MIF maker is a command line application to initialize the geometry, material, and simulation parameters and generate a valid OOMMF problem description. OOMMF solves the LLG equation (eqn.1 of Sec 1.3). OOMMF uses the FDM to solve the LLG equation. It calculates the magnetization value at a particular field from the given material parameter values. The magnetization output is the normalized output. During the magnetization reversal, the applied magnetic field tries to orient the magnetic moment along the field direction. The magnetic moment experiences torque. The simulation will run until the torque is minimum, in our case it is 10^{-5}.

2.4.1 Simulations using OOMMF: OOMMF works on the FD method [66]. Taylor series expansion is used to determine the partial differential equations. The basic idea of the method consists of approximating the partial derivatives of a function by finite difference quotients; this method divides the required geometry into cells of identical volume and shapes. When we use a particular geometry for simulation, that geometry should be divided in to unit cells and the size of the unit cell is (5 nm x 5 nm) to apply it for finite difference method. The magnetization is calculated on a uniform rectangular mesh at points ($x_0 + i\Delta x$, $y_0 + j\Delta y$, $z_0 + k\Delta z$) Here i,j,k are integers. To simulate the dynamics of the mangetic system from time t_o to t_{end} , the time has to be discretized to series of points [t_j]. The model is changed as follows.

$$\frac{dM(r_i,t_j)}{dt_i} = -|\bar{\gamma}|\, M(r_i,t_j) \times H_{eff}(r_i,t_j) - \frac{|\bar{\gamma}|\alpha}{M_s(r_j)} M(r_i,t_j) \times (M(r_i,t_j) \times H_{eff}(r_i,t_j) \text{----------(15)}$$

For the step wise solution for the magnetization above equation must be integrated numerically. The next values or the magnetization in each cell $M(r_j, t_j)$ are computed by multiplying the time derivative $\frac{dm}{dt}$ with a discrete time step *hi* and adding the result to the function values (r_i, t_{j-1}) as depicted in fig. 2.4. From the new values (r_i, t_j) the effective field components are then calculated and the integration is repeated until tend is reached.

The main advantages of the finite difference approach are ease of implementation, simplicity of meshing, efficient evaluation of the demagnetizing energy, and the accessibility of higher order methods [67, 68]. A main disadvantage of this approach is that we cannot handle curved boundaries easily with a rectangular mesh resulting in a staircase type approximation to the geometry. Each cell is approximated to a single particle [69]. The exchange length (l_{ex}) is greater than the length assumed by unit cell length and can be calculated by following equation

$$L_{ex} = \sqrt{\frac{2A}{\mu_0 M_s^2}} \quad \text{----------(16)}$$

Where A is the exchange energy, μ_0 is magnetic permeability, M_s is the saturation magnetization in A/m. Exchange length (l_{ex}) gives quantitative measurement for the mesh resolution.

The following screen shots explains how to run the micromagnetic simulations using OOMMF. Fig. 2.5 shows the OOMMF launch window. This contains seven programs as shown in the screen shot. In these, mmSolve2D is for running the two dimensional (2D) simulations and Oxsii is for three dimensional (3D) simulations. mmArchive, mmDataTable, mmDisp and mmGraph are common to both 2D and 3D simulations. Opening the mmArchive window saves the vector fields and the data table. mmDisp saves the magnetization orientation. It can also be

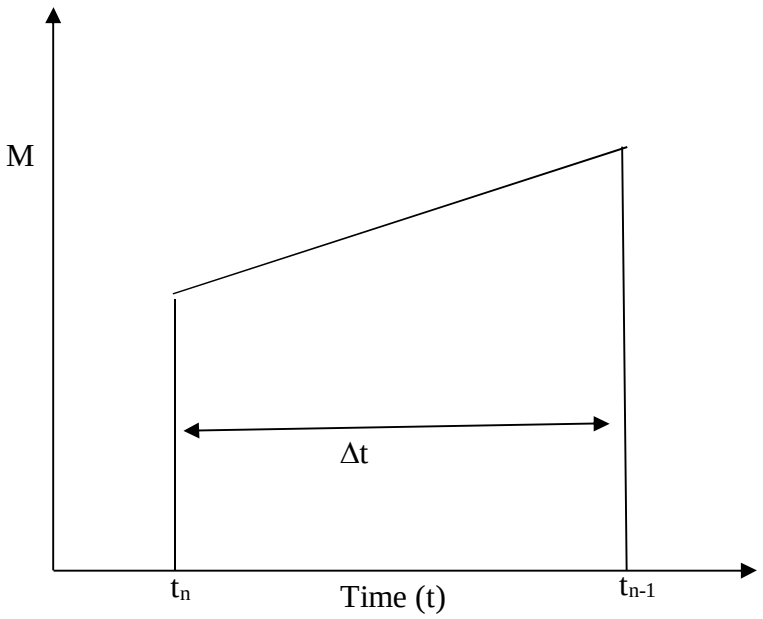

Fig. 2.4: Numerical Computaiton of Integral of the Landau-Lifshitz-equation

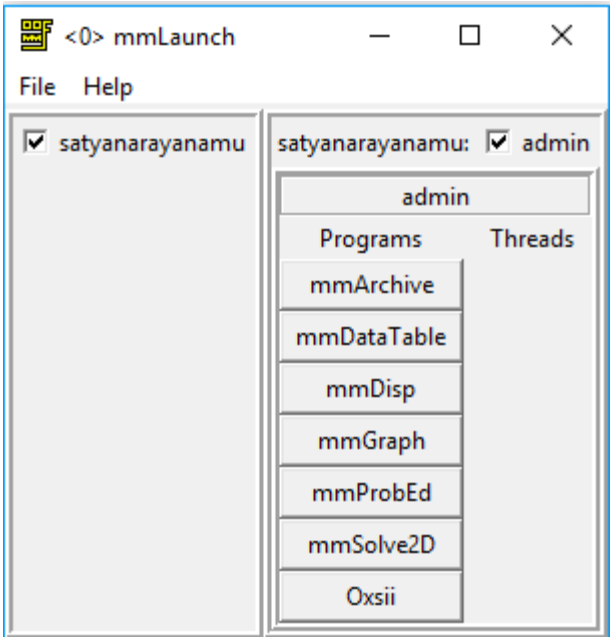

Fig. 2.5: OOMMF launch window

used to open the saved magnetization orientaitions after completing the simulations. mmGraph is used to save and replot the magnetization [70].

In the OOMMF launch window, the mmProbEd is used for giving the input parameters to run the 2D simulations. Fig. 2.6 shows the screen shot of mmProbEd. In this window the first tab indicates the material parameters. Fig. 2.7 shows the screen shot of the material parameters window.

The following are the material parameters used in simulations [48,71]..

- Saturation magnetization, $M_s = 1.9 \times 10^6$ A/m
- Anisotropy constant, $K_1 = 0$ and 3.5×10^5 J/m^3
- Exchange constant, $A = 3 \times 10^{-11}$ J/m
- Damping coefficient, $\alpha = 0.5$
- Mesh size 5 nm x 5 nm

The next tab is the simulation details in which the demagnetization type of the sample is to be entered. Since these are 2D simulations constant demagnetization is used in the present study. Fig. 2.8 shows the screen shot of this window.

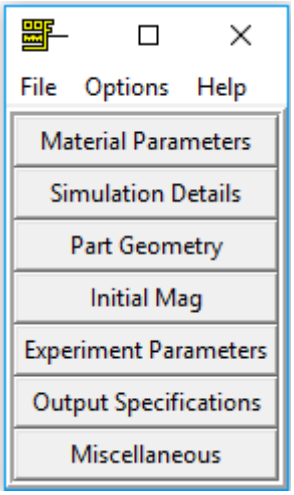

Fig. 2.6: mmProbEd window

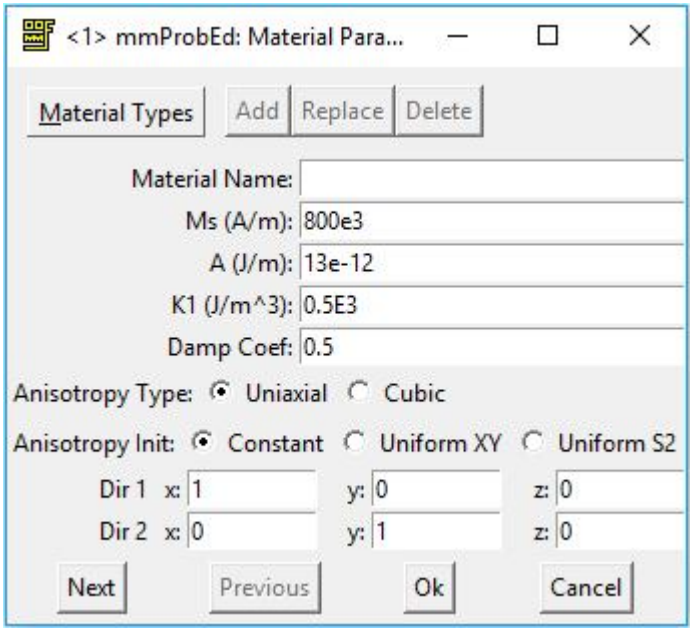

Fig. 2.7: Material parameters window

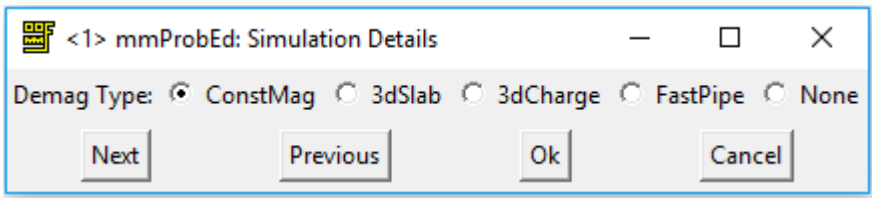

Fig. 2.8: Demagnetization type window

The third tab in mmProbEd where the geometry is specified. In this tab the geometry details of the nanostructure are specified . Fig. 2.9 shows the screen shot of the part geometry. If the geometry is other than the given geometries in the window, then jpeg or bitmap file of the nanostructure can be used. The path of the file can be specified in the mask. In the present study, circular, elliptical, square and rectangular nanostructures of CoFe were used in the thickness range from 10 nm to 60 nm. Fig. 2.10 shows the dimensions and thickness of the above mentioned nanostructures.

Next to part geometry is the initial magnetization direction. In this the magnetization orientation at the start of the simulation is to be given. Fig. 2.11 shows the screen shot of the initial magnetization window. Since the nanostructure magnetization is zero initially hence random magnetization was chosen for the simulation

Fig. 2.12 shows the experimental parameters window. In this the magnetic field values and the field orientation are given. The field can be applied along any of the directions (x, y, z). It can be divided into any number of ranges and ranges can be divided into number of steps. Field range from -500 Oe to +500 Oe are used in the simulations in steps of 120 Oe

The next two tabs indicate the output specifications and other miscellaneous details. They contain the output file name and path and the convergence value of the $m_x h$. The calculated $m_x h$ value converges to the given input value, then it completes one iteration and gives the output data. Figs. 2.13 and 2.14 show the screen shots of the above mentioned windows.

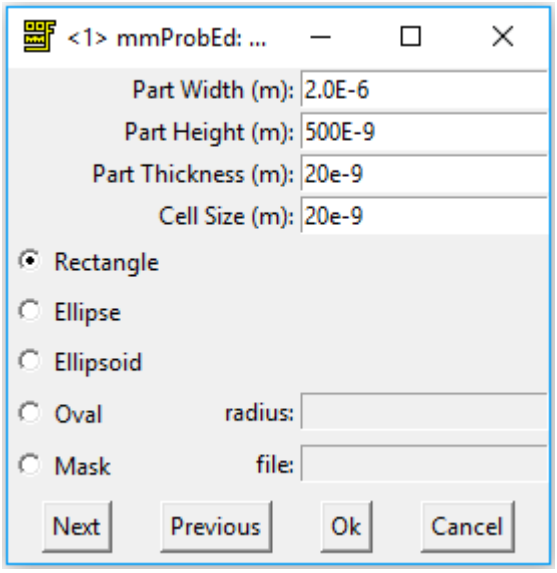

Fig. 2.9: Part geometry window

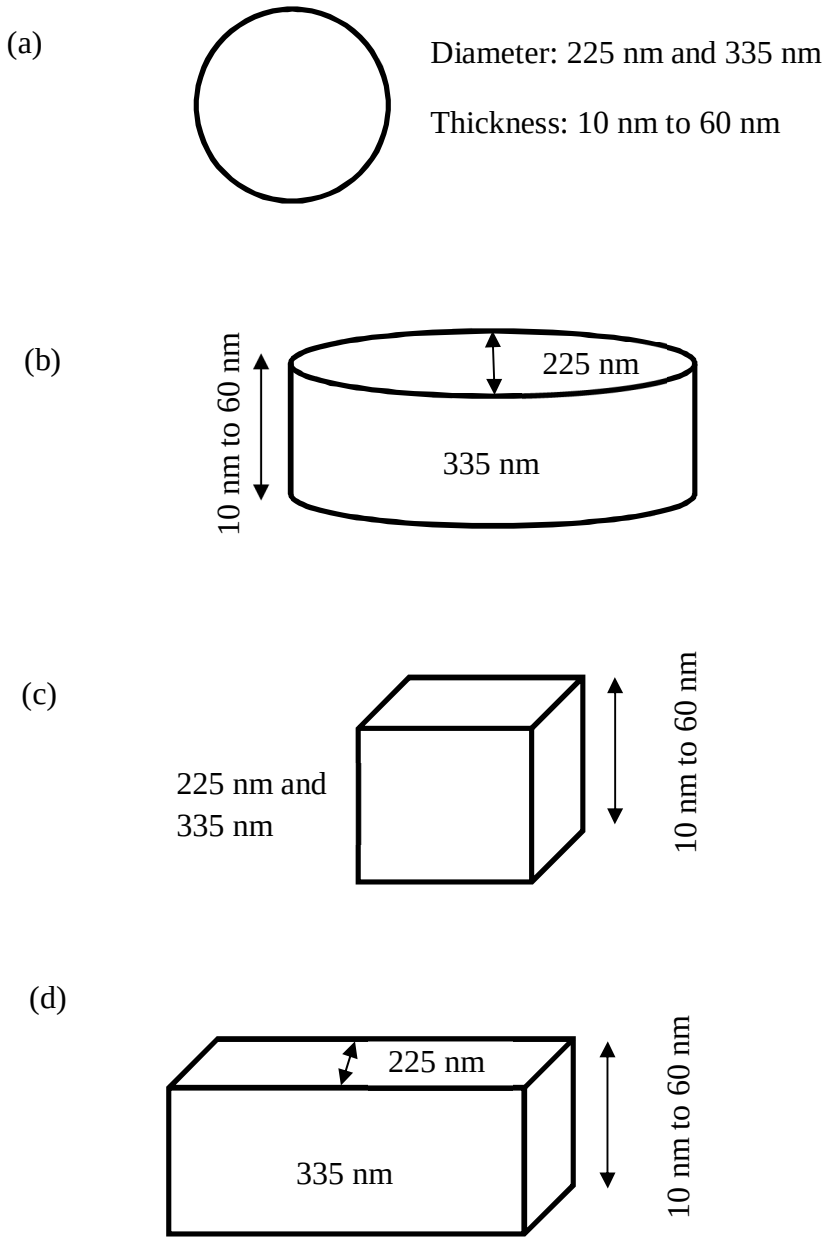

Fig. 2.10: Nanomagnets used in the simulations (a) circular, (b) elliptical, (c) square and (d) rectangular

.

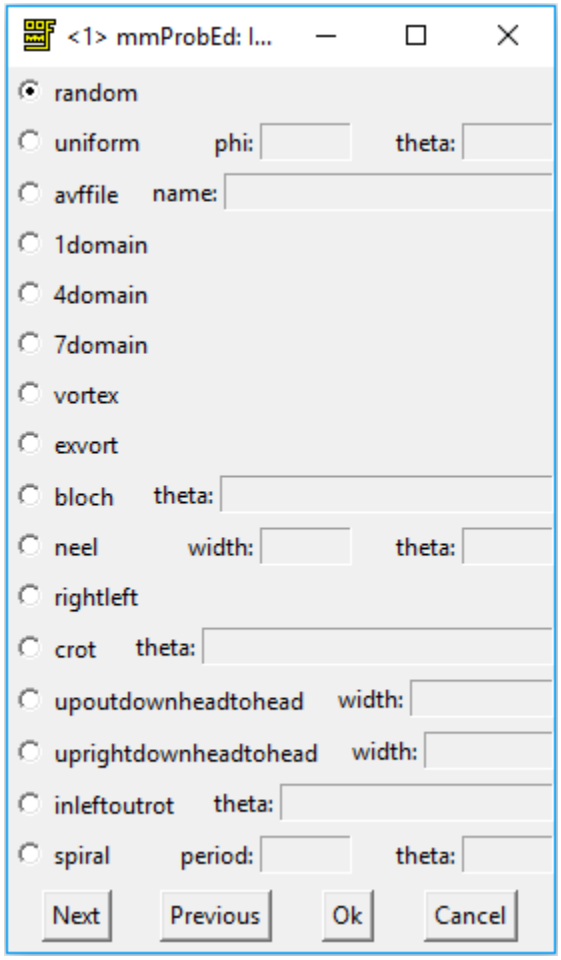

Fig. 2.11: Initial magnetization window

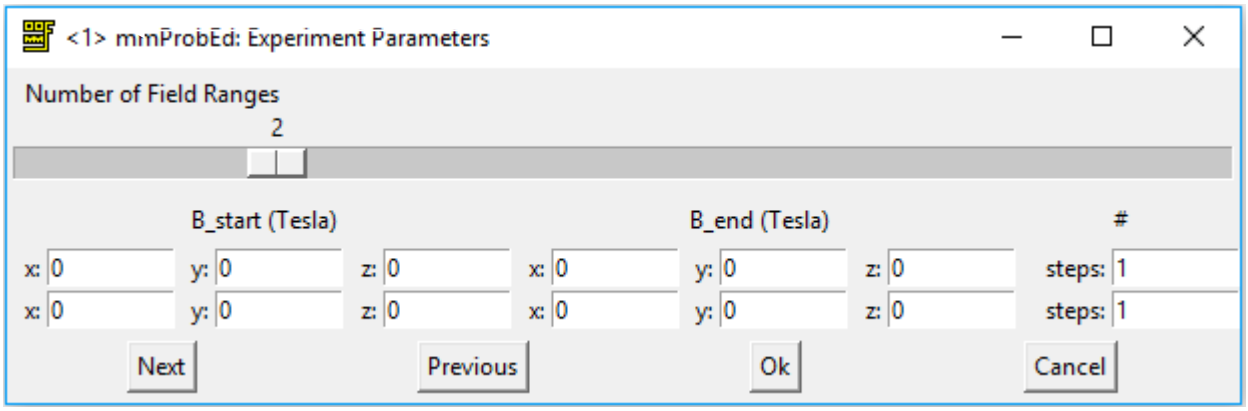

Fig. 2.12: Experiment parameters – magnetic field range window

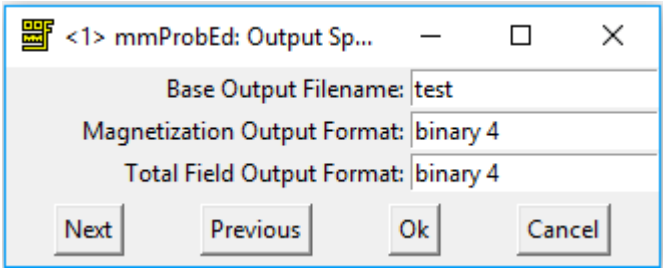

Fig. 2.13: Output specifications window

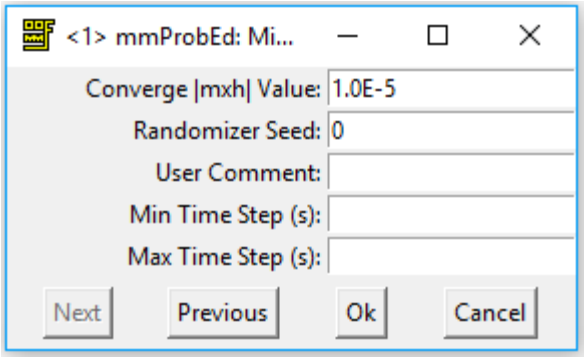

Fig. 2.14: Miscellaneous window

After editing the mmProbEd window, the mmLaunch window looks like Fig. 2.15. In the next step the mmSolve2D is to be selected to run the 2D simulations. Fig. 2.16 shows the screen shot of this window. The mmProbEd, load problem and scheduled outputs are to be selected before run the simulations. The data is saved for every one iteration.

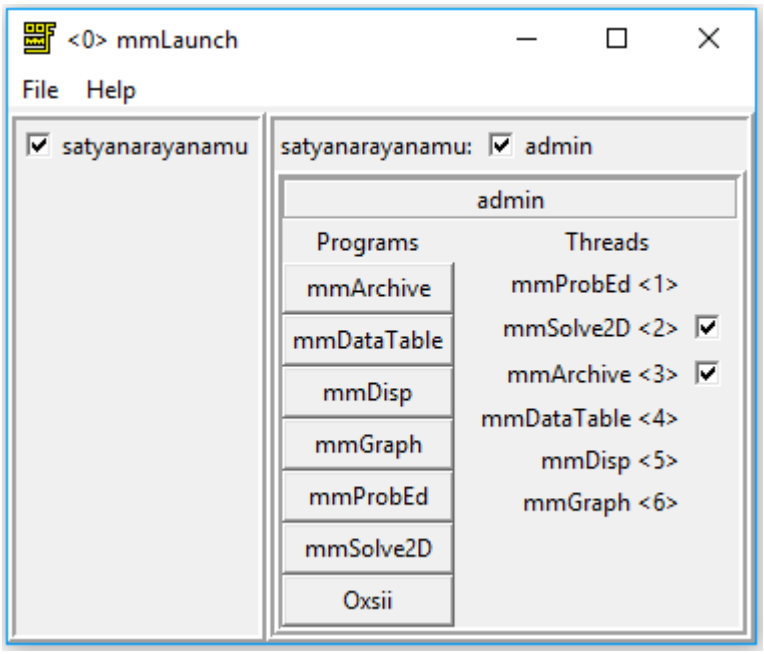

Fig. 2.15: Launch window after selecting the parameters in the programs

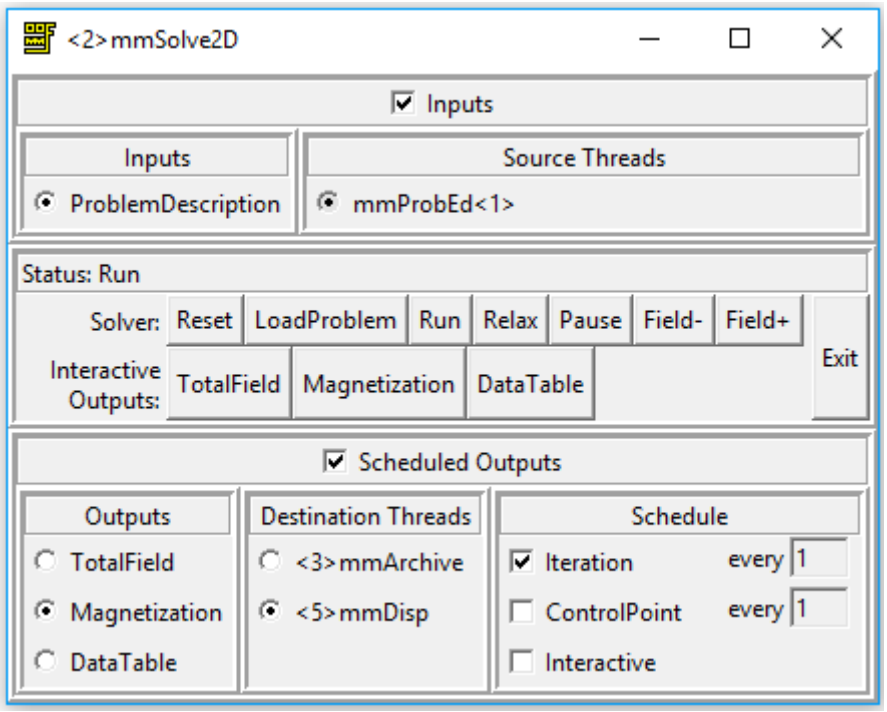

Fig. 2.16: mmSolve2D window

Chapter III

Magnetization reversal study in elliptical and circular nanomagnets

This chapter presents the micromagnetic simulation study of magnetization reversal in elliptical and circular nanomagnets. The elliptical nanomagnets major axis is 335 nm and minor axis is 225 nm and the circular nanomagnets are 225 nm and 335 nm in diameter. This chapter also presents the experimental magnetization reversal and magnetic force microscopy results of elliptical nanomagnets.

3.1 Elliptical Nanostructures

The magnetocrystalline anisotropy of as deposited films on nanostrucutres can be zero because of their amorphous nature and the same can be varied by heat treatment. Therefore we have done the micromagnetic simulations by taking the magnetocrystalline anisotropy of CoFe, K_1 = 0 J/m^3 and the bulk K_1 value, 3.5 x 10^5 J/m^3.

3.1.1 Simulation study with crystalline anisotropy constant K_1= 0 J/m^3

3.1.1.1 Applied field direction along the major axis (335 nm) of the ellipse

The thickness of the nanomagnets varied from 10 nm to 60 nm and the applied field from -500 Oe to +500 Oe. Fig. 3.1 (a) and (b) show the magnetization reversal in elliptical nanomagnets of thickness 10 nm and 20 nm respectively. These nanomagnets show similar type of reversal. When the field is changed from -500 Oe to +500 Oe, there is an abrupt reversal of magnetization

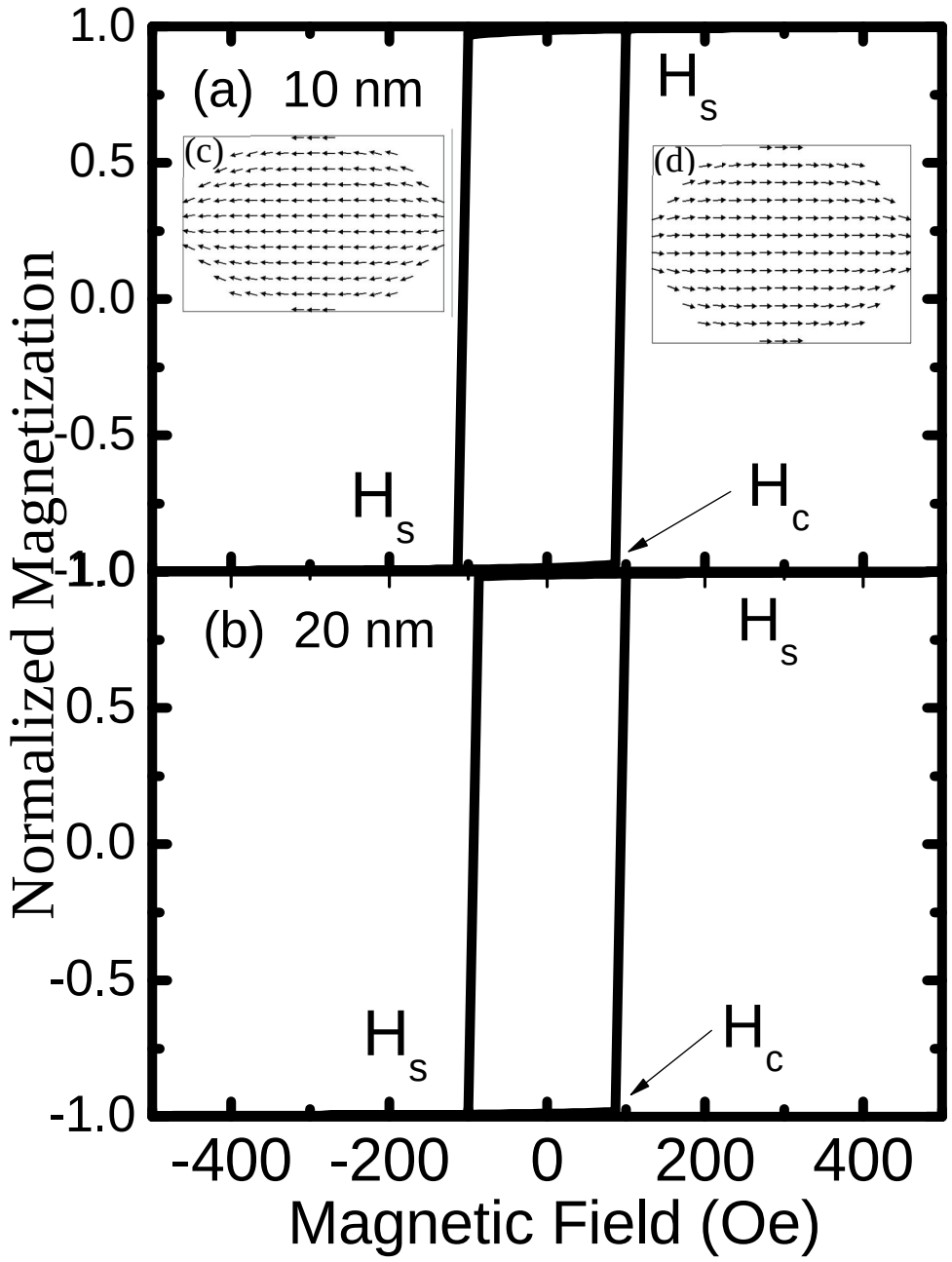

Fig. 3.1: Magnetization reversal along the major axis in (a) 10 nm and (b) 20 nm thick elliptical nanomagnets and magnetic orientations at saturating field along (c) –ve field and (d) +ve field

at field, H_c = 87 Oe in both the nanomagnets. This type of reversal behavior can be explained using Stoner – Wohlfarth model [72]. A field of -500 Oe makes the nanomagnet to saturate along the field direction. The orientation of magnetic moment at H_s is shown in figs. 3.1 (c) and (d) for fields along the negative and positive directions respectively. When the field is reduced to zero, The magnetization still lies along the field direction indicating that nanomagnets has remanent magnetization to the nanomagnet. When the field is increased in the positive direction, the magnetization would reverse and become parallel to the field direction at H_c = 87 Oe. Thus there is an abrupt reversal at this field. This type of reversal gives rectangle or square hysteresis loop which is the main criteria for magnetic data storage. Reversal process in nanostrucutres is largely controlled by the region within the structure that has the smallest nucleation field, smaller structures will on average have larger switching fields [48, 49, 73].

In the case of 30 nm nanostructure the magnetization reversal happens through the formation of intermediate double vortex state. Fig. 3.2 (a) shows the magnetization reversal and the formation and annihilation of double vortex states in 30 nm nanostructure. At saturating field all the magnetic moments in the nanomagnets are along the field direction. When the field is decreased towards zero the magnetic moment lies along the field direction. With increasing field, nucleation of double vortex occurs at H_{ndv} = 47 Oe. Fig. 3.2 (b) shows the nucleation of double vortex. Further increasing in the field makes the double vortex move towards the edges of the nanostructure. This can be seen at fields H_1 and H_2. Figs. 3.2 (c) and (d) show the movement of double vortex towards the edges of the nanostructure. At H_a complete annihilation of the double vortex happens and the magnetic moments orient along the positive field direction.

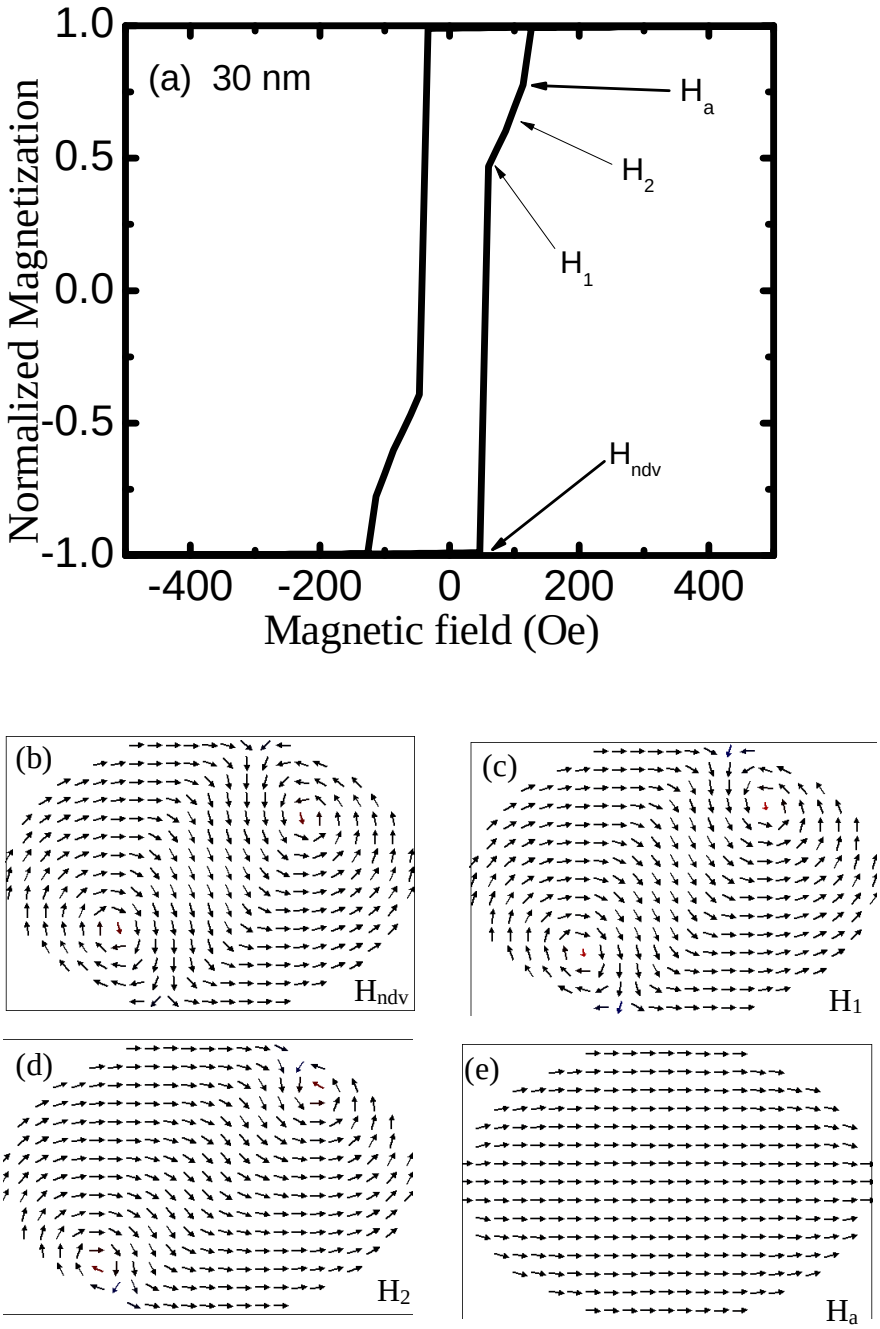

Fig. 3.2: (a) Magnetization reversal along the major axis in 30 nm thick elliptical nanomagnet and magnetic orientation at (b) nucleation field H_{ndv}, (c) field H_1, (d) field H_2 and (e) annihilation field H_a

Fig. 3.3 (a) - (c) show the magnetization reversal in 40 nm - 60 nm nanomagnets respectively. Initially the magnetic moment of the nanomagnets is aligned along the field direction. When the field is decreased towards zero, nucleation of double vortex occurred at field H_{ndv}. Fig. 3.3 (d) shows the double vortex formation in the above said nanomagnets. With further decrease in the field the two vortices combine to form a single vortex at field H_{sv}. Fig. 3.3 (e) shows the single vortex in the nanomagnets. This extra intermediate state is not observed in 30 nm nanomagnet as it depends on the direction of the applied field that is relative to the orientation of the central part of nanostructure. The single vortex moves towards the edges of the nanomagnets and then completely annihilates at field H_a. Fig. 3.3 (f) shows the single vortex at the edge of the nanomagnet just before annihilation.

For nanostrucutres of the same size and thickness, the double-vortex state is less energetically favorable than a single-vortex state due to higher exchange energy [74]. Surface energy controls the growth of the films the competition between the magnetostatic energy and exchange energy forms the domain wall. As the thickness of the film increases, the magnetostatc energy dominates the exchange energy. This leads to the formation of vortex states . For dimensions well above the exchange length (L_{ex}) the exchange energy will be minimum and there is reduction in magnetostatic energy by having a nonuniform magnetization reversal process in nanostructures. Hence we get zero magnetization by the formation of vortex states that reduces the stray field energy that was created by the domains and domain wall propagation. This single vortex state lowers the energy by reducing the stray fields and there by magnetostatic energy. Increasing the field towards the positive direction then deforms the vortex by pushing the core

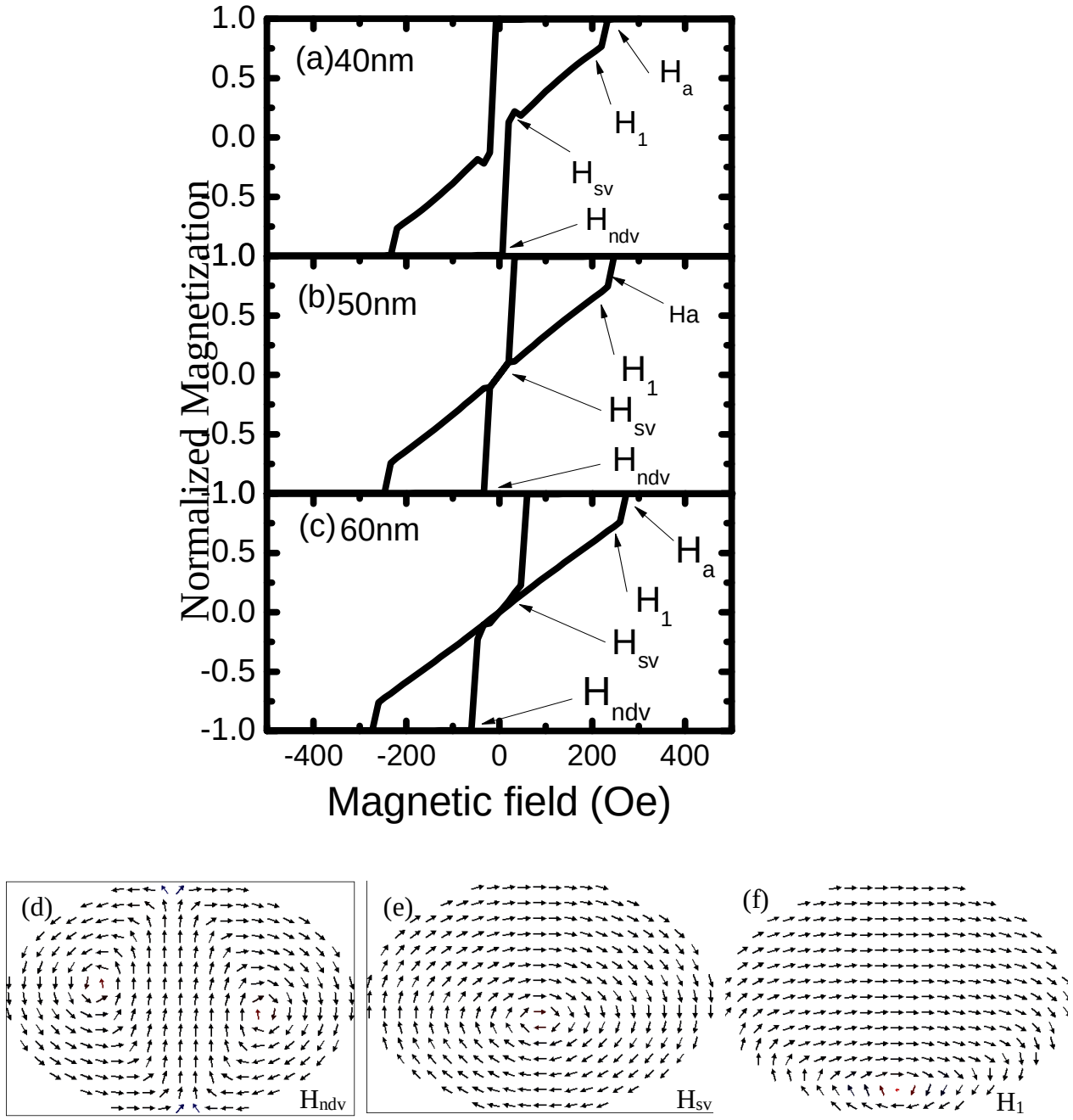

Fig. 3.3: Magnetization reversal along the major axis in (a) 40 nm (b) 50 nm and (c) 60 nm thick elliptical nanomagnets and magnetic orientation at (d) nucleation of double vortex H_{ndv}, (e) single vortex H_{sv}, (f) at field H_1

away from the center of the nanomagnet, until it becomes unstable and the vortex eventually annihilates. The vortex state only occurs for approximately exchange constant (A) > 10 L_{ex}.

The calculated value of the exchange length using equation (16) (of chapter 2) from the material parameter values (M_s = 1.9 x 10^6 A/m and A = 3 x 10^{-11} J/m) is 2.5 nm. Above the exchange length of 20 nm we observed the formation of vortex and multivortex states. For the vortex state the magnetization is nearly zero. Once the single vortex state is nucleated it is stable with in the structures until another stage is reached at large fields. Here the vortices are annihilated at the edges of the nanostructures to complete the reversal process. This highly ordered reversal mechanism have explained the hysteresis loops of single Co particles of different size. [75 - 78].

3.1.1.2 Applied field along the minor axis (225 nm) of the ellipse

Fig. 3.4 (a) shows the magnetization reversal along the minor axis of the 10 nm thick elliptical nanomagnet. Initially the magnetization is aligned along the negative field direction as shown in fig. 3.4 (b). The strength of the demagnetizing fields are larger along the minor axis than the major axis. When we decrease the field towards zero the magnetization reversal happens through the formation of s – type state. The nucleation of the state happens at H_{ns}. Complete formation of s – type state happens at field H_1. Figs. 3.4 (c) and (d) show the s – type state at fields H_{ns} and H_1 respectively. With further increasing the field in the positive direction, the magnetic moments align along the field direction through the direction change of S – type state as shown in Figs. 3.4 (e) – (g).

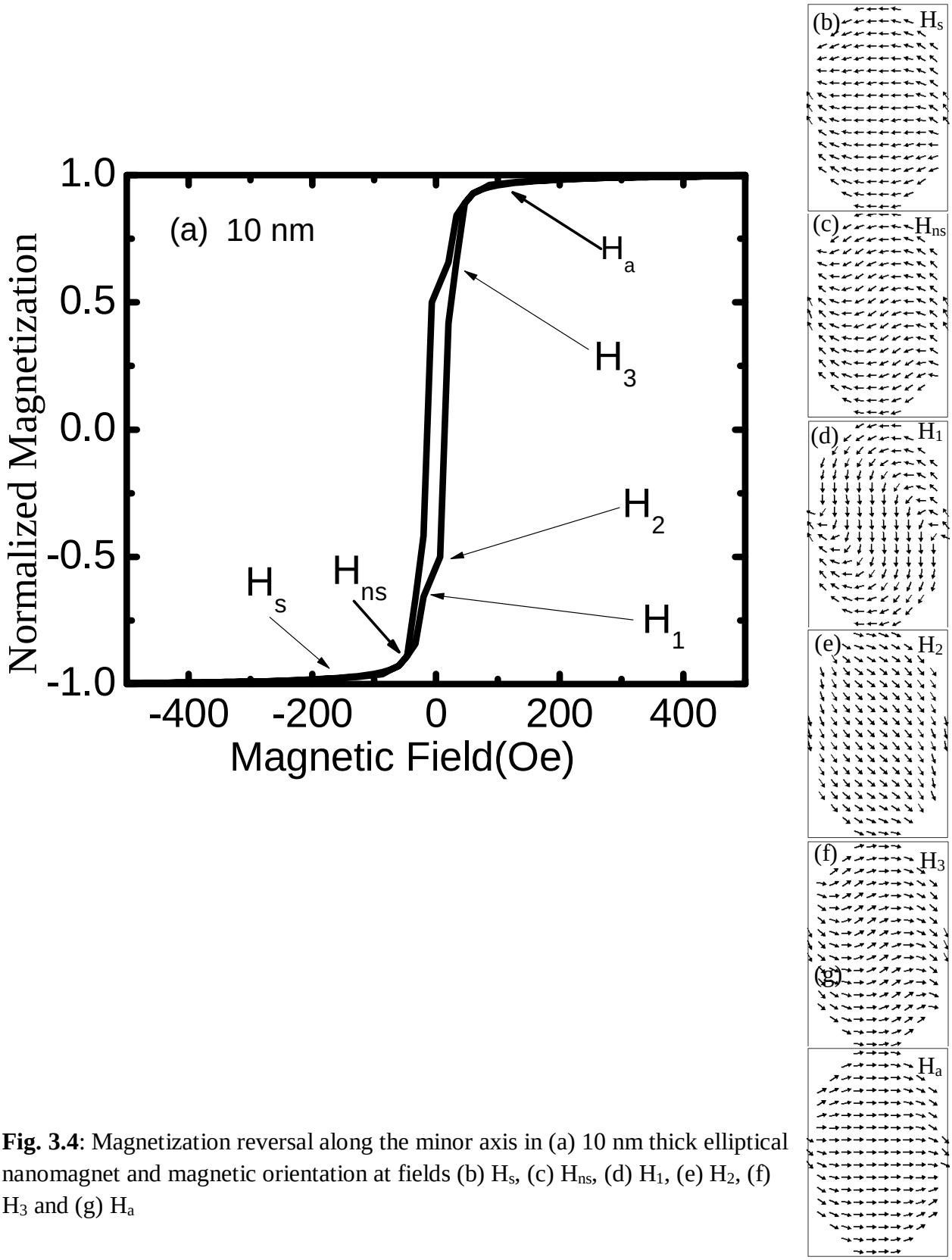

Fig. 3.4: Magnetization reversal along the minor axis in (a) 10 nm thick elliptical nanomagnet and magnetic orientation at fields (b) H_s, (c) H_{ns}, (d) H_1, (e) H_2, (f) H_3 and (g) H_a

Soft magnetic thin film nanostructures are magnetized in plane because of the foremost influences of stray field energy called shape anisotropy. If a nanostructure is magnetized along the short edge, surface charges and stray field energy are reduced by the formation of end domains that lead to C- states and S-states [4, 8,79].

Fig. 3.5 (a) - (c) show the magnetization reversal in 20 nm - 40 nm nanomagnets respectively. In these nanomagnets, the reversal happens through the formation of S – type and double vortex states. First the nucleation of s – type state happens with decreasing field at H_{ns}. This state is shown in Fig. 3.5 (d). With further decrease in the field towards zero, the S – type state converts into double vortex state at field H_1. Fig. 3.5 (e) shows the formation of double vortex state. The double vortex state moves towards the edges of the nanostructure. Fig. 3.5 (f) shows the captured image of the movement of the double vortex state at field H_2. Finally at higher fields, H_a the double vortex state annihilates.

The magnetization reversal in 50 nm and 60 nm nanomagnets happens through the nucleation of double vortex state and then the formation of single vortex state. This reversal process is same as that observed in the case of 50 nm and 60 nm elliptical magnets along the major axis. Fig. 3.6 shows the magnetization reversal and the captured images of the double and single vortex states. In 20 - 40 nm thickness when the field is applied along the minor axis (225nm) annihilation of double vortex could not takes place to single vortex as it depends on the direction of the applied field that is relative to the orientation of the central part of the nanostructure [80].

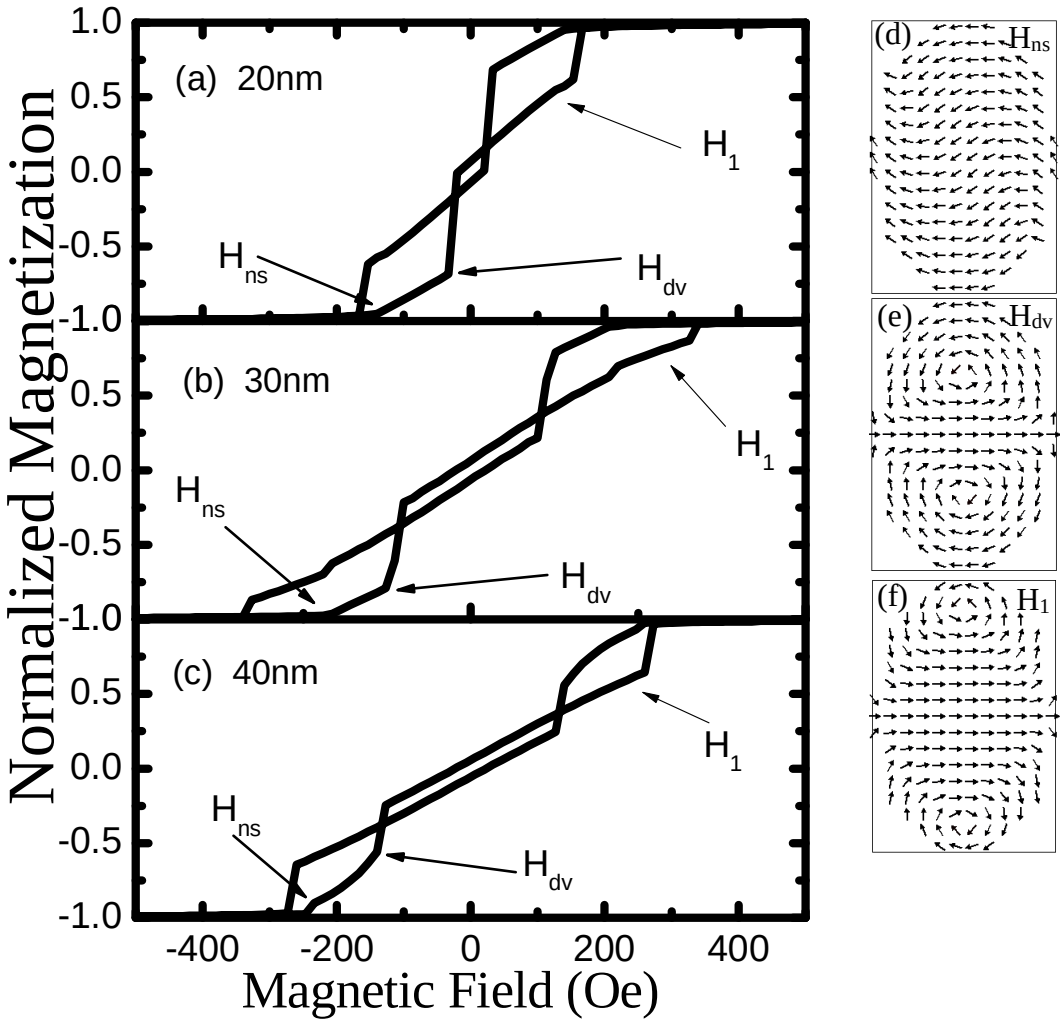

Fig. 3.5: Magnetization reversal along the minor axis in (a) 20 nm (b) 30 nm and (c) 40 nm thick elliptical nanomagnets and magnetic orientation at fields (d) H_{ns}, (e) H_{dv}, (f) H_1

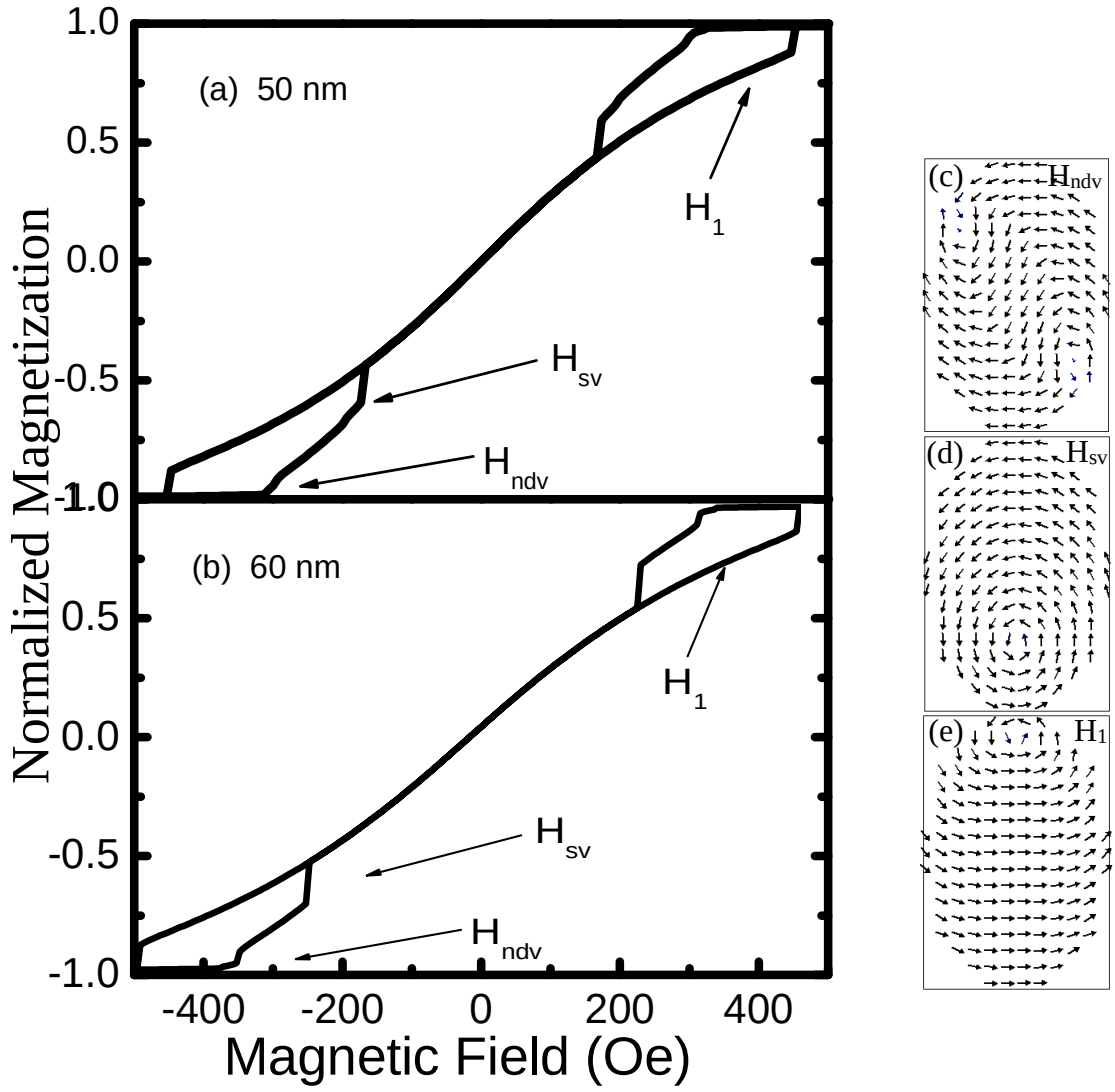

Fig. 3.6: Magnetization reversal along the minor axis in (a) 50 nm and (b) 60 nm thick elliptical nanomagnets and magnetic orientation at fields (c) H_{dv} (d) H_s and (e) H_1

3.1.1.3 Experimental results of magnetization reversal in elliptical nanomagnets

The simulation results were verified experimentally in the case of elliptical nanomagnets. For this, nanomagnets of thickness 10 nm and 60 nm were chosen. The X – ray diffractogram patterns of as deposited films on plain Si substrates shows the amorphous nature of the films. Fig. 3.7 (a) and (b) shows the XRD patterns of 10 nm and 60 nm thick films.

Fig. 3.8 (a) and (b) shows the magnetization reversal in these nanomagnets. The 10 nm nanomagnets shows the rectangular hysteresis loop. Abrupt reversal of magnetization happens at field H_c. In the demagnetized state the 10 nm nanomagnet shows the single domain behavior. Fig. 3.9 (a) shows the AFM and MFM images of 10 nm nanomagnets. The brown color in the MFM images confirm the formation of single domains in the demagnetized state. The images were captured by first magnetizing the nanomagnets along the major axis using an electromagnet. The magnetized samples were then used in MFM to see the domain orientation in the demagnetized state. The experimental results are comparable to the simulations (fig. 3.1). The field reversal observed experimentally is more gradual could be due to the thermal fluctuations, magnetostatic interactions between the neighboring nanomagnets and the switching field distribution.

The magnetization reversal for 60 nm nanomagnets was same as that observed in simulations (fig. 3.3(c)). Here the reversal happens through the formation of single vortex state. Fig. 3.9 (b) shows the AFM and MFM images of the 60 nm nanomagnets. In the case of simulations the double vortex state is observed at field H_{ndv} as shown in Fig. 3.3 (c). In the case of MFM the image is captured at zero field, which shows only the single domain state. This single domain

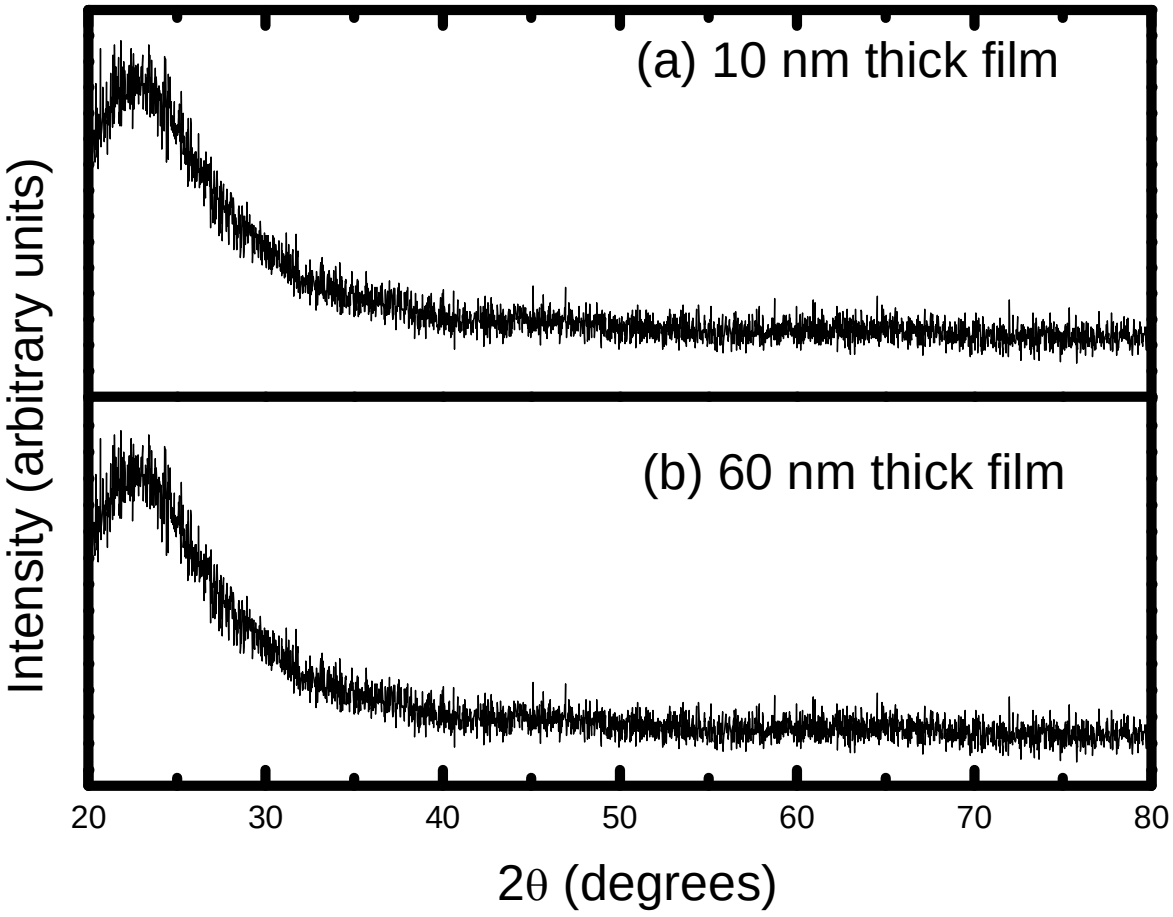

Fig. 3.7: XRD patterns of (a) 10 nm thick and (b) 60 nm thick films

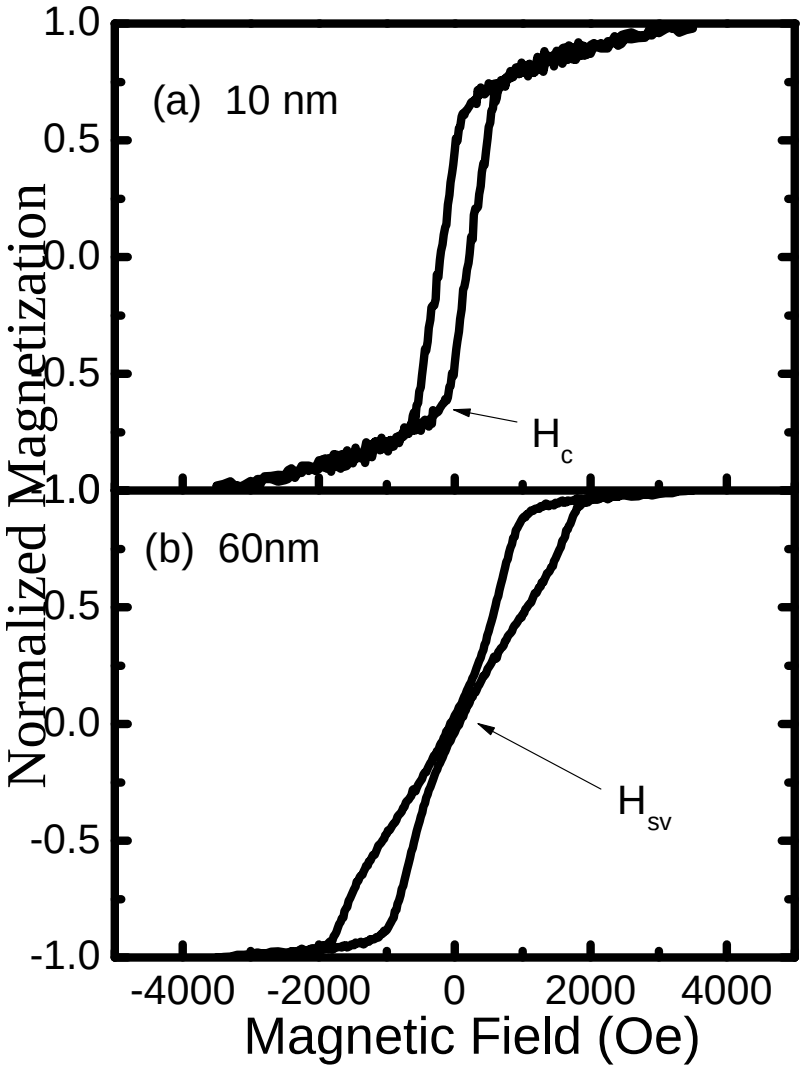

Fig. 3.8: Experimental magnetization reversal along the major axis in (a) 10 nm and (b) 60 nm thick elliptical nanomagnets

(a)

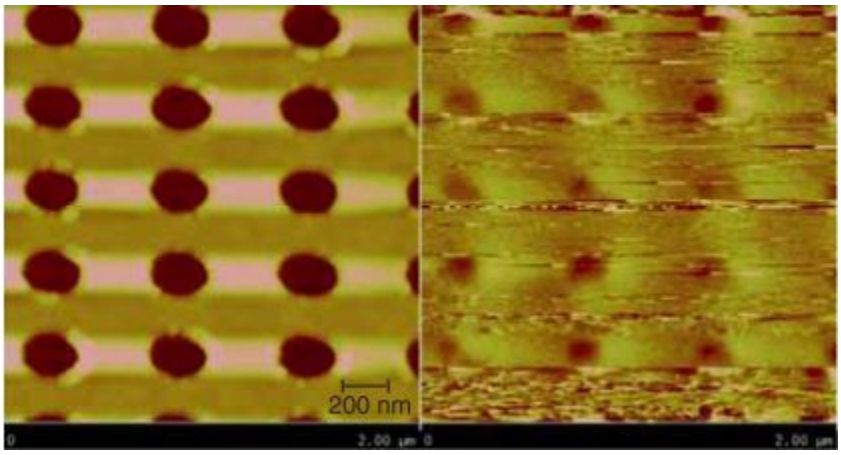

(b)

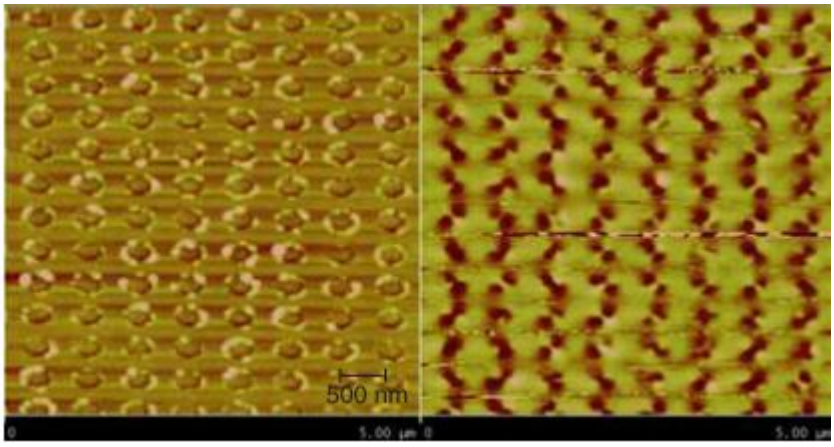

Fig. 3.9: AFM and MFM images of (a) 10 nm and (b) 60 nm thick elliptical nanomagnets

state is formed by the annihilation of two vortex states into single vortex as observed in simulations.

3.1.2 Simulation study with crystalline anisotropy constant K_1= 3.5 x 10^5 J/m^3

The as deposited films on nanostructures can be amorphous in nature. The magnetocrystalline anisotropy is zero for amorphous nanomagnets. Because of this the simulation results with K_1 = 0 J/m^3 are matching with the experimental observations as explained in the previous section. The amorphous films can be heat treated to make them crystalline. For these films the crystalline anisotropy plays a prominent role. Hence the micromagnetic simulations were carried out with the bulk anisotropy constant, K_1 = 3.5 x 10^5 J/m^3.

3.1.2.1 Applied field direction along the major axis (335 nm) of the ellipse

Fig. 3.10 shows the magnetization reversal along the major axis. In all the nanomagnets the reversal is the coherent rotation of the magnetization. An abrupt reversal happens at field H_c, the coercive field. The H_c is large for 10 nm nanomagnets. As the thickness of the nanomagnets increases the H_c decreases. 60 nm nanomagnets shows the minimum H_c. Increase in thickness of the nanomagnets increases the magnetostatic energy as a result decrease in coercivity.

3.1.2.2 Applied field direction along the minor axis (225 nm) of the ellipse

The 10 nm and 20 nm nanomagnets shows the abrupt reversal as shown in fig. 3.11 (a) and (b) respectively. Increase in thickness of the nanomagnets and the magnetization axis which is the minor axis makes the magnetostatic energy very high. Because of this high magnetostatic energy the magnetization reversal in 30 nm to 60 nm nanomagnets happens through the

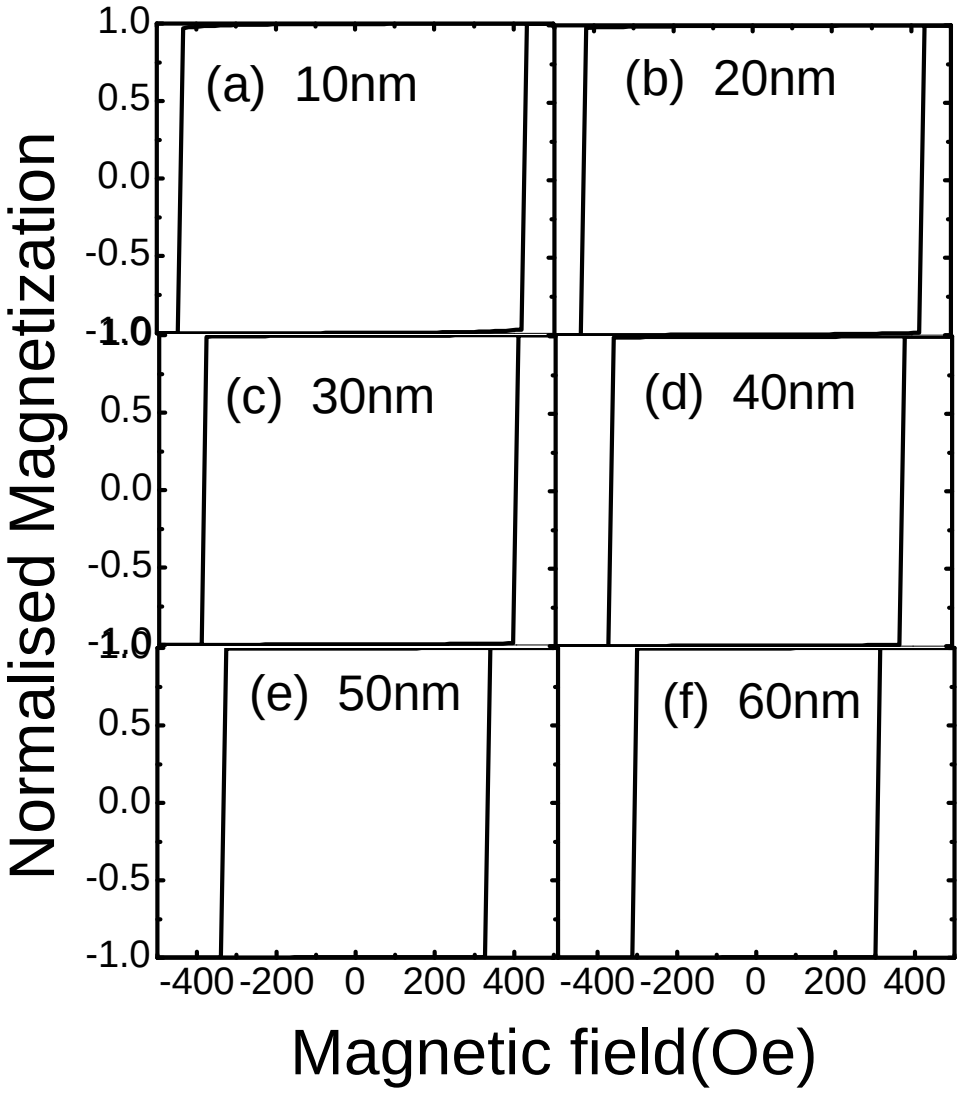

Fig. 3.10: Magnetization reversal along the major axis for (a) 10 nm, (b) 20 nm, (c) 30 nm, (d) 40 nm, (e) 50 nm and (f) 60 nm thick elliptical nanomagnets

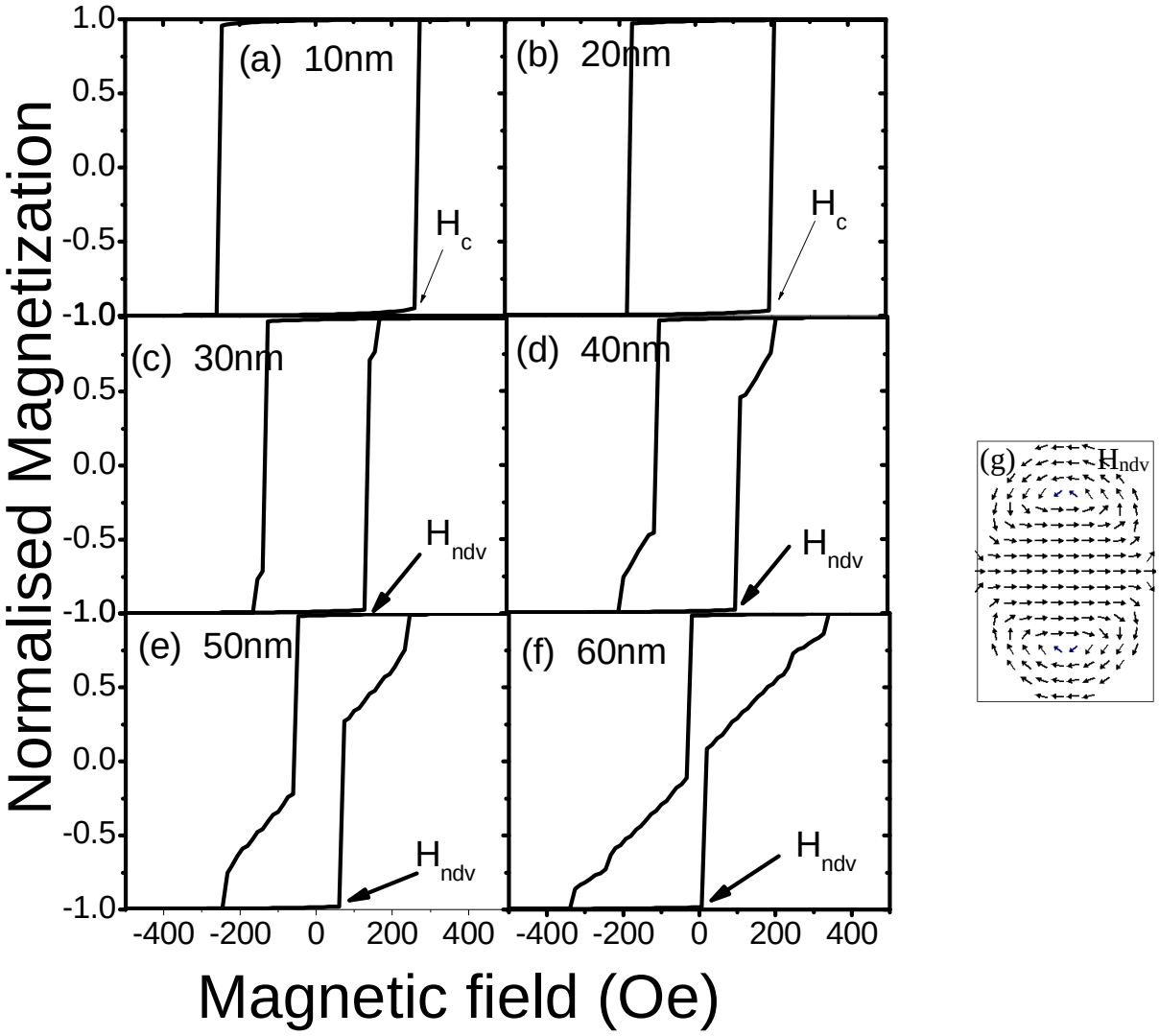

Fig. 3.11: Magnetization reversal along the minor axis for (a) 10 nm, (b) 20 nm, (c) 30 nm, (d) 40 nm, (e) 50 nm and (f) 60 nm thick elliptical nanomagnets and (g) nucleation of double vortex in 30 nm to 60 nm thick nanomagnets at field H_{ndv}

formation of intermediate double vortex state. This intermediate state decreases the coercivity with the thickness. Fig. 3.11 (c) to (f) shows the magnetization reversal along the minor axis in the thickness range 30 nm to 60 nm. The captured magnetic orientation of the nanomagnets showing the formation and annihilation of the double vortex state is shown in the fig.3.11 (g) and (h).

3.2 Circular Nanostructures

Magnetization reversal and magnetic pattern in circular nanostructures of diameter 335 nm and 225 nm with magnetocrystalline anisotropy constant $K_1 = 0$ J/m^3 and 3.5 x 10^5 J/m^{3}were studied.

3.2.1 Crystalline magnetic anisotropy constant $K_1 = 0$ J/ m^3

3.2.1.1 Circular nanostructures of diameter 335 nm

The 10 nm nanomagnets exhibit the coherent reversal of magnetization. Fig. 3.12 (a) shows the magnetization reversal in 10 nm nanomagnet. Initially the magnetic moment is along the negative field direction. As the field decreases the magnetization continues to be in the same direction which can be explained using Stoner – Wolfforth model [72,81]. At field Hc = 7 Oe the magnetization changes the direction towards positive field. Figs. 3.12 (b) and (c) show the magnetic orientation in the nanomagnet along the negative and positive field directions.

Unlike in 10 nm nanomagnet, the 20 nm nanomagnet shows the magnetization reversal through the formation of single vortex state [82]. As the thickness increases the magnetostatic energy dominates the exchange energy. This results in the formation of single vortex state. Fig. 3.12

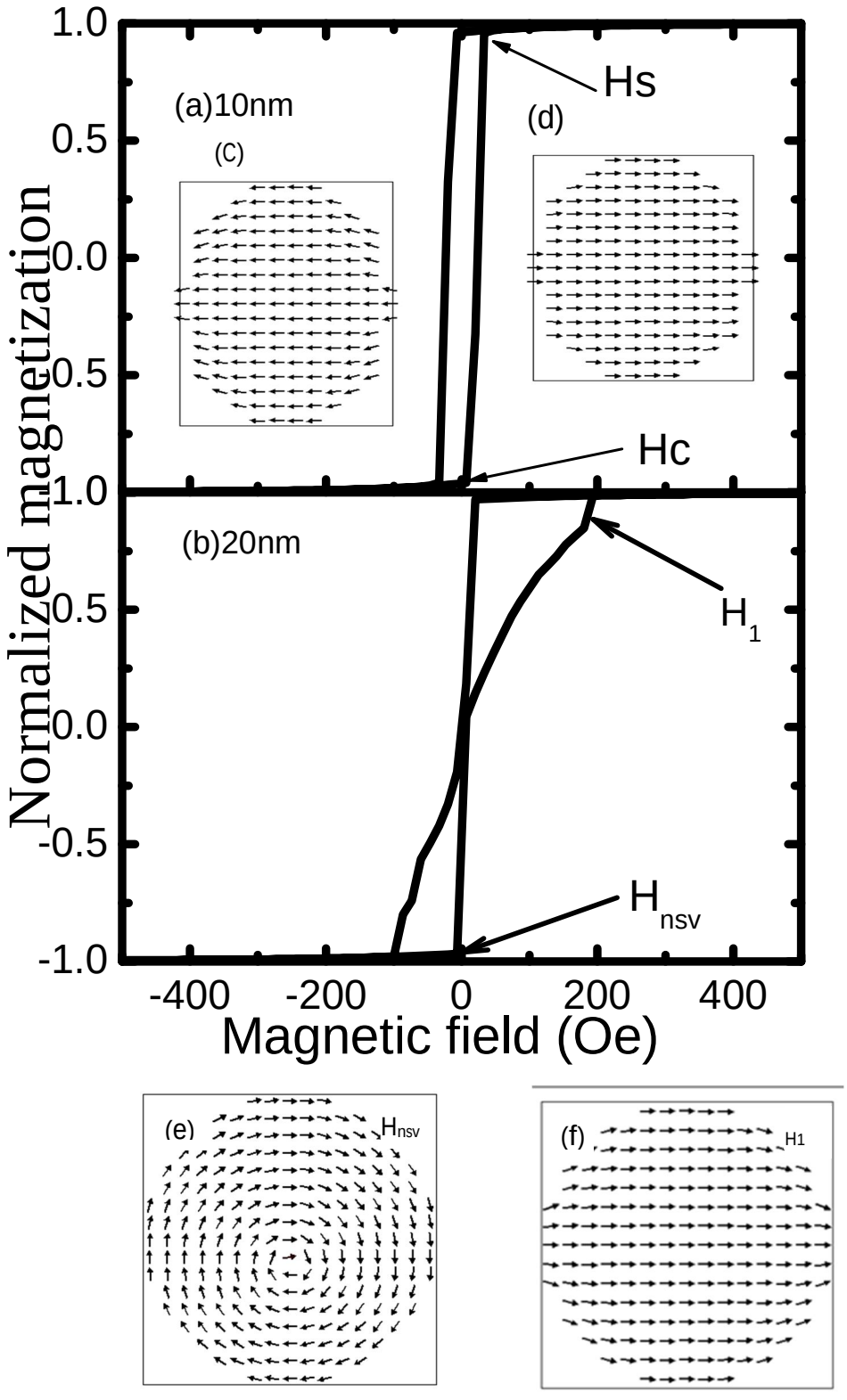

Fig. 3.12: Magnetization reversal in circular nanomagnets of diameter 335 nm and of thickness (a) 10 nm and (b) 20 nm and magnetic orientation at saturating field along (c) –ve field and (d) +ve field directions (e) Hnsv, ,and (f) H1

(d) shows the magnetization reversal and fig. 3.12 (e) and (f) shows the nucleation of single vortex state at H_{nsv} and the movement of vortex towards the edges at higher field H_1. After field H_1 the annihilation of vortex occurs and the magnetization saturates along the positive field direction.

Figs. 3.13 (a) – (d) show the magnetization reversal in 30 nm – 60 nm nanomagnets respectively. Like in the elliptical nanomagnets (fig. 3.3), the reversal occurs through the formation of double and single vortex states. The nucleation of double vortex occurs at field H_{ndv}, as the field increases the double vortex converts into single vortex at field H_{sv} and the movement of single vortex towards the edges and then annihilation takes place as the field increases. Figs. 3.13 (e) and (f) show the nucleation of vortex at field H_{nsv} and the movement of vortex towards the edges at field H_1. The double-vortex state is less energetically favorable than a single-vortex state due to higher exchange energy [83,84]. For dimensions well above the exchange length (L_{ex}) the exchange energy will be minimum and there is reduction in magnetostatic energy by having a nonuniform magnetization reversal process in nanostructures. The decrease in exchange leads to the formation of double vortex state [85-88].

3.2.1.2 Circular nanostructures of diameter 225 nm

There is no difference in the magnetization reversal when the diameter is decreased to 225 nm. Coherent rotation of magnetization is observed in 10 nm and 20 nm nanomagnets and the other nanomagnets of thickness 30 nm - 60 nm showed the reversal through the formation of double and single vortex states. Figs. 3.14 shows the reversal in 10 nm and 20 nm nanomagnets and

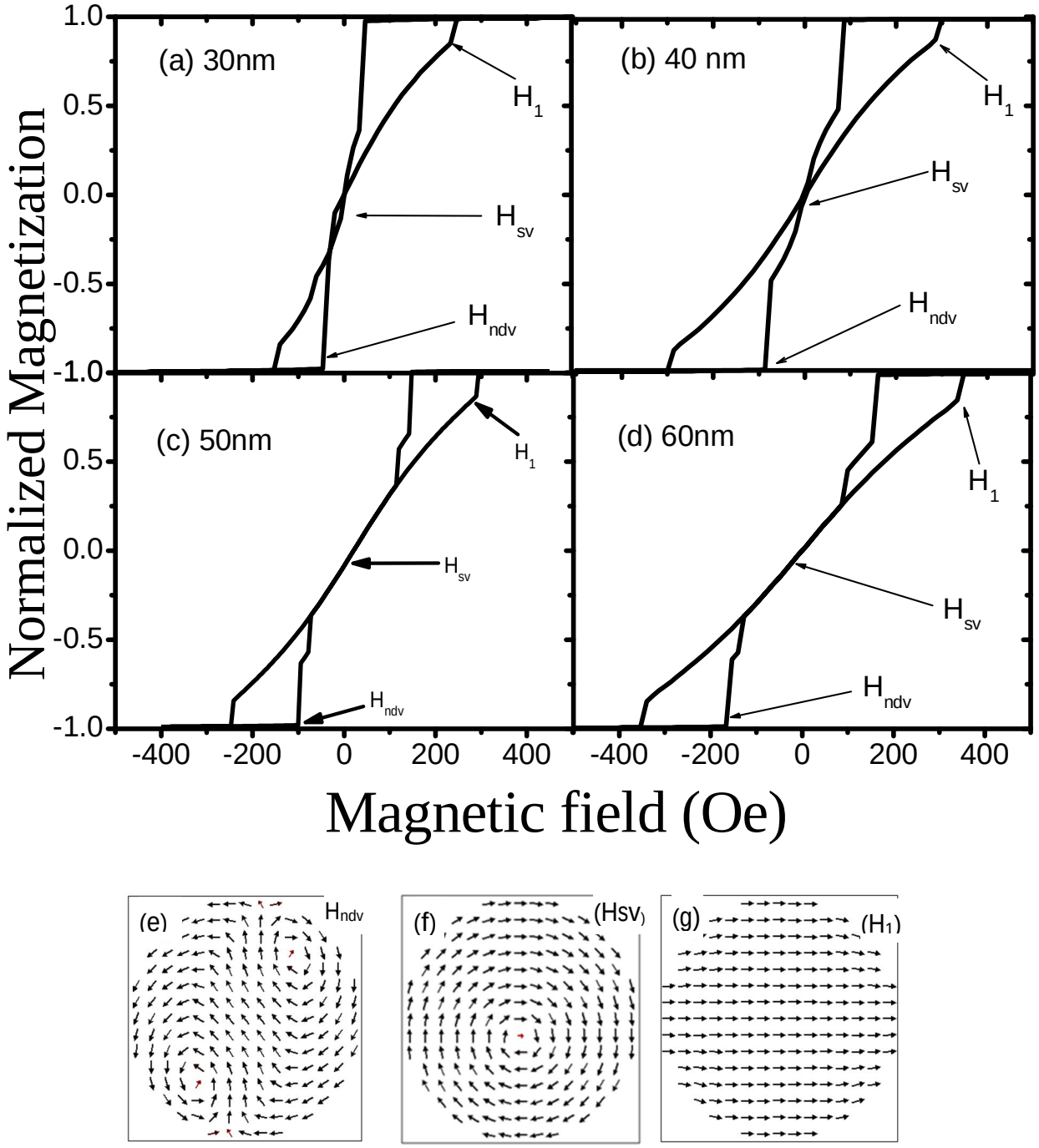

Fig. 3.13 : Magnetization reversal in circular nanomagnets of diameter 335 nm and of thickness (a) 30 nm (b) 40 nm (c) 50nm (d) 60 nm and magnetic orientation at (e) nucleation field H_{ndv}, (f) field at H_{sv}, (g) and H_1 field

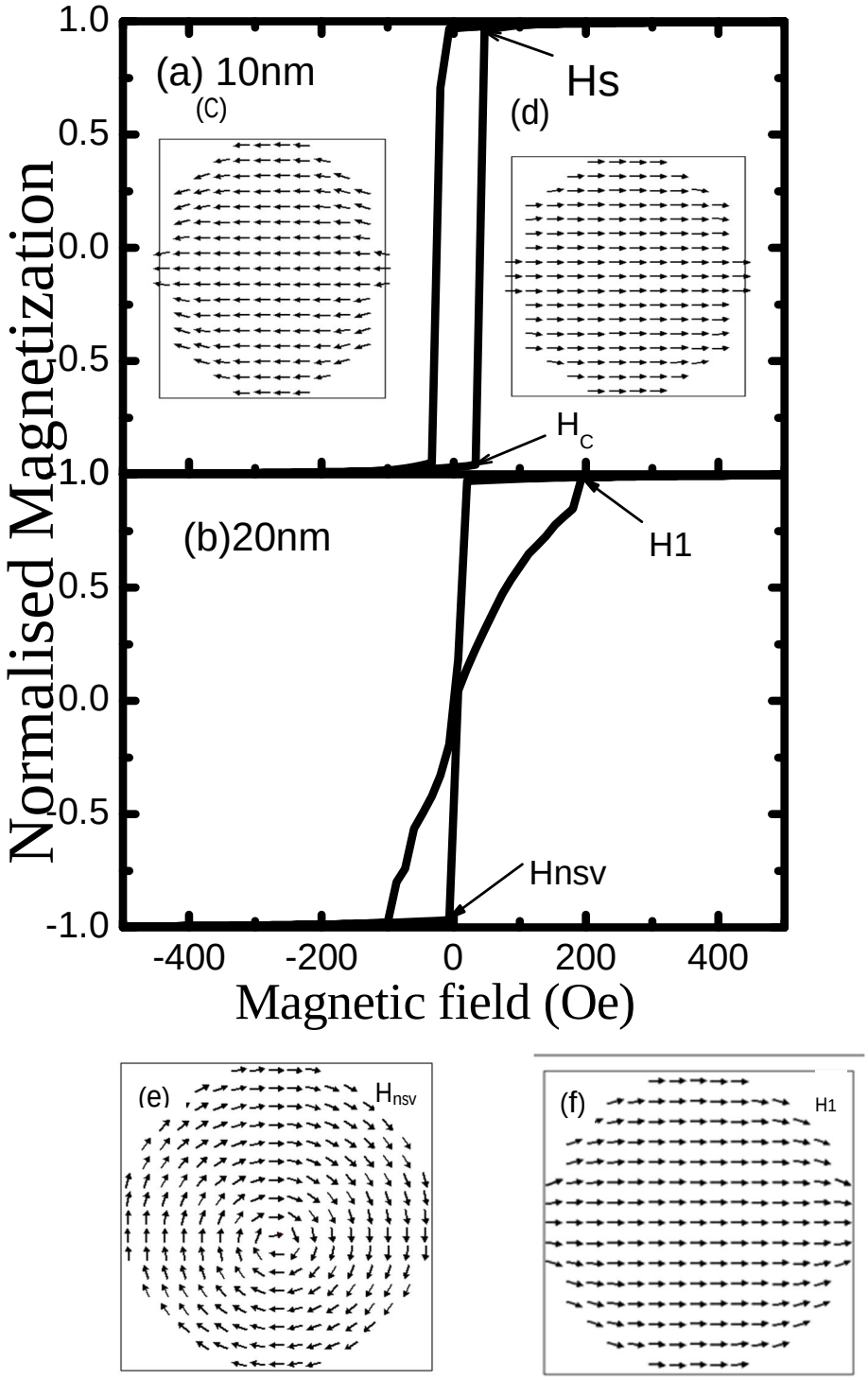

Fig. 3.14: Magnetization reversal in circular nanomagnets of diameter 225 nm and of thickness (a) 10 nm and (b) 20 nm and magnetic orientation at saturating field along (c) –ve field and (d) +ve field directions (e) H_{nsv} and (f) H_1

figs. 3.15 shows the reversal and the intermediate states during reversal in 30 nm – 60 nm nanomagnets.

3.2.2 Crystalline magnetic anisotropy constant $K_1 = 3.5 \times 10^5$ J/ m^3

The magnetization reversal in 335 nm and 225 nm diameter circular nanomagnets shows the rectangular hysteresis loop. Abrupt reversal of magnetization occurs at field H_c because of high magnetocrystalline anisotropy in these nanomagnets. Figs. 3.16 and 3.17 shows the reversal in 335 nm and 225 nm respectively. The magnetization reversal in 335 nm and 225 nm diameter circular nanomagnets shows the rectangular hysteresis loop. Abrupt reversal of magnetization occurs at field H_c because of high magnetocrystalline anisotropy in these nanomagnets.

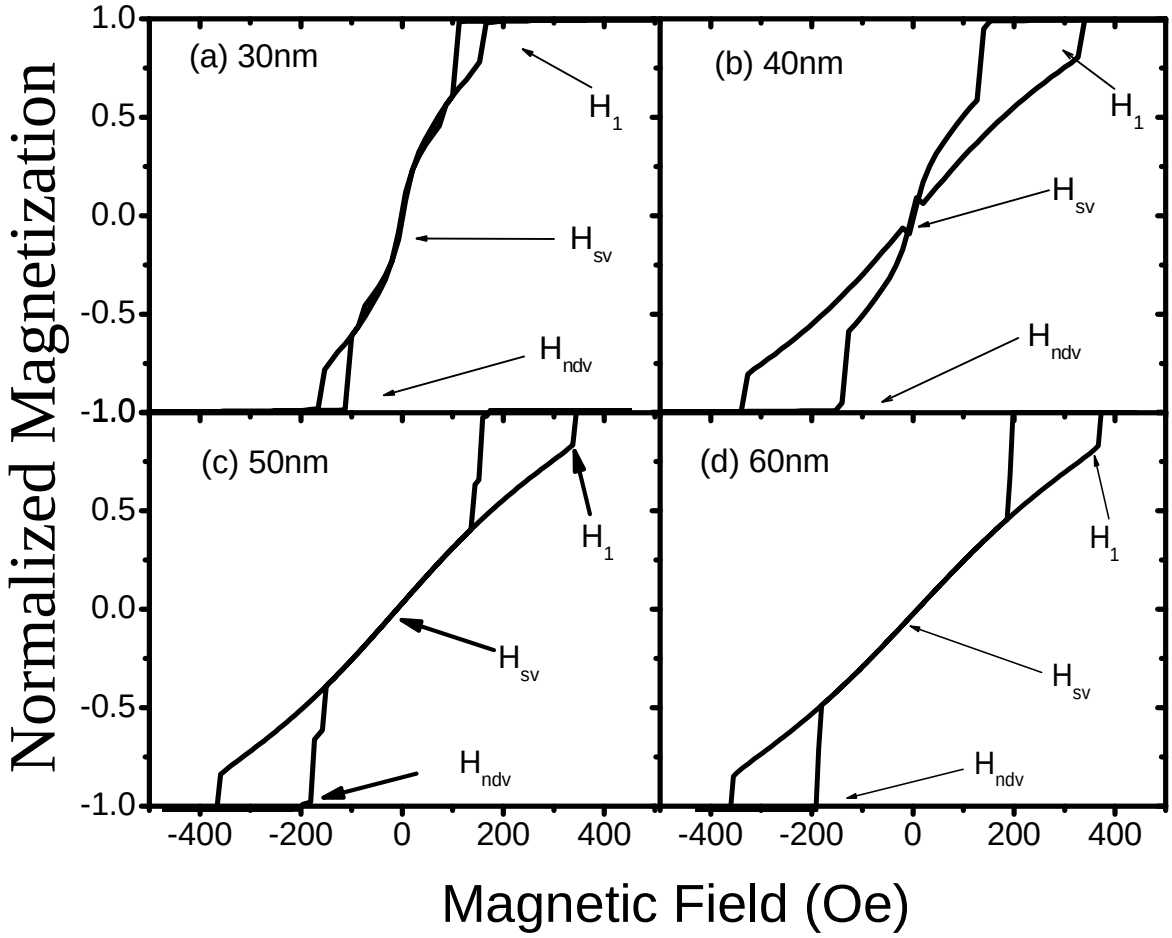

Fig. 3.15 : Magnetization reversal in circular nanomagnets of diameter 225 nm and of thickness (a) 30 nm (b) 40 nm (c) 50nm (d) 60 nm and magnetic orientation at (e) nucleation field H_{ndv}, (f) field at H_{sv}, (g) and H_1 field

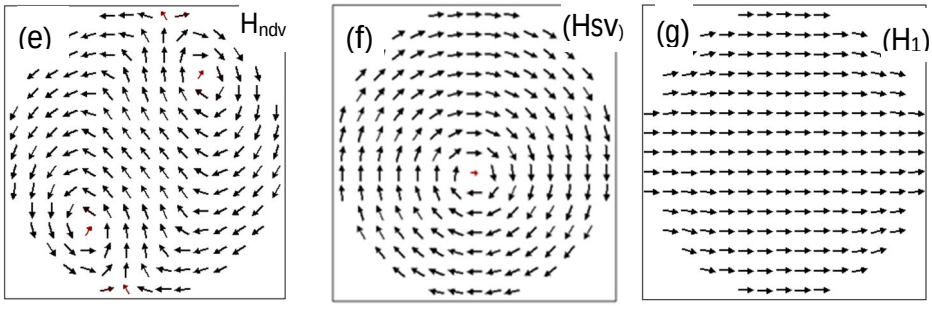

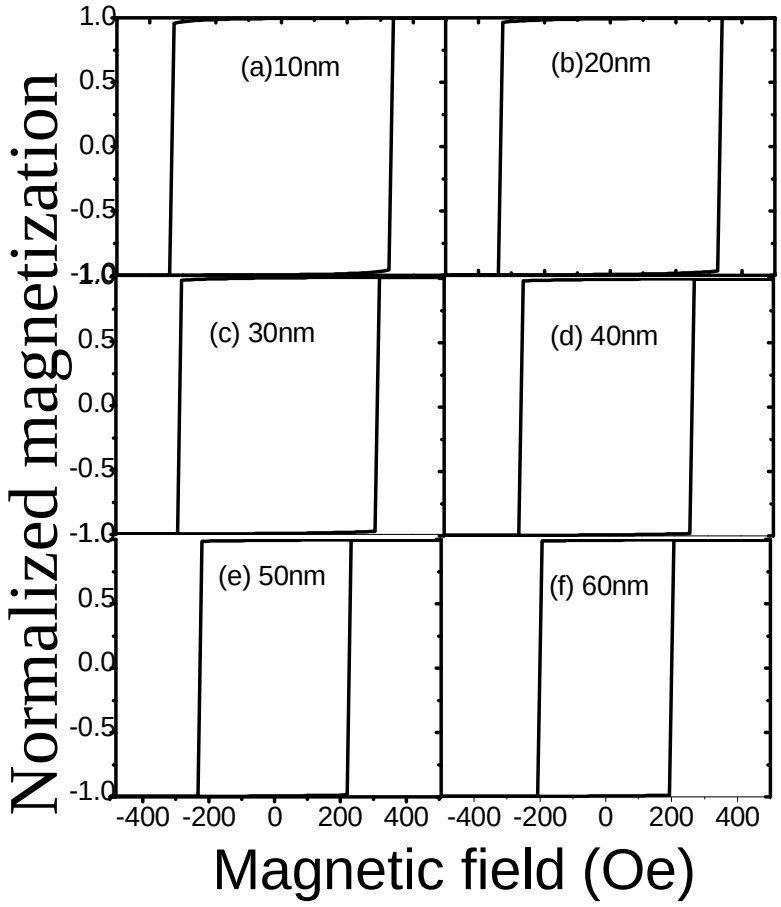

Fig. 3.16: Magnetization reversal for the circular nanomagnets of diameter 335 nm and of thickness (a) 10 nm, (b) 20 nm, (c) 30 nm, (d) 40 nm, (e) 50 nm and (f) 60 nm

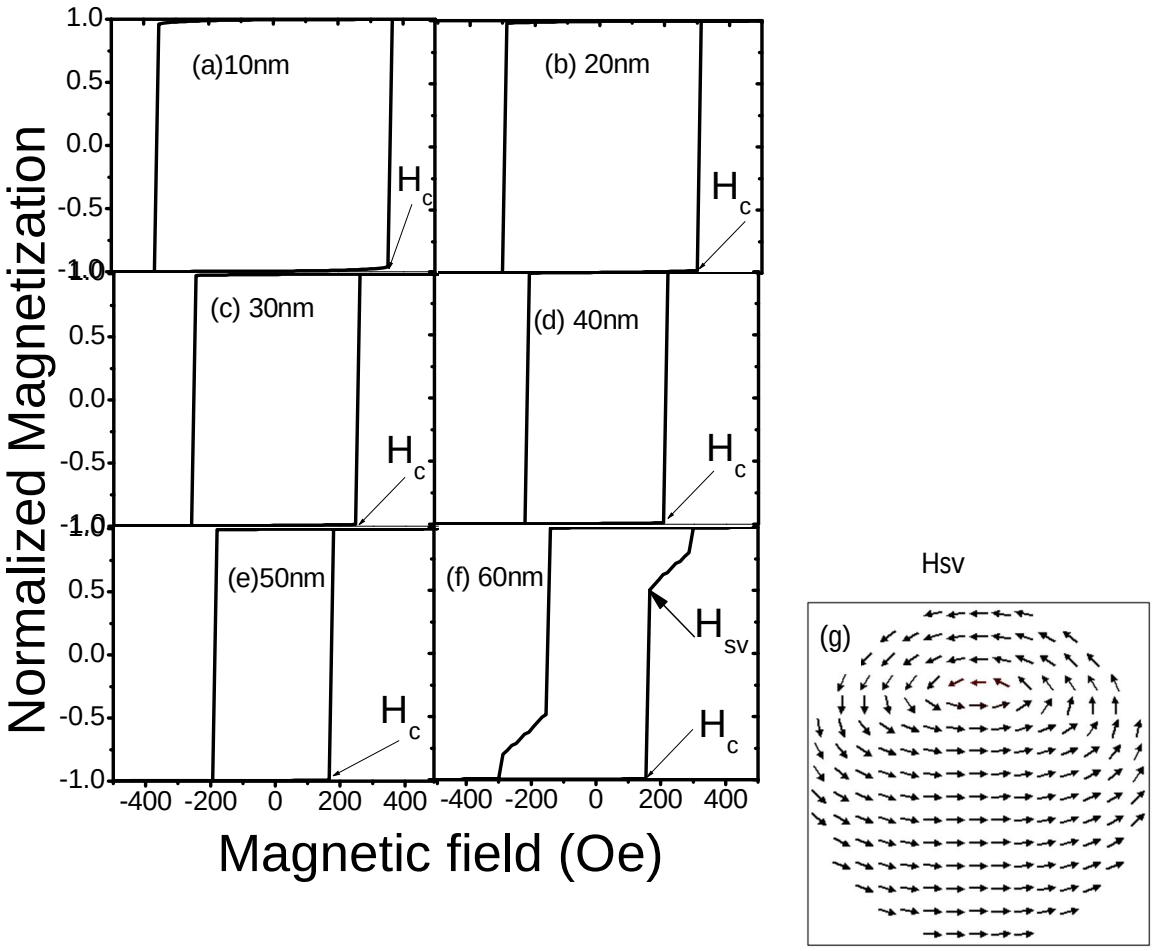

Fig. 3.17: Magnetization reversal in circular nanomagnets of diameter 225 nm and of thickness (a) 10 nm, (b) 20 nm, (c) 30 nm, (d) 40 nm, (e) 50 nm and (f) 60 nm nanomagnets (g) nucleation of single vortex in 60nm nanomagnets at field H_{sv}

Chapter IV

Magnetization reversal study in rectangular and square nanomagnets

This chapter presents the micromagnetic simulation study of magnetization reversal in rectangular and square nanomagnets. The rectangular nanomagnets length is 335 nm and width is 225 nm and the square nanomagnets are 225 nm and 335 nm in dimension.

4.1 Rectangular Nanostructures

Like in the elliptical and circular nanostructures here also the simulations were done for CoFe nanostrucutres by taking the magnetocrystalline anisotropy K_1 = 0 J/m^3 and for the bulk anisotropy constant, $K_1 = 3.5 \times 10^5$ J/m^3.

4.1.1 Simulation study with crystalline anisotropy constant K_1= 0 J/m^3

4.1.1.1 Applied field direction along the length (335 nm) of the rectangle

The thickness of the nanomagnets varied from 10 nm to 60 nm and the applied field from -500 Oe to +500 Oe. Fig. 4.1 (a) and (b) shows the magnetization reversal in rectangular nanomagnets of thickness 10 nm and 20 nm respectively. The magnetization reversal happens in the same fashion in both the nanomagnets. A field of -500 Oe makes the nanomagnet to saturate along the field direction. The orientation of magnetic moment at H_s is shown in figs. 4.1 (c) and (d) for fields along the negative and positive directions respectively. When the field is reduced to zero the system does not become demagnetized. The magnetization still lies along the field

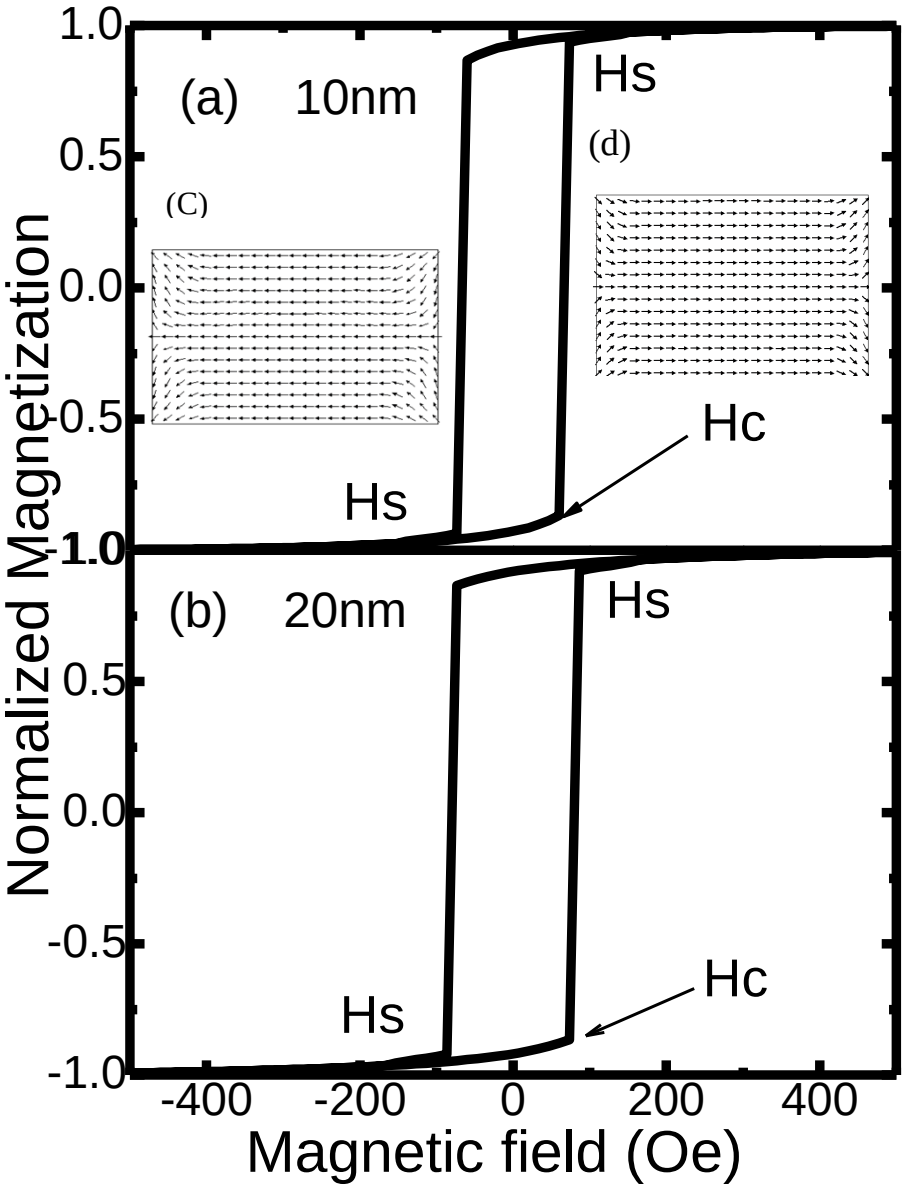

Fig. 4.1: Magnetization reversal along the length of rectangular nanomagnets of thickness (a) 10 nm and (b) 20 nm and magnetic orientations at saturating field along (c) –ve field and (d) +ve field directions

direction. This gives remanent magnetization to the nanomagnet. When the field is increased in the positive direction the magnetization would prefer to reverse parallel to the field direction at H_c = 73 Oe. Thus there is an abrupt reversal at this field. This type of reversal gives rectangle or square hysteresis loop which is the main criteria for magnetic data storage. This type of reversal behavior can be explained using Stoner – Wohlfarth model [72].

In the case of 30 nm – 60 nm nanostructures the magnetization reversal happens through the formation of intermediate double vortex state. Fig. 4.2 (a) - (d) shows the magnetization reversal in 30 nm - 60 nm nanomagnets respectively. The formation and annihilation of double vortex states in 30 nm - 60 nm nanostructures are shown in fig. 4.2 (e) – (g). At saturating field all the magnetic moments in the nanomagnets are along the field direction. When the field is decreased towards zero the magnetic moment lies along the field direction because of the high energy. With increasing field along the positive direction nucleation of double vortex occurs at H_{ndv} = 46 Oe. With further increasing the field complete formation of double vortex takes place. This can be seen at field H_1 as shown in fig. 4.2 (f). Here the field is zero and the magnetic orientations are in the demagnetized state so that the total magnetic moment is zero. At H_a complete annihilation of the double vortex happens.

4.1.1.2 Applied field along the width (225 nm) of the rectangle

If a rectangular thin film element is magnetized along the short edge, surface charges and stray field energy are reduced by the formation of end domains that lead to C- states [89, 90]. Fig. 4.3 (a) shows the magnetization reversal along the minor axis of the 10 nm thick elliptical

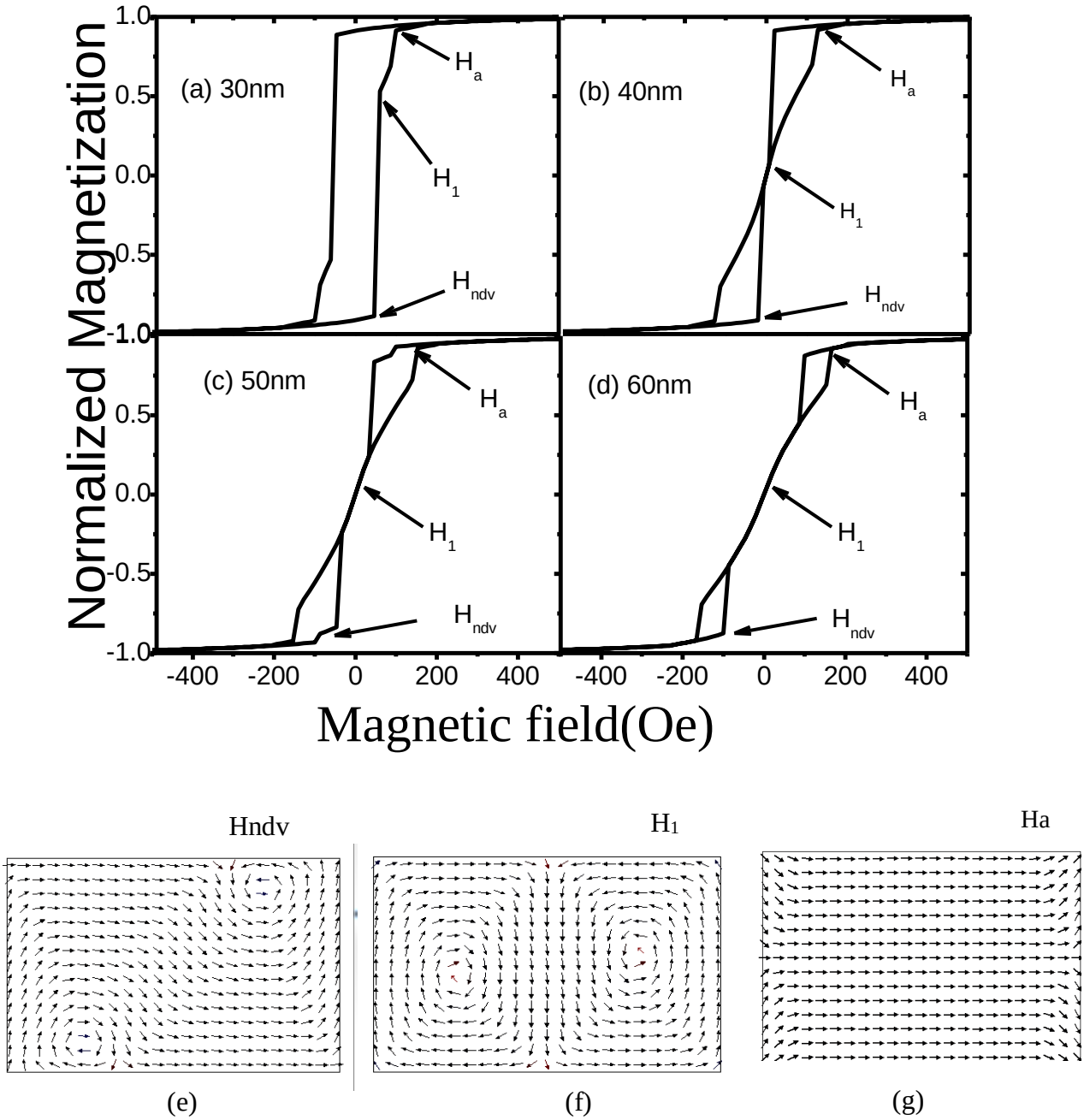

Fig. 4.2: Magnetization reversal along length of rectangular nanomagnets of thickness (a) 30 nm (b) 40 nm (c) 50nm (d) 60 nm and magnetic orientations at (e) nucleation field H_{ndv}, (f) field H_1, (g) and annihilation field H_a

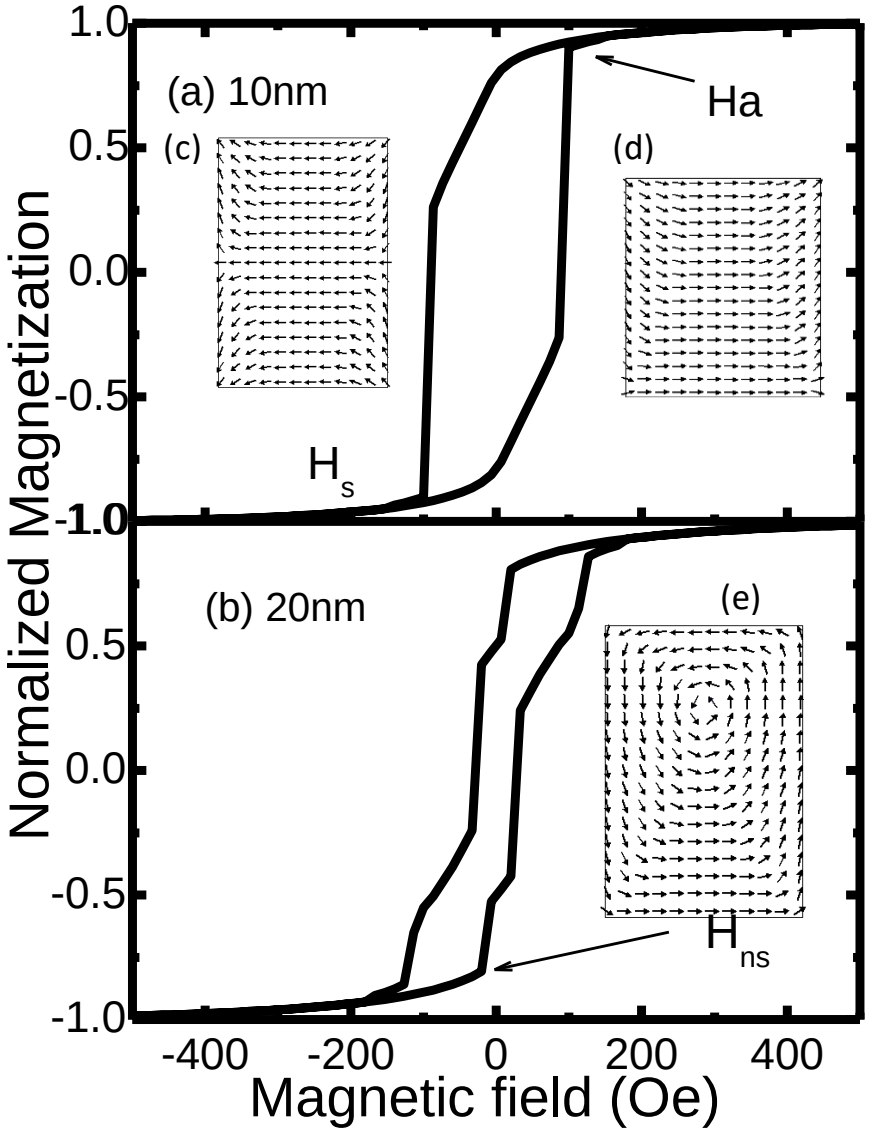

Fig. 4.3: Magnetization reversal along the width of rectangular nanomagnets of thickness (a) 10 nm and (b) 20 nm and magnetic orientation at fields (c) H_s, (d) H_a, (e) H_{ns}, (f) H_a

nanomagnet. Initially the magnetization is aligned along the negative field direction. The strength of the demagnetizing fields is larger along the width than the length. When we decrease the field towards zero the magnetization reversal happens through the formation of c – type state as shown in Fig. 4.3 (b). Increasing the field towards positive direction makes the annihilation of the c-type state. Fig. 4.3 (c) shows the orientation of magnetic moments along the positive direction of the field.

The reversal in 20 nm nanomagnets happens through the formation of vortex state. Fig. 4.3 (d) shows the magnetization reversal in the above said nanomagnet. In this nanostructure the reversal happens through the formation of single vortex state. Figs. 4.3 (e) show the formation of single vortex state.

Fig. 4.4 (a) - (c) shows the magnetization reversal in 30 nm - 50 nm nanomagnets. In these nanomagnets the reversal happens through the formation of multivortex states. The nucleation of multivortex occurs at field H_{nmv}. Fig. 4.4 (d) shows the multivortex state. With further decreasing the field towards zero and increasing in the positive direction the movement of multivortex towards the edges of the nanostructure takes place. Fig. 4.4 (e) shows the multivortex at the edges of the nanostructure and at field H_1. Finally at higher fields, H_a the multivortex state annihilates.

The magnetization reversal in 60 nm nanomagnets happens through the formation of multi and single vortex states. Fig. 4.5 shows the magnetization reversal and the orientations. At H_{ndv} the nucleation of multivortex occurs and complete formation of multivortex takes place at field H_{mv}.

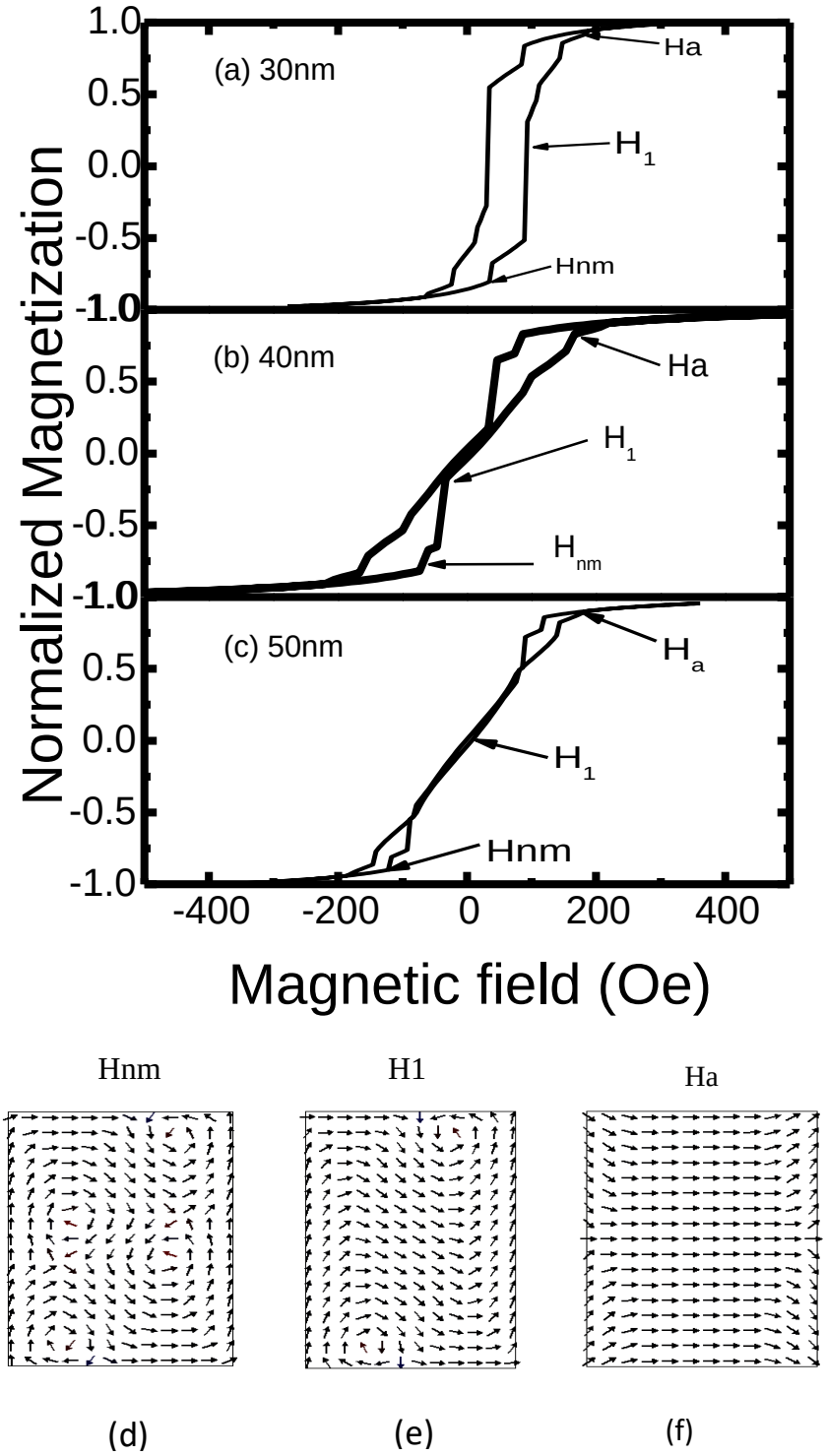

Fig. 4.4: Magnetization reversal along the width of rectangular nanomagnets of thickenss (a) 30 nm (b) 40 nm and (c) 50 nm and magnetic orientation at fields (d) H_{nm}, (e) H_1, (f) H_a

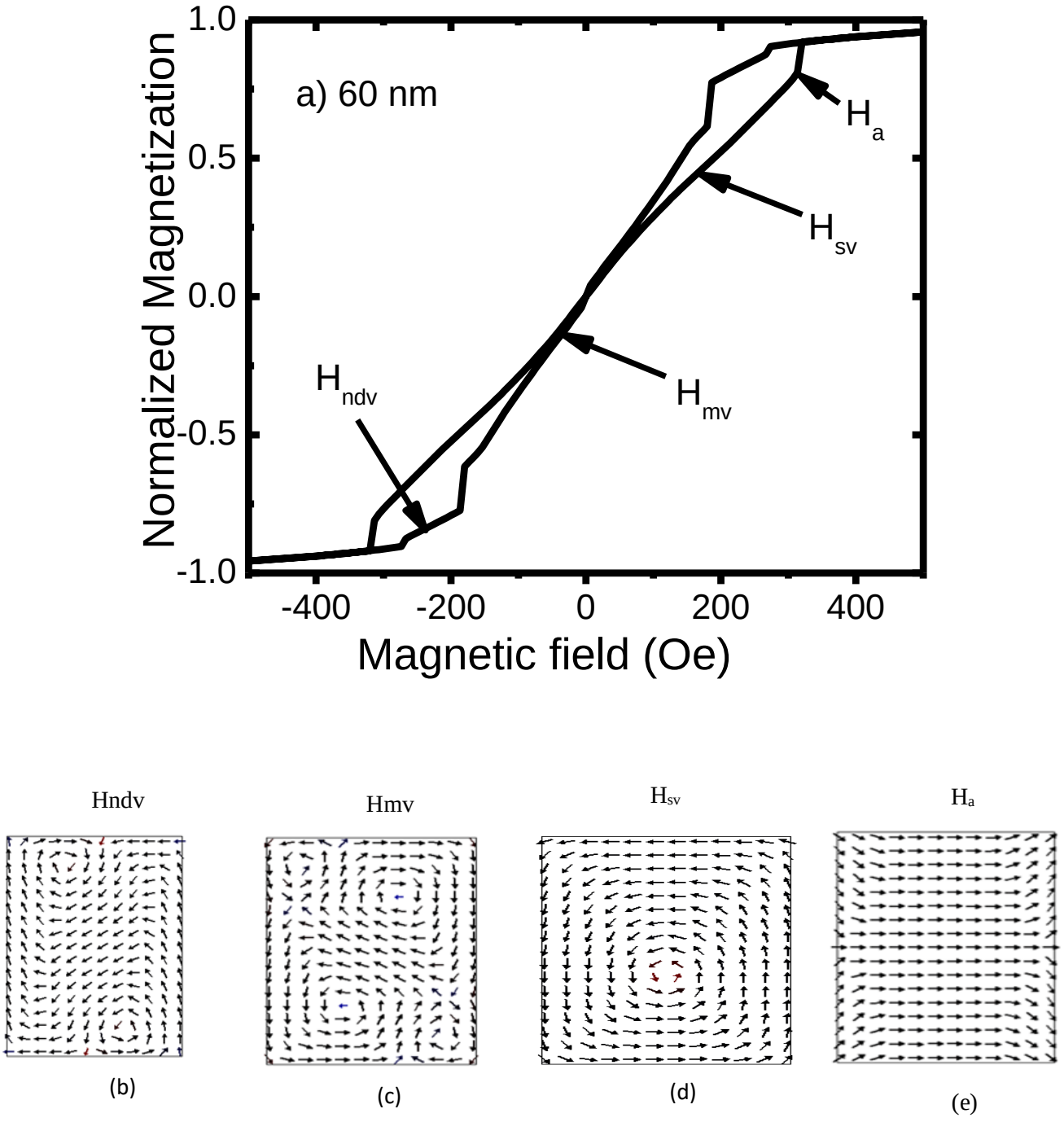

Fig. 4.5: Magnetization reversal along the width of rectangular nanomagnet of thickness (a) 60 nm and magnetic orientations at fields (b) H_{ndv} (c) H_{mv} (d) H_{sv} and (e) H_a

At higher fields the multivortex states merge into single vortex. Further increasing the field causes the annihilation of the vortex states.

If a rectangular thin film is magnetized stray field energies are reduced by the formation of end domains that lead to C-states [36 - 38, 90]. Still these structures have stray field energy that can be decreased by flux closure arrangements even though at the expense of exchange energy due to domain walls. The thickness dependence of the stray field energy eventually leads to a transition from single domain state to multi-domain states [91 - 93].

4.1.2 Simulation study with crystalline anisotropy constant $K_1 = 3.5 \times 10^5$ J/m^3

Like in elliptical and circular nanostructures the micromagnetic simulations were carried out with the bulk anisotropy constant, $K_1 = 3.5 \times 10^5$ J/m^3.

4.1.2.1 Applied field direction along the length (335 nm) of the rectangle

Fig. 4.6 shows the magnetization reversal along the length. In all the nanomagnets the reversal is the coherent rotation of the magnetization. An abrupt reversal happens at field H_c, the coercive field. The H_c is large for 10 nm nanomagnets. As the thickness of the nanomagnets increases the H_c decreases. 60 nm nanomagnets shows the minimum H_c. Increase in thickness of the nanomagnets increases the magnetostatic energy as a result decrease in coercivity.

4.1.2.2 Applied field direction along the width (225 nm) of the rectangle:

The 10 nm - 40 nm nanomagnets shows the abrupt reversal as shown in fig. 4.7 (a) – (d). Increase in thickness of the nanomagnets and the magnetization direction which is along the width makes the magnetostatic energy very high. Because of this high magnetostatic energy the

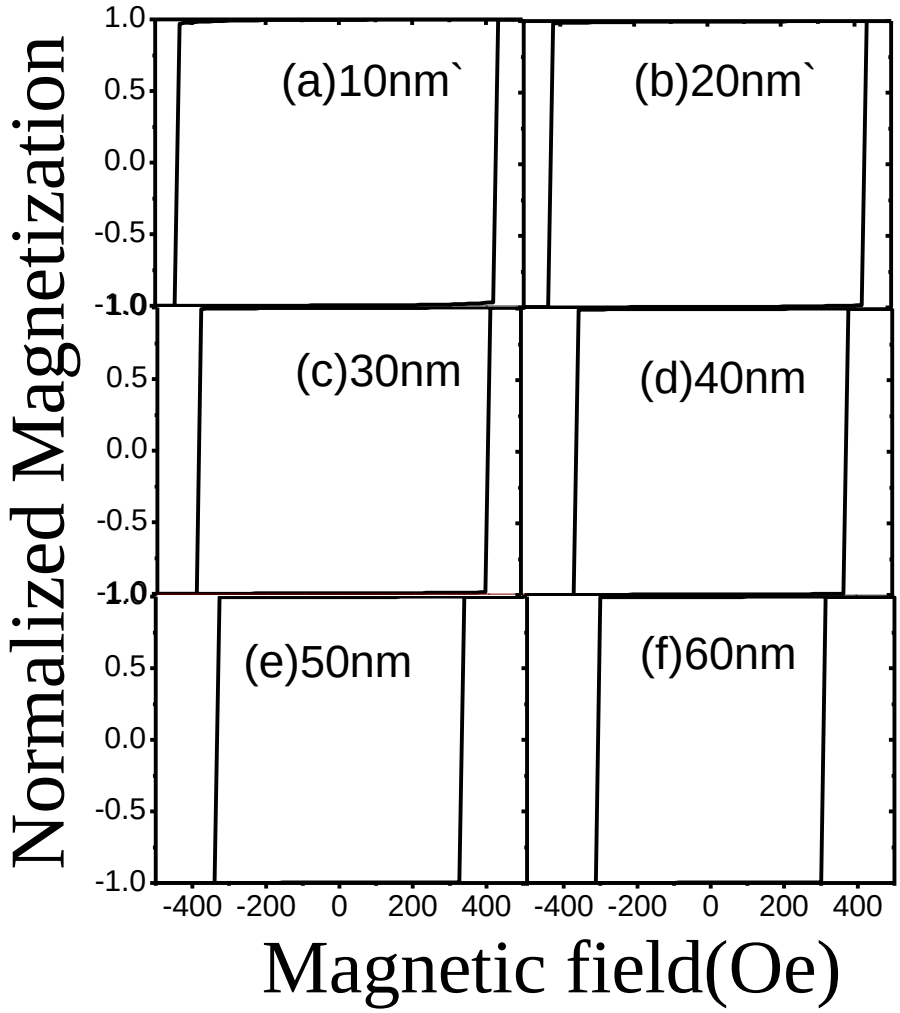

Fig. 4.6: Magnetization reversal along the length of rectangular nanomagnets of thickness (a) 10 nm, (b) 20 nm, (c) 30 nm, (d) 40 nm, (e) 50 nm and (f) 60 nm

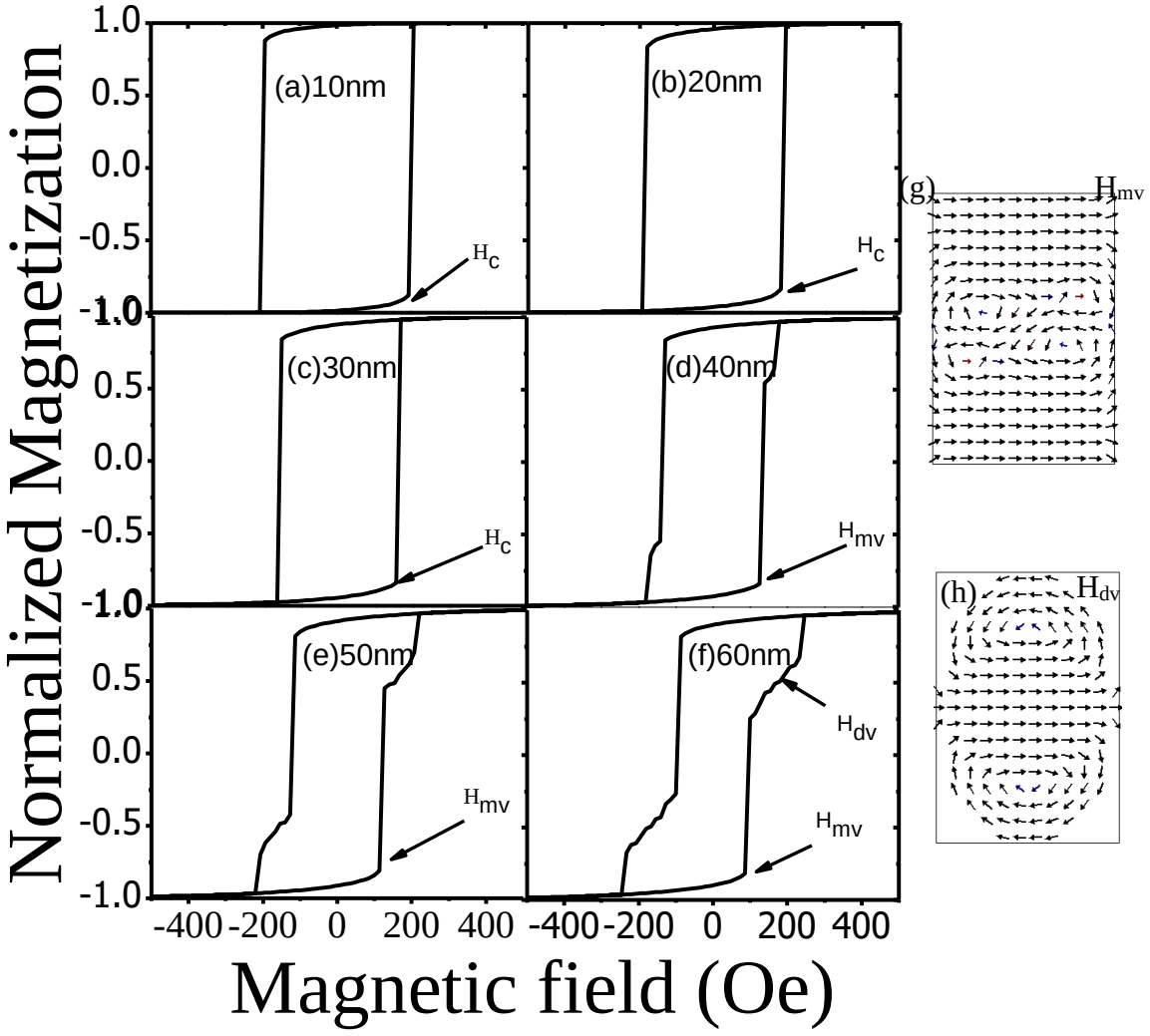

Fig. 4.7: Magnetization reversal along the width of rectangular nanomagnets of thickness (a) 10 nm, (b) 20 nm, (c) 30 nm, (d) 40 nm, (e) 50 nm, (f) 60 nm, (g) nucleation of multivortex vortex in 40 nm - 60 nm nanomagnets at field H_{mdv} and (h) H_{dv}

magnetization reversal in 50 nm and 60 nm nanomagnets happens through the formation of intermediate multivortex states and double vortex state. This intermediate state decreases the coercivity. Fig. 4.7 (e) – (h) shows the magnetization reversal and the magnetic orientation in nanomagnets.

4.2 Square Nanostructures

4.2.1 Crystalline magnetic anisotropy constant $K_1 = 0$ J/ m^3

4.2.1.1 Square nanostructures of edge 335 nm

The 10 nm and 20 nm nanomagnets exhibit the coherent reversal of magnetization. Fig. 4.8 (a) and (b) shows the magnetization reversal in 10 nm and 20 nm nanomagnets. At field H_c = 33 Oe the magnetization changes the direction towards positive field.

In 30 nm nanomagnet the magnetization reversal happens through the formation of double vortex state. As the thickness increases the magnetostatic energy dominates the exchange energy. This results in the formation of double vortex state. Fig. 4.9 (a) shows the magnetization reversal and fig. 4.9 (b) - (d) shows the nucleation of double vortex state at H_{ndv} and the movement of vortex towards the edges at higher field H_1. After field H_1 the annihilation of vortex occurs and the magnetization saturates along the positive field direction at Ha.

Fig. 4.10 (a) – (c) show the magnetization reversal in 40 nm – 60 nm nanomagnets respectively. Like in the rectangular nanomagnets (fig. 3.3), the reversal occurs through the formation and annihilation of multivortex states. Figs. 4.10 (d), (e) and (f) show the nucleation of vortex at field H_{nmv} and the movement of vortex towards the edges at field H_{dv}.

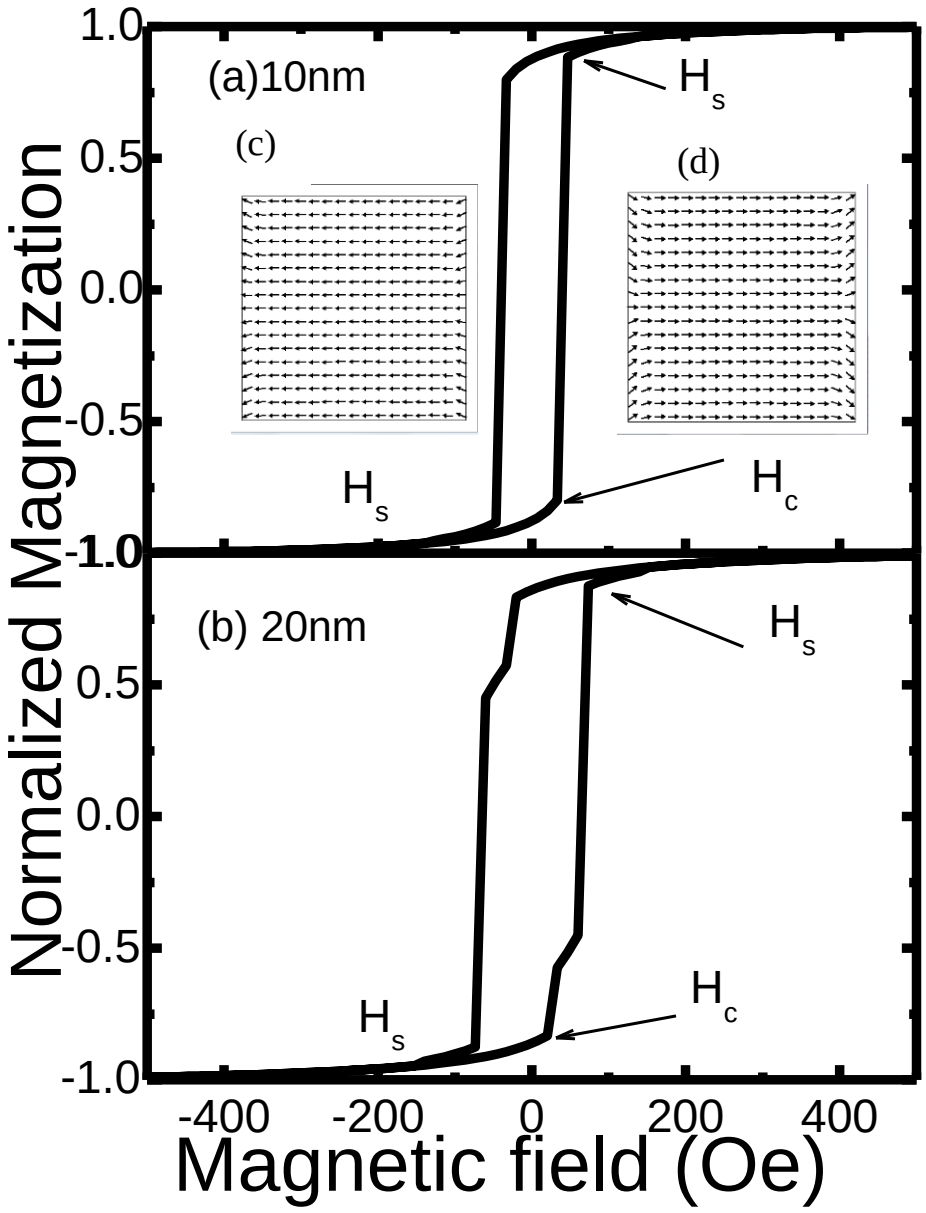

Fig. 4.8: Magnetization reversal in square nanostructures of size 335 nm and of thickness (a) 10 nm and (b) 20 nm and magnetic orientations at saturating field along (c) –ve field and (d) +ve field directions

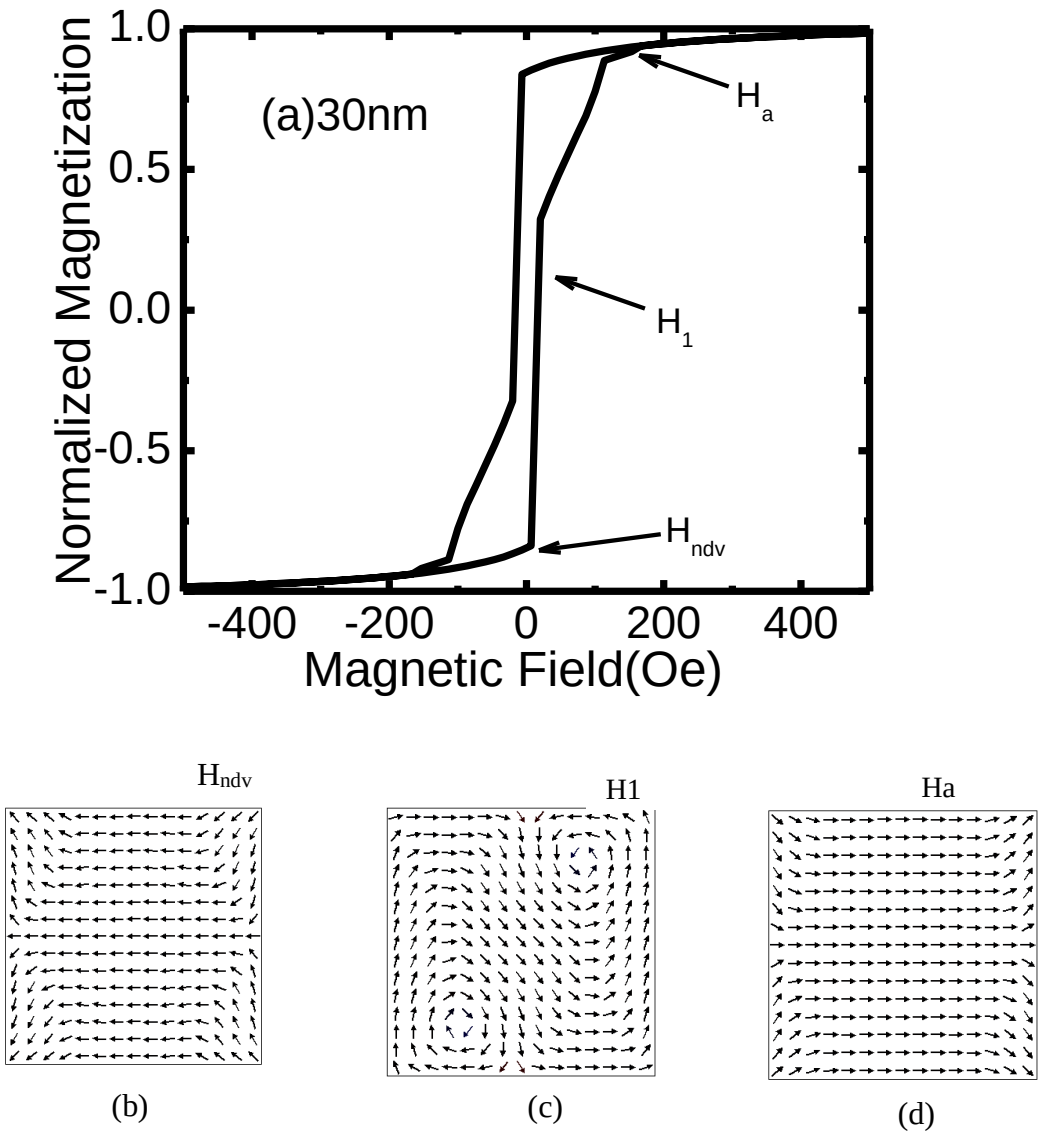

Fig. 4.9: (a) Magnetization reversal in square nanostructure of size 335 nm and of thickness 30 nm and magnetic orientation at (b) nucleation field H_{ndv}, (c) field H_1, and (d) annihilation field H_a

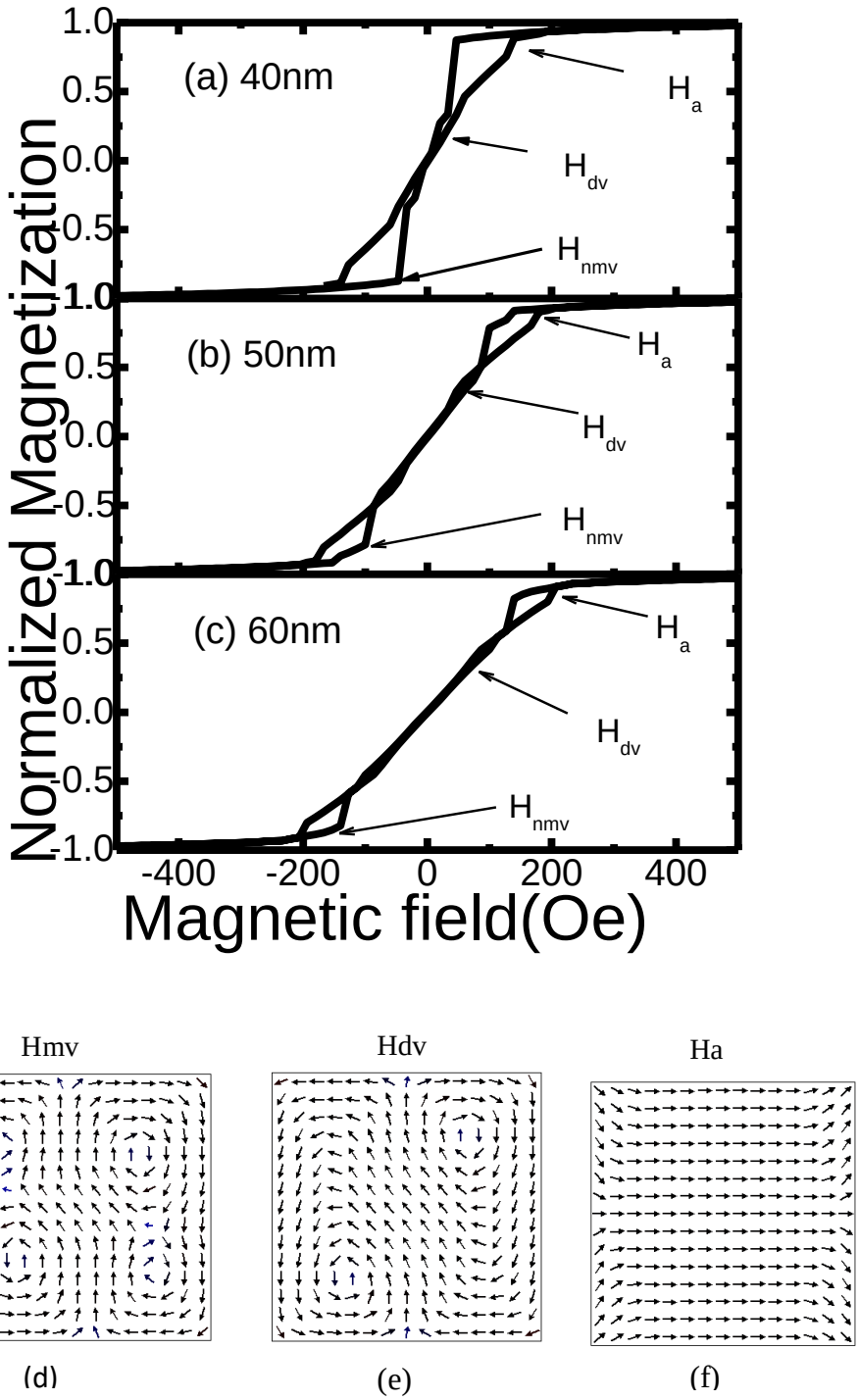

Fig. 4.10 : Magnetization reversal in square nanostructures of size 335 nm and of thickness (a) 40 nm (b) 50 nm and (c) 60 nm and magnetic orientation at (d) nucleation of multi vortex H_{mv}, (e) double vortex H_{dv}, (f) at field H_a

4.2.1.2 Square nanostructures of edge 225 nm

There is no difference in the magnetization reversal when the edge length is decreased to 225 nm. Coherent rotation of magnetization is observed in 10 nm - 50 nm nanomagnets. The 60 nm nanomagnet showed the reversal through the formation of multivortexes state. Figs. 4.11 - 4.13 shows the reversal in square nanomagnets of edge 225 nm.

4.2.2 Simulation study with crystalline anisotropy constant $K_1 = 3.5 \times 10^5$ J/m^3

4.2.2.1 Applied field direction along 335 nm edge of the square

Fig. 4.14 shows the magnetization reversal along 335 nm nanomagnets of thickness 10 nm – 60 nm. The reversal is the coherent rotation of the magnetization. An abrupt reversal happens at field H_c, the coercive field. The H_c is large for 10 nm nanomagnets. As the thickness of the nanomagnets increases the H_c decreases. 60 nm nanomagnets shows the minimum H_c. Increase in thickness of the nanomagnets increases the magnetostatic energy as a result decrease in coercivity.

4.2.2.2 Applied field direction along 225 nm edge of the Square

Like in 335 nm the reversal happens without formation of any intermediate state in nanomagnets of thickness 10 nm – 50 nm. Fig. 4.15 shows the magnetization reversal in 10 nm – 60 nm thick nanomagnets. In the case of 60 nm nanomagnets the reversal happens through the formation of multivortex state. This behavior is same as observed in circular nanostructure diameter 225 nm where the reversal happens through the formation of single vortex state (fig. 3.16).

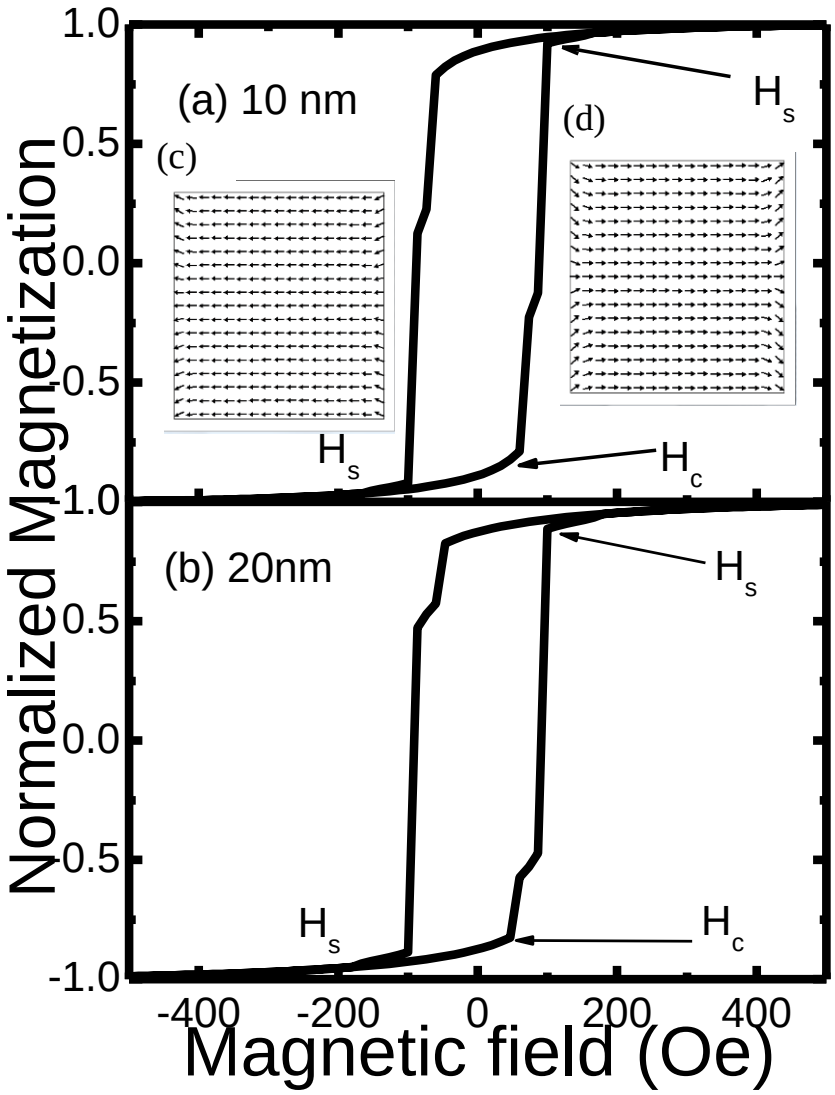

Fig. 4.11: Magnetization reversal in square nanostructures of size 225 nm and of thickness (a) 10 nm and (b) 20 nm and magnetic orientations at saturating field along (c) –ve field and (d) +ve field directions

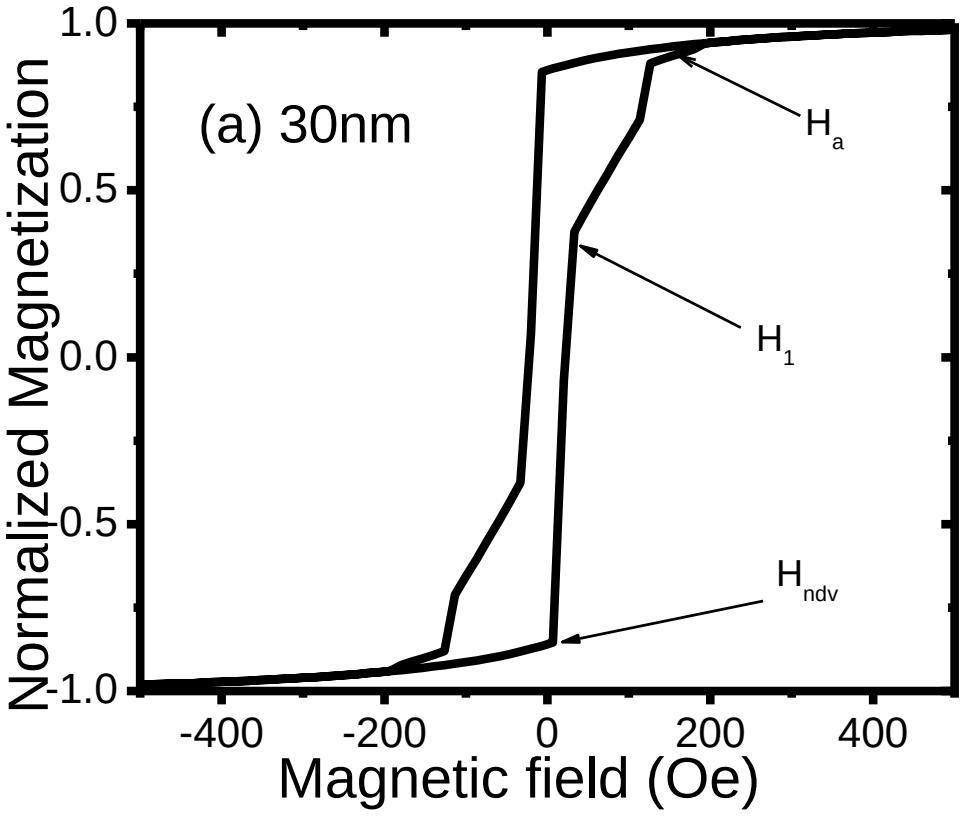

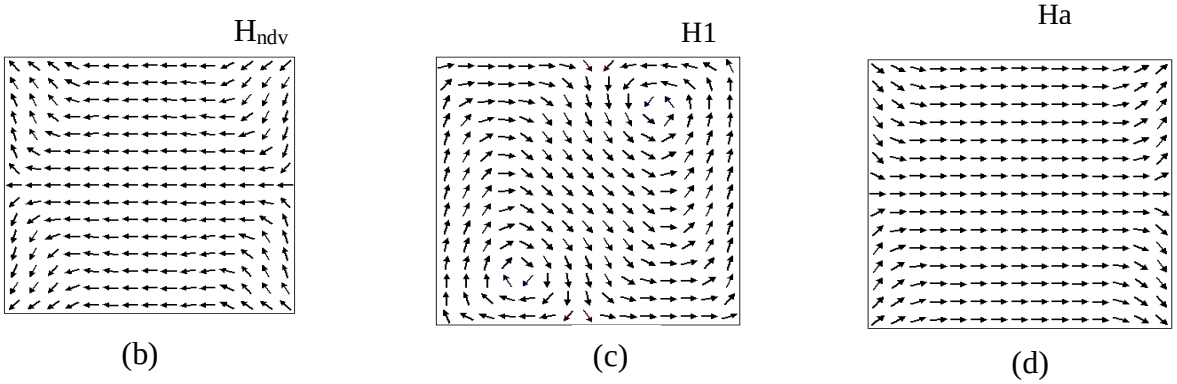

Fig. 4.12: (a) Magnetization reversal in square nanostructure of size 225 nm and of thickens 30 nm and magnetic orientation at (b) nucleation field H_{ndv}, (c) field H_1, and (d) annihilation field H_a

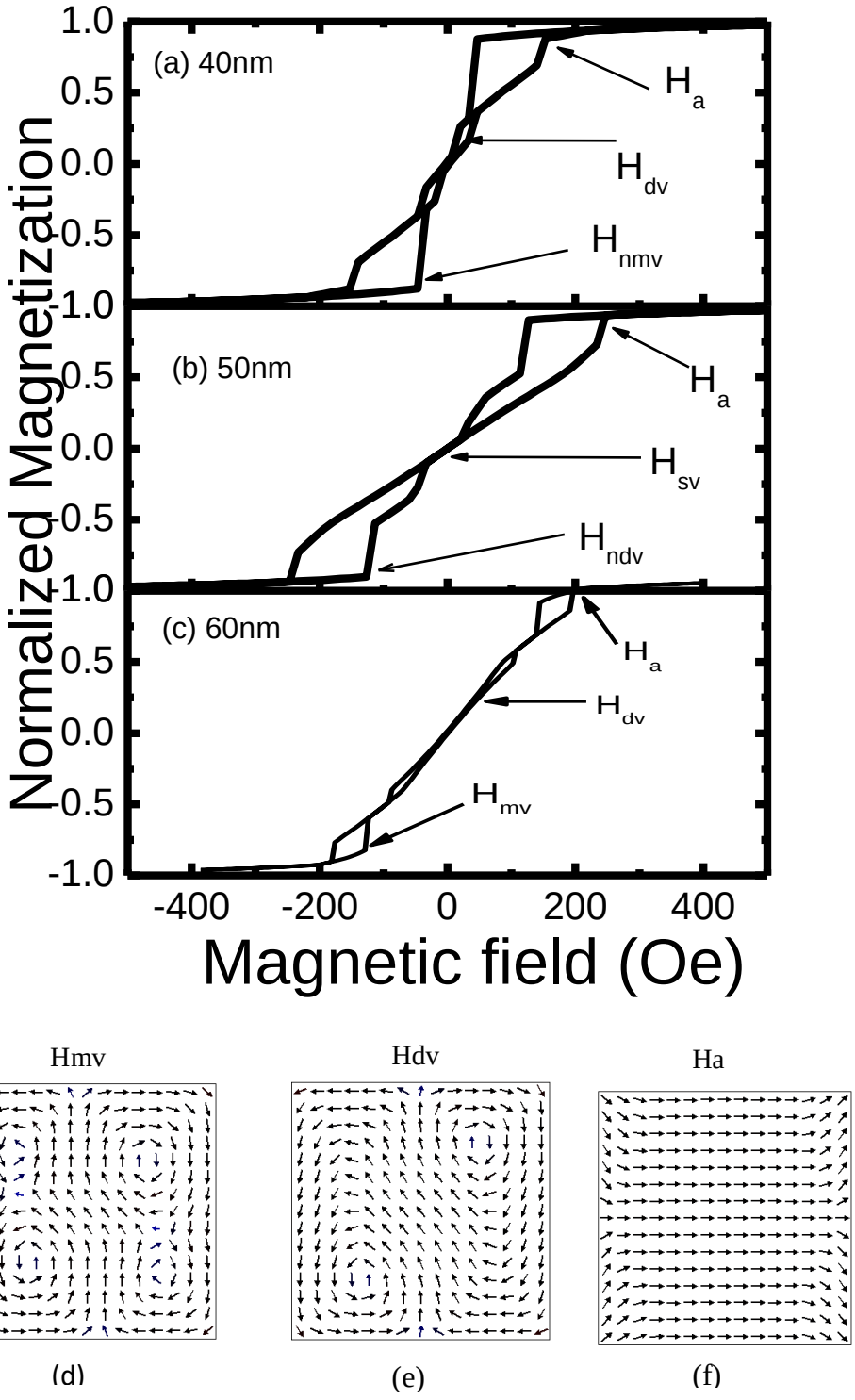

Fig. 4.13 : Magnetization reversal in square nanostructures of size 225 nm and of thickness (a) 40 nm (b) 50 nm and (c) 60 nm and magnetic orientation at (d) nucleation of multi vortex H_{mv}, (e) double vortex H_{dv}, (f) at field H_a

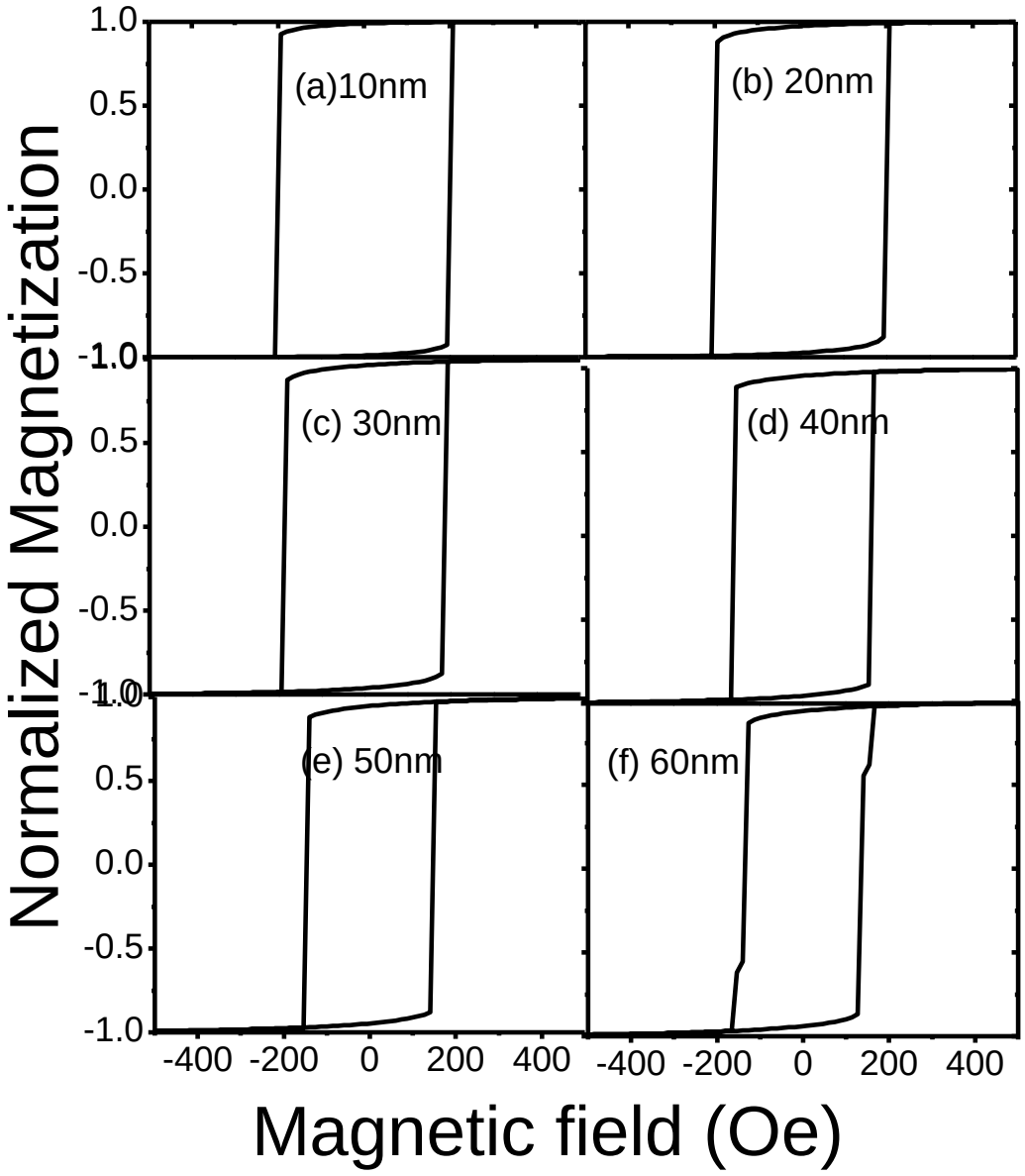

Fig. 4.14: Magnetization reversal in square nanomagnets of size 335 nm and of thickness (a) 10 nm, (b) 20 nm, (c) 30 nm, (d) 40 nm, (e) 50 nm and (f) 60 nm

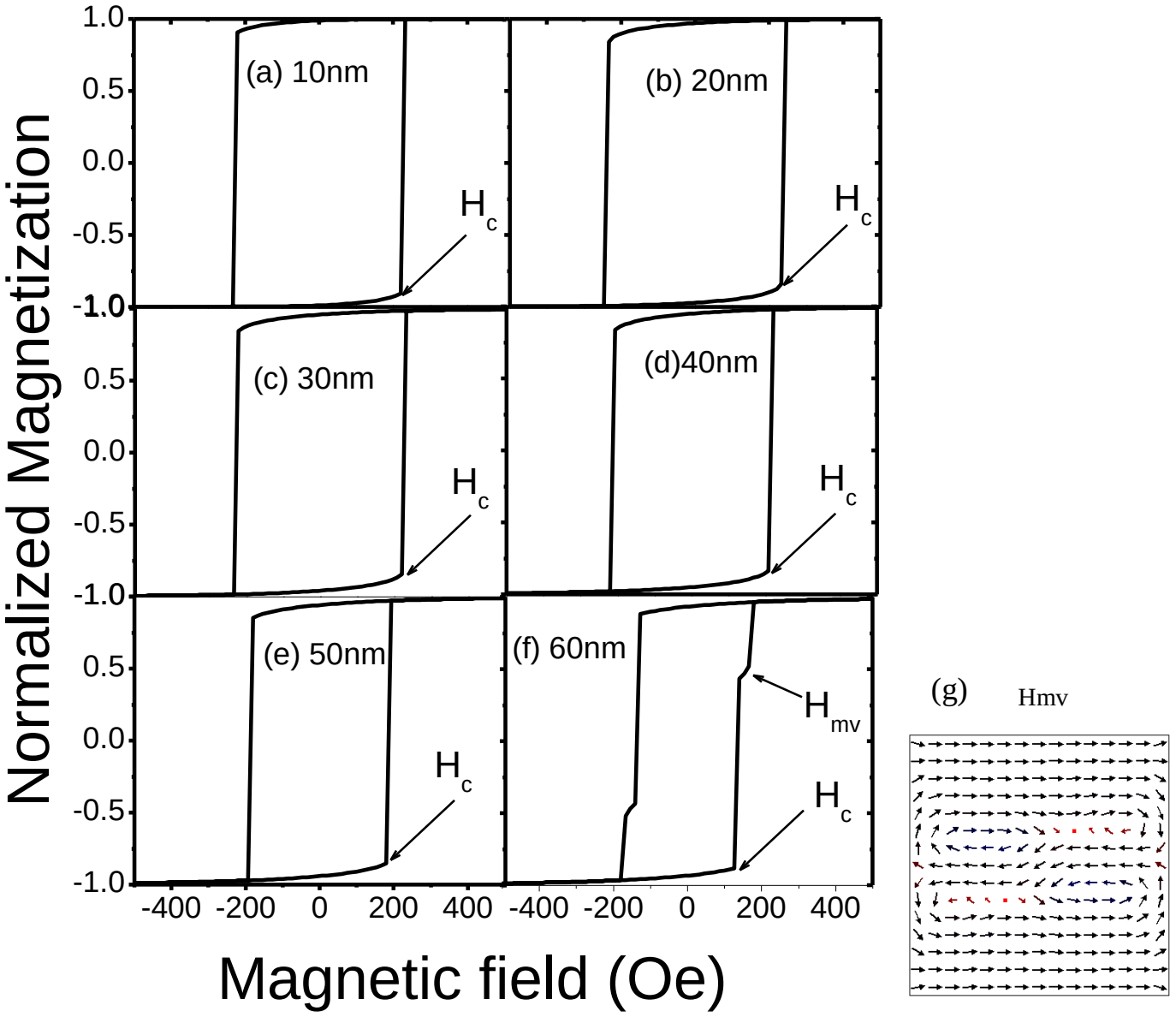

Fig. 4.15: Magnetization reversal in square nanomagnets of size 225 nm and of thickness (a) 10 nm, (b) 20 nm, (c) 30 nm, (d) 40 nm, (e) 50 nm and (f) 60 nm and (g) nucleation of multi vortex in 60 nm nanomagnets at field H_{mv}

Chapter V

Summary and Conclusions

5.1 Summary

This chapter summarizes the thesis work on magnetization reversal in soft magnetic CoFe nanostructures using micromagnetic simulations. Some of the simulation results were verified experimentally. The shape and size dependence of CoFe magnetization reversal were studied.

Elliptical (major axis 335 nm and minor axis 225 nm), circular (335 nm or 225 nm diameters), rectangular (length 335 nm and width 225 nm) and square (335 nm or 225 nm edge lengths) nanostructures are used in the simulations. The thickness of the nanostructures varied from 10 nm to 60 nm.

The reversal in 10 nm nanostructure is independent of the shape of the nanostructure. When the field is changed from -500 Oe to +500 Oe, there is an abrupt reversal of magnetization. This type of reversal behavior can be explained using Stoner – Wohlfarth model. A field of -500 Oe makes the nanomagnet to saturate along the field direction. When the field is reduced to zero stops the system does not become demagnetized. The magnetization still lies along the field direction. This gives remanent magnetization to the nanomagnet. When the field is increased in the positive direction, the magnetization would prefer to reverse parallel to the field direction. Thus, there is an abrupt reversal at this field. This type of reversal gives rectangle or square hysteresis loop which is the main criteria for magnetic data storage.

As the thickness is increased (20 nm – 60 nm) the reversal happens through the formation of double vortex and single vortex states in the case of elliptical and circular nanostructures of dimension 335 nm. In the case of rectangular and square nanostructure of same dimension, in addition to the above said two intermediate states multivortex state was also observed.

The variation of coercivity with the thickness of the nanostructure also confirms that the reversal in higher thickness (> 10 nm, for elliptical and circular; > 20 nm for rectangular and square nanostructures) occurs through formation of some intermediate states. Fig. 5.1 shows the coercivity variation for nanostructures of dimensions (a) 335 nm and (b) 225 nm respectively. The coercivity decreases with the increase of thickness due to the formation of single and multivortex states.

Reversal along the 225 nm shows s – type states in elliptical nanostructures and c – type states in rectangular nanostructures of lower thickness (10 nm). As the thickness increases, the reversal happens through the formation of intermediate states. Table 1 summarizes the magnetization reversal in nanostructures of different shapes and sizes.

Soft magnetic thin film nanostructures are magnetized in plane because of the foremost influences of stray field energy called shape anisotropy. If a nanostructure is magnetized along the short edge, stray field energy is reduced by the formation of end domains that lead to C-

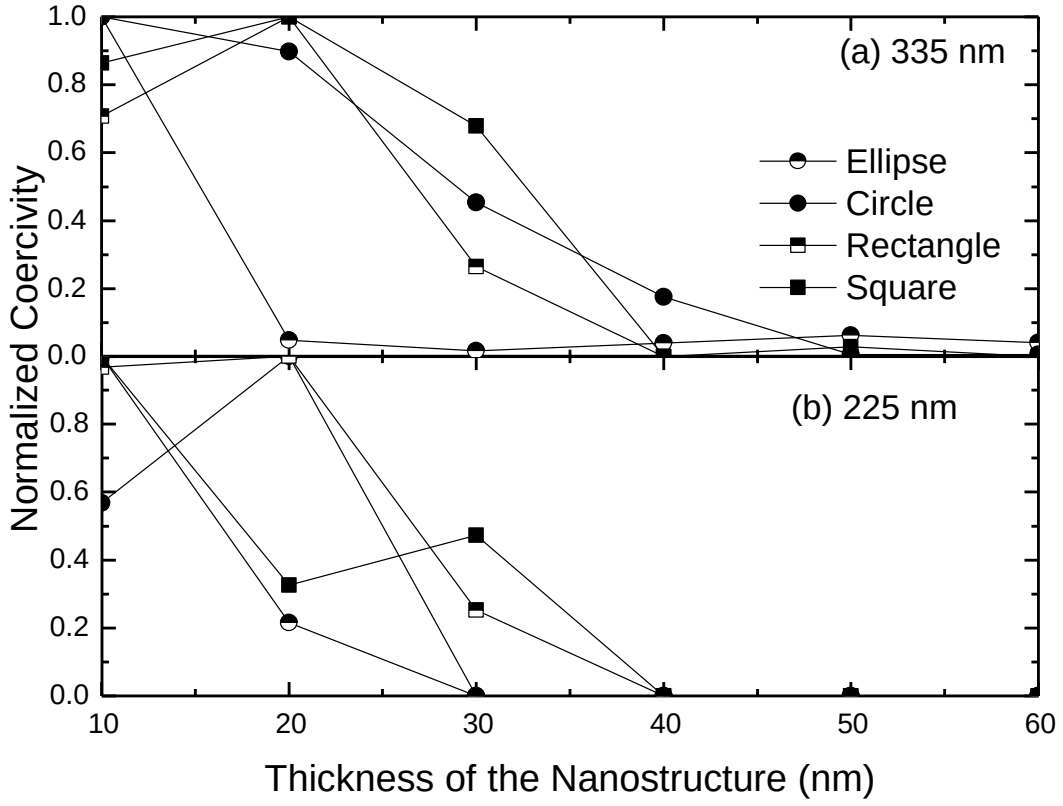

Fig. 5.1: Coercivity variation with the thickness of the nanostructures of dimension (a) 335 nm and (b) 225 nm having $K_1 = 0$ J/m^3

states and S-states. For nanostrucutres of the same size and thickness, the double-vortex state is less energetically favorable than a single-vortex state due to higher exchange energy. For dimensions well above the exchange length (L_{ex}) the exchange energy will be minimum and there is reduction in magnetostatic energy by having a nonuniform magnetization reversal process in nanostructures. Hence, we get zero magnetization by the formation of vortex states. If a rectangular thin film is, magnetized stray field energies are reduced by the formation of end domains that lead to c-sates. Still these structures have stray field energy that can be decreased by flux closure arrangements even though at the expense of exchange energy due to domain walls. The thickness dependence of the stray field energy eventually leads to a transition from single domain state to multi-domain states.

Table 1: Comparison of magnetization reversal in nanomagnets of different shape and size having magnetocrystalline anisotropy constant, $K_1 = 0$ J/m^3

Nanostructure		Thickness					
	Size	10 nm	20 nm	30 nm	40 nm	50 nm	60 nm
Elliptical	335 nm	AR	AR	DV	DV & SV	DV & SV	DV & SV
	225 nm	S	S & DV	S & DV	S & DV	DV & SV	DV & SV
Circular	335 nm	AR	SV	DV & SV	DV & SV	DV & SV	DV & SV
	225 nm	AR	SV	DV & SV	DV & SV	DV & SV	DV & SV
Rectangular	335 nm	AR	AR	DV	DV	DV	DV
	225 nm	C	SV	MV	MV	MV	MV & SV
Square	335 nm	AR	AR	DV	MV	MV	MV
	225 nm	AR	AR	DV	MV	MV	MV

The simulation results were verified experimentally in the case of elliptical nanomagnets. For this, nanomagnets of thickness 10 nm and 60 nm were chosen. The 10 nm nanomagnets shows the rectangular hysteresis loop. Abrupt reversal of magnetization happens at coercive field. In the demagnetized state, the 10 nm nanomagnet shows the single domain behavior. The MFM images captured in the demagnetized state also shows the single domain behavior. The magnetization reversal for 60 nm nanomagnets was same as that observed in simulations. Here the reversal happens through the formation of single vortex state.

The as deposited films on nanostructures can be amorphous in nature. The magnetocrystalline anisotropy is zero for amorphous nanomagnets. Because of this the simulation results with K_1 = 0 J/m^3 are matching with the experimental observations as explained in the previous section. The amorphous films can be heat treated to make them crystalline. For these films, the crystalline anisotropy plays a prominent role. Hence the micromagnetic simulations were carried out with the bulk anisotropy constant, $K_1 = 3.5 \times 10^5$ J/m^3. Table 2 summarizes the magnetization reversal in nanostructures of different shapes and sizes. The coercivity is high for these nanostructures because of the magnetocrystalline anisotropy. The magnetocrystalline anisotropy plays a prominent role in the reversal. Fig. 5.2 shows the coercivity variation for nanostructures of dimension (a) 335 nm and (b) 225 nm respectively. Here also we observed decrease in coercivity with the increase of thickness. The rapid decrease in the case of 225 nm nanostructures is explained based on the magnetostatic energy, which is large for smaller structures.

Table 2: Comparison of magnetization reversal in nanomagnets of different shape and size having magnetocrystalline anisotropy constant, $K_1 = 3.5 \times 10^5$ J/m^3

Nanostructure		Thickness					
	Size	10 nm	20 nm	30 nm	40 nm	50 nm	60 nm
Elliptical	335 nm	AR	AR	AR	AR	AR	AR
	225 nm	AR	AR	DV	DV	DV	DV
Circular	335 nm	AR	AR	AR	AR	AR	AR
	225 nm	AR	AR	AR	AR	AR	SV
Rectangular	335 nm	AR	AR	AR	AR	AR	AR
	225 nm	AR	AR	AR	AR	MV & DV	MV & DV
Square	335 nm	AR	AR	AR	AR	AR	AR
	225 nm	AR	AR	AR	AR	AR	MV

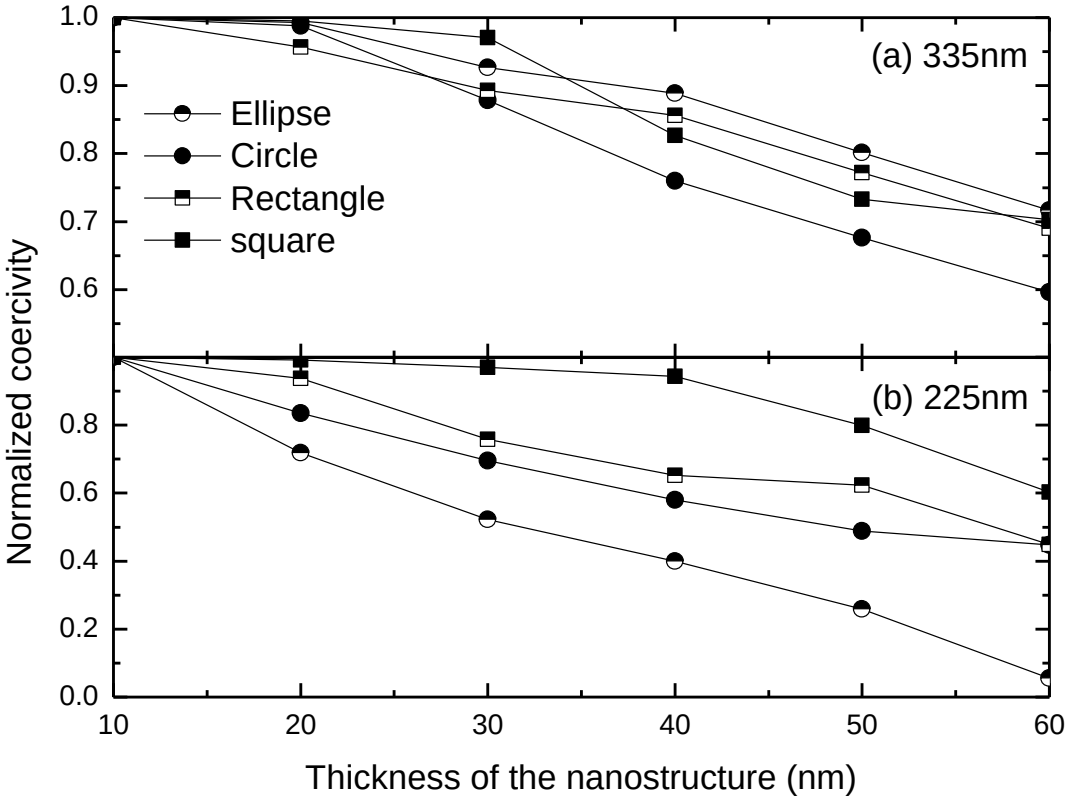

Fig. 5.2: Coercivity variation with the thickness of the nanostructures of dimension (a) 335 nm and (b) 225 nm having $K_1 = 3.5 \times 10^5$ J/m^3

5.2 Scope for Future Work

The development of flexible magnetoelectronics requires magnetic nanostrucutres on flexible substrates. The magnetocrystalline anisotropy constant depends on the nature of the film, which can be controlled by selecting the substrate and heat treatment. Micromagnetic simulations help in choosing the substrate for a given application. The present study can be extended to 3 dimensional (3D) structures having multi layers. There is plenty of scope for the 3D micromagnetic simulations for spintronic applications such as spin transfer torque, current induced domain wall motion, etc. The new emerging topic, magnetic skyrmions, can also be studied using micromagnetic simulations.

References

1. Frank J. Owens, Physics of Magnetic Nanostructures (2015), *by John Wiley & Sons*

2. B.D.Culity, C.D.Graham, Introduction to Magnetic Materials (2009), *by John Wiley & Sons*

3. Jiles D., Introduction to Magnetism and Magnetic Materials (1998)., *Taylor & Francis Inc*. U.S.,

4. A. Hamadeh, N. Locatelli, V.V. Naletov, R. Lebrun, G.de Loubens, J.Grollier, O.Klein, and V.Cros, *Appl.Phys.Lett*. **104** (2014) 022408

5. J. Li, A. Tan, K. W. Moon, A. Doran, M. A. Marcus, A. T. Young, E. Arenholz, S. Ma, R. F. Yang, C. Hwang and Z. Q. Qiu, *Appl.Phys.Lett*. **104** (2014) 262409

6. J. A. J. Burgess, A. E. Fraser, F. Fani Sani. D. Vick, B. D. Hauer, J. P. Davis, and M. R. Freeman, *Science* **339** (2013) 1051

7. S. Agramunt-Puig, N. Del-Valle, C. Navau, and A. Sanchez, Press, Cambridge *Appl. Phys. Lett.*, **104** (2014) 012407

8. J. Tóbik, V. Cambel, G. Karapetrov, *Sci. Rep*. **5** (2015) 12301

9. M.lakshamanan, *Phil. Trans. R. Soc. A* **369** (2011) 1280

10. H**.** Kronmiiller , R. Fischer, R. Hertel, T. Leineweber, **175** (1997) 177

11. Junqin Li, Yong Wang, Jiefeng Cao, XiangyuMeng, Fangyuan Zhu, Yanqing Wu, Renzhong Tai, *J. Magn. Magn. Mater*, **435**, (2017) 167

12. J. Lohau, A. Moser, C.T. Rettner, M.E. Best and B.D. Terris, *Appl. Phys. Lett*. **78** (2001) 990

13. S.S.P. Parkin, K.P. Roche, M.G. Samant, P.M. Rice, R.B. Beyers, R.E. Scheuerlein, E. J. O' Sullivan, S.L.Brown, J. Bucchigano, D.W. Abraham, Y. Lu, M. Rooks, P.L.Trouilloud, R.A. Wanner and W.J. Gallagher, *J.Appl. Phys*. **85**, (1999) 5828

14. H. Ardhuin, J.N. Chapman, P.R. Aitchison, M.F. Gillies, K.J. Kirk and C.D.W. Wilkinson, *J. Appl. Phys*. **88**, (2000) 2760

15. Wang K L, Alzate J G and Amiri P K *J. Phys. D: Appl. Phys*. **46** (2013) 074003

16. Khvalkovskiy A V, Apalkov D, Watts S, Chepulskii R, Beach R S, Ong A, Tang X, Smith A D, Butler W H, Visscher P B, Lottis D, Chen E,Nikitin V and Krounbi M *J. Phys. D: Appl. Phys.* **46** (2013) 074001

17. D.Sander *J.phy: Condens.Matter* **16** (2004) R603

18. S. Yakata, M. Miyata, S. Honda, H. Itoh, H. Wada, and T. Kimura, *Appl. Phys. Lett*., **99** (2011) 242507

19. Rosa M. Corona, Ali C. Basaran, Juan Escrig, Dora Altbir , *Journal of Magnetism and Magnetic materials* ***438*** (2017) 168

20. Takanashi ,K. Fundamentals of Magnetoresistance Effects in Spintronics for Next generation Innovative Devices; Wiley:Newyork, NY, USA, 1, (2015)

21. K.Ando , S.Fujita , J.Ito, S.Yuasa, Y.Suzuki, Y.Nakatani, T.Miyazaki and H.Yoda, *Journal of Applied Physics*, **115**, (2014) 172607

22. J. Daughton, Thin solid Films, **216** (1992) 162

23. J. Barnas, A.Fuss, R.Camley, P.Grunberg, and W.Zinn, *Physical Review* B **42** (1990) 8110

24. G.Panning, D. Erstad, W. Heikkila, A.Hurst and H. Kaakani, GOMAC Conference, March 8-11, ,Monterey, CA, (1999)

25. A.Pohm, B.Everitt, R.Beech, and J.Daughton, *IEEE Trans.Magn*., **33** (1997) 3280

26. A. Pohm, B. Everitt, R. Beech, A. Fink ,and J. Daughton, *IEEE Trans.Magn*., **34**, 4 (1998) 1060

27. Evgeny Y Tsymbal, Oleg N Mryasov and Patrick R LeClair, *J. Phy. s: Condens. matter*, **15** (2003) 4

28. Wang SG, Ward RC, Hesjedal T, Zhang XG, Wang C, Kohn A, Ma Ql, Zhang J, Liu HF, HanXF., *J. Nanoscience and Nanotechnology*, **12** (2012) 1006-23

29. Kalitsov A,Zermatten PJ,Bonell F,Gaudin G,Andrieu S,Tiusan C,Chshiev M,Velev JP, *J.Phys. Condens. matter*, **25** (2013) 496005

30. Ortega N, Kumar A, Scott JF, Katiyar RS, *J.Phys Condens. matter*, **27** (2015) 504002

31. Kasuni Nanayakkara, Alexander Anferov, Ajey P.Jacob, S.James Allen and Alexander Kozhanov, *IEEE Trans. on Magn.*, **11** (2014) 50

32. C. J. Garcia-Cervera, Z. Gimbutas and E. Weinan, *J. Comput. Phys*. **184** (2003) 37

33. Jain S, Re n Y, Adeyeye A O and Singh N *Phys. Rev. B* **80** (2009) 132401

34. P.Vavassori, N.Zaluzec.V.Metlushko, V.Novosad, B.Ilic, and M.Grimsditch, *Physical Review B* **69** (2004) 214404

35. F.Carace, P.Vavassori, G.Gubbiotti, S.Tacchi, M.Madami, G.Carlotti, T.Okuno, *Thin solid Films* **515** (2006) 727

36. Mei-Feng Lai, Zuang-Hang Wei, J.C.Wu, Ching-Ray Chang, N.A.Usov, Ida Chang, and Jun-Yang Lai, *IEEE Trans. Magnetics*, **41** (2005) 953

37. Junqin Li, YongWang, Jiefeng Cao, Xiangyu Meng, Fangyuan Zhu and Renzhong Tai *Journal of Magnetism and Magnetic Materials* (2017), doi: https : // doi.org/ 10.1016/ j.jmmm.2017.11.081

38. Mei-Feng Lai, Zuang-Hang Wei, J.C.Wu, Ching-Ray Chang, W.Z.Hsieh, and Jun-Yang Lai, *IEEE Trans. Magnetics*, **41** (2005) 944

39. G. Shimon, A.O.Adeyeye and C.A.Ross, *J. Appl. Phys.* **111** (2012) 013909.

40. A.O.Adeyeye and N.singh . *J. Phys.D* **41** (2008) 153001

41. S.S.P.Parkin, M.Hayashi and L.Thomas, *Science* **320** (2008) 5873, 190

42. Jyh-Shinn,Ching –Rang chang ,W.c.Lin and Denny D.Tang *IEEE Trans. Magnetics*, **41** (2005) 879

43. J. G. Zhu and Y. Zhang, *I*, B Hillebrands and K. Ounadjela, Eds. Newyork*: Springer – verlag*, (2002) 289

44. J.Fidler, T.Schrefl, W.Schloz, D.Suess, V.D.Tsiantos, *Physica B* **306** (2001) 112

45. Luu Van Thiem, Le Tuan Tu and Manh-Huong Phan , *Sensors*, **15** (2015) 5687

46. L.Torres, E.Martinez, L.Lopez-Diaz and J.Iniguez, *J. Appl. Phys*. **89** (2001) 7585

47. R.P.Cowburn *J.Phys.D* **33** (2000) R16

48. V. Satya Narayana Murthy, C. Krishnamoorthi, R. Mahendiran and A. O. Adeyeye, *J. Appl. Phys.* **105** (2009) 023916

49. N. Singh, S. Goolaup, and A. O. Adeyeye, Nanotechnology **15** (2004) 1539

50. K.L. Chopra, S. Major, D.K. Pandya, Thin Solid Films, **102** (1983) 1

51. Ivor Brodie and Julius J.Muray , The Physics of Micro/Nanofabrication, *Springer Sciences*- (2013)

52. Siracusano G, Tomasello R, Puliafito V, Giordano A, Azzerboni B, La Corte A, Carpentieri M and Finocchio G *J. Appl. Phys*. **117** (2015) 17E504

53. Jing Yin, Cheng Liang Pan, Hong Bo Wang, and Zhi Hua Feng, Rev. Sci. Instrum. **82** (2011) 124702

54. A. Niazi, P. Poddar and A. K. Rastogi, *current science*, **79**, (2000) 1

55. I V Yaminsky, A.M. Tishin Russian Chemical Review **68 (3)** (1999) 165

56. Hartmann U. Magnetic Force Microscopy , *Annual Review of Materials Research* , 29 (1999) 53

57. Porthun S, Abelmann L., and Lodder C., *Journal of Magnetism and Magnetic Materials*, **182 ,** 1-2 (1998) 238

58. S.Zhang, and S.S.-L.Zhang,Phys.Rev.Lett,. **102** (2009) 086601,

59. Brown, W.F., Jr., La Bonte, A.E. *J. Appl. Phys*. **36** 4 (1965) 1380

60. T.Dietl, *Phys.Rev. B* **77** (2008) 085208.

61. T. Fischbacher, M.Franchin, G.Bordignon, and H.Fangohr , *IEEE Trans. Magn.* **43**, (2007) 2896

62. D.Suess, R.Dittrich, H.Forster, J.Fidler,T.Schrefl, W.Scholz, V.D.Tsiantos, Comput.Mater.Sci., **28** (2003) 366

63. W.Wang, M.-A.Bisotti, D.Cortes, T.Kluyver, M.Vousden, R.Pepper, O.Laslett, R.Carey, and H.Fangohr, (2016). https:/ github.com/ computational modelling / fidimag

64. Donahue M J and McMichael RD. *National Institute of Standards and Technology*, Gaithersburg, MD, USA (2002)

65. Mykola Dvornik , Arne Vansteenkiste, Jonathan Leliaert, , Mathias Helsen, Felipe Garcia-Sanchez, and Bartel Van Waeyenberge , *AIP Advances*, **4** (2014) 107133

66. J. Miltat and M. Donahue, Mathematical & Computational Sciences Division, National Institute of Standards and Technology, Gaithersburg MD U. S. A. (2001) 20899

67. Huang Z. Department of Mathematical Sciences, Tsinghua University, Beijing, P. R. China (2003) 100084

68. A. Bagneres- iallix and P. Baras. *J. Appl. Phys*. **69** (1991) 4599

69. Thomas L. Gilbert, *IEEE Trans. on Magn.* **40** (2004) 6

70. Donahue M J et al, OOMF User's guide, version 1.0. interagency report NISITR 6376, *National Institute of Standards and Technology*, Gaithersburg, MD, (1999).

71. Zhengang Guo, Liqing Pan, Hongmei Qiu, M.Yasir Rafique, Shuai Zeng, Advanced Materials research, **710** (2013) 80

72. Stoner E.C and Wohlfarth E P , *Philos.Trans.R.Soc.London,Ser.A* **, 74** (1948) 240

73. Dunin-Borkowski R E ,McCartney M R,Kardynal B and Smith D J ,*J.Appl.Phys*. **84,** (1998) 374

74. F. Carace, P. Vavassori, G. Gubbiotti, S. Tacchi, M. Madami, G. Carlotti, T. Okuno, *Thin solid Films* **515** (2006) 727

75. W. Wernsdorfer, K. Hasselbach, A. Benoit, W. Wernsdorfer, B. Barbara, D. Mailly, J. Tuaillon, J. P. Perez, V. Dupuis, J. P. Dupin, G. Guiraud, and A. Perex, *J.Appl.Phys.*, **78,** (1995) 7192,

76. R.Morales, A.C.Basaran, J.E.Villegas, D.Navas,N.soriano, B.Mora, C.Redono, X.Batlle, and I. K. Schuller, *Phys.Rev.Lett.* ,**114** (2015) 097202.

77. K. K. M. Pandey, J S Chen, J F Hu and G M Chow, *J. Phys. D: Appl. Phys.* **42,** (2009) 015009

78. P. Lupo, Z. Haghshenasfard, M. G. Cottam, and A. O. Adeyeye, *Phys. Rev. B* **94** (2016) 214431

79. Baek B, Rippard W H, Pufall M R, Benz S P, Russek S E, Rogalla H, Dresselhaus P D *Phys. Rev. Appl*. **3** (2015) 011001

80. D. M. Burn, M. Chadha, and W. R. Branford, *Phys. Rev. B* **92**, (2015) 214425

81. D. K. Koltsov, R. P. Cowburn, A. O. Adeyeye and M. E. Welland, *Phys. Rev. lett*. **83** (1999) 5

82. K.Y. Guslienko, J. Nanosci. Nanotechn., **8** (2008) 2745

83. C A F Vaz, M Kläui, J A C Bland, and L Lopez-Diaz, 2003 , *J. Physics: Conden.Matter. Phys.* , **21** (2003) 15

84. F J Castaño, C A Ross and A Eilez , *Journal of Physics* : D **36** (2003) 17

85. J.P. Davis , J. A. J. Burgess, A. E. Fraser, F. Fani Sani, D. Vick, B.D. Hauer, , M. R. Freeman, *Science*, **339** (2013) 1051

86. K. Muthukumar, H.O. Jeschke, R. Valenti, E. Begun, J. Schwenk, F. Porrati, M. Huth, Beilstein , *J. Nanotech*. **3** (2012) 546

87. Z –H.Wei, C.-R.Chang, N.A.Usov, M.-F.Lai, and J.C.Wu, *J. Magn. Magn. Matter.* **95** (2002) 1

88. Arabinda Haldar and A. O. Adeyeye, *J. Appl. Phys* **106** (2015) 032404

89. R.Hertel and H.kronmuller, *Physica B* **275** (2000) 1

90. Y.Zheng and J.Zhu, *J.Appl.Phys*. **81** (1997) 4336

91. W.L.Gan, M.ChandraSekhar, D.W. Wong ,I.Purnama, S.Y.Chiam, L.m.Yong and W.S.Lew, *Appl.Phys.Lett*. **105** (2014) 152405

92. A.lara , O.V.Dobrovolskiy, J.L.Prieto, M. Huth, and F.G. Aliev, *J. Appl. Phys.* , **105** (2014) 182402

93. Z.M.Dai, Y.Y.Dai, W.Liu, T.T.Wang, X.T.Zhao, X.G.Zhao and Z.D.Zhang. *Appl.Phys.Lett*. **111** (2017) 022404

Publications

Journal Papers

1. N. V. S. S. Seshagiri Rao and V. Satya Narayana Murthy, "Comparitive study of magnetization reversal process between elliptical and rectangular CoFe nanomagnets", *Trans Indian Inst Met* **70** (2017) 567

2. N. V. S. S. Seshagiri Rao, V. Satya Narayana Murthy and YJVS.Ramakrishna Sharma, "Magnetic force microscopy and simulation studies on $Co_{50}Fe_{50}$ elliptical nanomagnets", *Bull. Mater. Sci.* **39** (2016) 725

3. N. V. S. S. Seshagiri Rao and V. Satya Narayana Murthy, "Multivortex formation during magnetization reversal in rectangular and square CoFe nanomagnets" (*To be communicated*)

Conferences

1. N. V. S. S. Seshagiri Rao and V. Satya Narayana Murthy (2017) Comparitive study of magnetization reversal process in anisotropic elliptical and rectangular CoFe nanomagnets, *Prensed in 17th International Conference on Thin Films (ICTF 2017), held in New Delhi, India*

2. N. V. S. S. Seshagiri Rao and V. Satya Narayana Murthy (2017) Comparitive study of magnetization reversal process between elliptical and rectangular CoFe nanomagnets,*Prensed in International Conference on Emerging Trends in Materials and Manufacturing Engineering (IMEE17), held in Tiruchirappalli, India*

3. N. V. S. S. Seshagiri Rao and V. Satya Narayana Murthy (2017) Comparitive study of magnetization reversal process between circular and elliptical CoFe Nanomagnets, *Prensed in*

International Conference on Magnetic Materials and Applications (ICMAGMA), held in Hyderabad, India

4. N. V. S. S. Seshagiri Rao and V. Satya Narayana Murthy (2014), 2D micromagnetic simulations of permandur circular nanostructures, *Presented in National Conference on Advanced Materials for Defense and Aerospace Applications, held at Bits Pilani, Hyderabad, India*

Biography of the candidate

My self N.V.S.S.Seshagiri Rao completed my M.Sc. with first class of 65 percentage form Andhra University Vishakhapatnam in 2001 and M.Tech.with 69 percentage in Atmospheric Sciences from Andhra University Vishakhapatnam in 2004. From 2004 August onwards I have worked as Assistant Professor of Physics at various engineering colleges till June 2013. From July 2013 I joined as a Project Associate in DST SERB project no. SR/FTP/PS – 014 /2011, 02/07/2012 under Dr. V. Satya Narayana Murthy, Assistant Professor, Department of Physics, BITS Pilani Hyderabad Campus. At the same time, I registered for Ph.D under his guidance. I completed my PhD work and submitted my thesis on "Magnetization Reversal Study in CoFe Magnetic Nanostructures". I have experience on preparation and characterization of soft magnetic thin films and simulating the magnetic nanostructures. I have published my thesis work in reputed international journals and presented in national and international conferences held in India.

Biography of the supervisor

Dr. V. Satya Narayana Murthy is working as Assistant Professor in Department of Physics, BITS Pilani Hyderabad Campus. He joined in BITS in 2010. Dr. Murthy completed his PhD in the year 2007 from Indian Institute of Technology Madras. 2008 he was in Department of Electrical Engineering, National University of Singapore as a postdoctoral fellow. 2009 – 2010 he was in Center for Nondestructive Evaluation of Materials, Department of Mechanical Engineering, Indian Institute of Technology Madras as a postdoctoral fellow. His research experience comprises of preparation and characterization of soft magnetic materials in bulk, thin film and nanostructure form. He has designed magnetostrictive and electromagnetic acoustic sensors for nondestructive evaluation of the materials. He has good amount of experience on micromagnetic simulations. He has published his research work in reputed international and national journals.